Democratic and Popular Republic of Algeria Ministry of

Higher Educationand Scientific Research University Mohamed

Khider of Biskra

Faculty of Exact Sciences and Science of Nature and Life

Department of Mater Science

Thesis

Presented to obtain the diploma:

Doctorate of Science in
Chemistry

Specialty: Sciences of
Materials

The role of pH on the synthesis of a passivation layer comprising MgO-ZnO alloys

Presented by:

Nadjat Chaouch

Publicly defended on:

To the Jury composed by:

M^{r}. Abdallah Attaf	Professor	University of Biskra	President
M^{r}.Said Lakel	Professor	University of Biskra	Supervisor
M^{r}. Said Benramache	Professor	University of Biskra	Co-Supervisor
M^{rs}. Loubna Benamor	Lecturer ‘’A’’	University of Batna2	Examiner
Mr. Adel Bouhdjer	Lecturer ‘’A’’	University of Batna2	Examiner

Academic year: 2022-2023

ACKNOWLEDGEMENT

Firstly, I would like to thank ALLAH who gave me the health, courage, and patience to carry out this modest work.

I particularly thank my supervisor, Mr. **Said Lakel**, a Professor at the Mohamed Khider University of Biskra, for agreeing to direct this work with great availability and efficiency, for sharing his experience with me, and for the advice and encouragement throughout this work.

I am delighted to acknowledge a debt of gratitude to my co-supervisor professor **Said Benramache** from the University of Biskra for his endurance, patience, and encouragement. It has been a privilege to have his support and help. I hope the result will be as he wishes and wants.

It is a great honor for me, Pr. **Abdallah Attaf** is the head of the jury for my thesis at The Mohamed Khider University of Biskra, It is also my pleasant duty to thank Dr. **Loubna Benamor** from the University of Batna 2, and Dr. **Bouhdjer Adel** from the University of Batna 2, because they agreed to discuss my dissertation.

I would like Many thanks to all the teachers of the Department of Matter Sciences Section of Mohamed Khider University of Biskra,

Finally, I thank everyone who contributed directly or indirectly to the realization of this work.

Great thanks to all my teachers, especially Dr. **T. Tibermacine** for their valuable suggestions to fulfill my research successfully. I would like to thank all those who helped me here and there, especially all the teachers and Students of the Department of Matter Sciences Section of the Mohamed Khider University of Biskra and common base department in science and technology, University of Batna 2. I would also like to thank everyone who works in the laboratory of thin films at our university and the pedagogy laboratory

Finally, I express my sincere thanks to all my, family, friends, and colleagues, and to everyone who helped me to accomplish this research work.

Dedication

I dedicate this thesis to the special people who deserve much respect and great love:

In memory of my dear father.

A special feeling of gratitude to my loving mother whose words of

encouragement and push for success.

My sisters and my brothers have never left my side and are very special.

I also dedicate this dissertation to my many friends who have supported me, and to all those

who helped me without hesitation

Thank you a lot, indeed.

I dedicate this work In memory of my professor Ahmed Boutarfaia

Nadjat Chaouch

CONTENTS TABLE

General introduction

General introduction

Today, the nanotechnology gained great attention due to its potential applications; it also find it multi-use in: information technology, energy, environmental science, medicine, transportation, food safety, and among many others. However, the nanotechnology can also be categorized as one of the best sciences because having a size ranging from 1–100 nm. There are numerous developed methods for synthesizing nanoparticles, which were categorized as physical, chemical, and biological methods. These physical and chemical techniques can be carried out in the water, using organic solvents, ionic water, microemulsions, or wet chemical procedures. Other techniques for creating nanoparticles included gas condensation, vacuum deposition and vaporization, mechanical attrition, hydrolysis, condensation, growth and agglomeration, and electrodeposition. Most of these processes call for dangerous substances, stabilizing agents, and capping agents that may have negative effects in medical settings. An eco-friendly method of creating nanoparticles has been developed in response to this concern, and it has many advantages for use in medical and pharmaceutical applications [1].

Metal oxide semiconductor nanomaterial's exhibiting excellent physical and chemical properties are accepted as one of the most important parts of technological applications [2]. In addition Mixed metal oxides have found increasing research focus and applications in physics, chemistry, materials science and engineering. The combination of two or more metals in an oxide matrix can produce materials with novel physical and chemical properties leading to relatively higher performance in various technological applications [3].the alloying or combination-based wide-band gap semiconductors are attractive to various technological applications, such as photovoltaic's, and optoelectronic devices [4]. Among them, MgO is one of the most investigated metal oxides, because of its facile making and doping. The alloys made from ZnO and MgO give wide band gap semiconductors with highly tunable band gaps.Alloying with magnesium oxide (MgO) to make Mg-doped ZnO can increase the band-gap energy from 3.3 eV for wurtzite ZnO to 7.8 eV for rock salt[5].For the purpose of changing the electrical and optical properties of ZnO, MgO was often doped into or combined with ZnO in various ways. A number of research efforts have been focused on the artificial engineering of oxides and semiconductors for functional devices applications[6]. The fabrication of thin films and pH is important for those applications, because of the size-related effects of their performances [7].

The aim of this thesis is to investigate of the physical properties of the thin films of MgO-ZnO by the spray pyrolysis technique, which were prepared at different experimental parameters on the fundamental properties of MgO-ZnO films. The parameters investigated are (substrate

temperature, molarity and pH) to understand the effects of these parameters on the properties of this material in order to optimize their performance for use in optoelectronic applications. The layers developed have undergone morphological, structural, optical and electrical characterizations.

This thesis is composed of five chapters that are organized as follows: It began with an elaborate introduction and find by an general conclusion.

The first chapter presents a review of thin films MgO and ZnO, also summarize proprieties, structural, optical, and electrical, for the last studies. At the end of the chapter, it will outline the multiple applications of these films in optoelectronic and photovoltaic fields.

The second chapter presents a review of the Spray Pyrolysis technique and the different procedure effects for depositing undoped and doped Magnesium oxide thin films. In the present study, the obtained films will characterize using X-ray diffractometer (XRD), scanning electron microscopy (SEM), and energy-dispersive X-ray spectroscopy (EDX) techniques. The electrical and optical properties of the films will study using a four-probe setup and a UV- visible spectrophotometer, respectively.

The third chapter discusses the effect of different molar concentrations on the structural, optical, and electrical properties of MgO thin films.

The fourth chapter talks about the effect of pH solution on the structural, optical, morphological and electrical properties of MgO thin films.

The fifth chapter contains an explanation for the deposition of $Zn_{0.5}Mg_{0.5}O$ thin films. The films were deposited with different pH solution, on the structural and optical and properties.

Finally, there is a conclusion that includes a summary of the main findings, concluding remarks, and recommendations for further research.

References

[1] K. P. P. Bisquera, J. R. Salazar, E. S. Romero, L. Lou Mar, A. Lopez, and J. J. Monserate, "Synthesis and Characterization as Zinc Oxide Nanoparticles as a Source of Zinc micronutrient in Organic Fertilizer Synthesis and Characterization as Zinc Oxide Nanoparticles as a Source of Zinc micronutrient in Organic Fertilizer," no. January, 2017.

[2] E. Faculty, "The Role of Au Doping on the Structural and Optical Properties of Cu 2 O Films Emine Güneri *," vol. 58, pp. 49–67, 2019, doi: 10.4028/www.scientific.net/JNanoR.58.49.

[3] I. Journal and O. F. Engineering, "INTERNATIONAL JOURNAL OF ENGINEERING SCIENCES & RESEARCH TECHNOLOGY STRUCTURAL AND OPTICAL PROPERTIES OF (ZnO/MgO) NANOCOMPOSITES," vol. 7, no. 8, pp. 493–499, 2018.

[4] S. D. Senol, C. Boyraz, E. Ozugurlu, A. Gungor, and L. Arda, "Band Gap Engineering of Mg Doped ZnO Nanorods Prepared by a Hydrothermal Method," *Cryst. Res. Technol.*, vol. 54, no. 3, pp. 1–7, 2019,.

[5] S. K. Mahadeva, J. Fan, A. Biswas, K. S. Sreelatha, L. Belova, and K. V Rao, "Magnetism of Amorphous and Nano-Crystallized Dc-Sputter-Deposited MgO Thin Films," pp. 486–497, 2013,.

[6] S. Phanichphant, "Characterization of ZnO / MgO Nanocomposites Synthesized by Flame Spray Pyrolysis," no. July 2009, 2015,.

[7] F. Meydaner. Tezel, O. Özdemir, and I. Afsin Kariper, "THE EFFECTS of pH on STRUCTURAL and OPTICAL CHARACTERIZATION of IRON OXIDE THIN FILMS," *Surf. Rev. Lett.*, vol. 24, no. 4, pp. 1–10, 2017.

Chapter I

Introduction

and

Literature Review

This chapter deals Literature Review of the structural, optical, and electrical properties of Magnesium oxide MgO and MgO-ZnO, then exhibits their important applications in a variety of fields.

I.1.Introduction

Metal oxides are one of the most attractive types of functional materials because of their unusual chemical and physical properties, which cover almost all requirements of materials science and solid-state physics. Metal oxides are perfect materials for a wide range of applications in ceramics, catalysis, energy conservation and storage, sensing, and electronics [1]. Ceramic or metal/alloy oxide films are of scientific and technological importance due to their applications in They will continue to contribute to many applications and an enormous body of research (e.g., information technology, electronics, spintronics, displays, memory units, sensors, biosensors, actuators, active surfaces with different characteristics, catalysis, energy harvesting, energy storage, environmental and safety concerns, healthcare, bioengineering, medicine, the drug industry, etc.)Metal oxides are one of the most attractive types of functional materials because of their unusual chemical and physical properties, which cover almost all requirements of materials science and solid-state physics. [2].Metal oxides Metal oxides nanomaterials such as TiO2 [3],ZnO [4],CuO [5],SiO2 [6],SnO2[7] and MgO [8].

Magnesium oxide (MgO) materials have been attracted a great attention thanks to their wide range of technological applications. MgO compound has a cubic crystalline structure and belongs to the transparent oxide family. It was characterized as an interesting material due to its chemical and thermal stability properties [9], the non-toxicity and abundance of its constitution [10].and high transmission values near to 90% [11].and its refractive index and dielectric constant are 1.736 and 10 respectively [12]. MgO is an insulator material with wide band gap which is 7.8eV and high dielectric constant around 9.8 has attract much attention to be used as dielectric layer in order to replace the commonly used dielectric material which is silicon dioxide, SiO_2[13].

ZnO may be used as dopant to modify the luminescence of MgO crystals. because the ionic radius of Mg^{2+}(0.057 nm) is close with Zn^{2+}(0.06 nm) in ZnO films, and MgO has a larger bandgap (7.7 eV) than that of ZnO material [14].

For the fabrication of Mg_x Zn_{1-x} O (MZO) thin films These improvements make (MZO) material as useful in a broad area of applications in optoelectronic devices such as gas sensors, biosensors and spintronic devices. Furthermore, many researches focus on the enhancement of ultraviolet photodetectors based on MZO films [15]. different techniques have been carried out, such as sol-gel method [16], spray pyrolysis [17], pulsed laser deposition [18] and magnetron sputtering [19]. This last deposition technique results a very attractive growth method thanks to uniform deposition achieved on large area substrates; it also permits low temperature deposition, even at room temperature (RT), at high deposition rates. Finally, the sputtered films present good adhesion onto substrates, high chemical stability and high density[16].

I.2.Magnesium oxide (MgO)

MgO is wide band gap (~7.8eV) refractory material with melting point 2852^0C, boiling point 3600^oC and density 3.58 g/cm^3. It is a highly ionic insulating crystalline solid material with halite (rock salt) structure, as shown in Figure 2.1, and with a lattice parameter of 4.21**Å**. It consists of Mg^{2+} ions and O^{2-} ions held together with ionic bonds [20]. The radius ratio falls within the range of 0.41–0.73 A˚ , which is the radius ratio of stable octahedral coordination. Existing high bond strength in ionic crystal is due to the strong electrostatic forces between ions and hence MgO an ionic crystal, exhibits hardness and high melting point and low electrical conductivity. Its structural, physical, optical and electronic properties are listed in Table I.1[20].

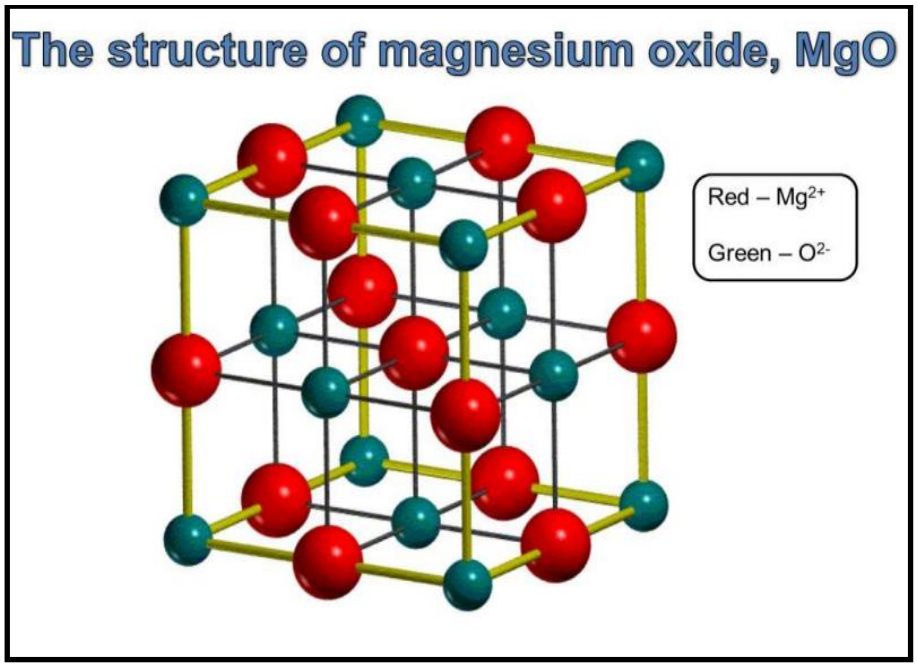

Figure I.1: Arrangement of Mg^{2+} and O^{2-} in Magnesium oxide(MgO).

Table I.1: Summary of Material properties of MgO[20.]

Property	Parameters	values
Physical	Crystal type Density Melting Point Boiling point	Cubic 3.85 g/cm^3 2800 °C 3600°C
Chemical	Color Chemical formula Molecular weight Number of atoms $/cm^2$	White MgO 40.304 g/mol 2×10^{23}
Optical	Optical band gap eV Absorption coefficient/cm (2µm)	7.2 0.05
Dielctric	Dielctric constant Refractive index	9.8 1.739

I.3.Zinc oxide (ZnO)

ZnO, one of the II-VI inorganic semiconductor materials, with a wide direct band gap (3.37 eV) near the UV range and with a large exciton binding energy (~ 60 MeV) at RT. Wurtzite structure model of ZnO is shown in **Figure I.2**.The lattice constants of ZnO unitcell are a = 3.250 Å and c = 5.206Å, with c/a ratio of 1.6 [21]. The number of nearest neighbor atoms in wurtzite structure is four. Each O (or Zn) ion is tetrahedrally surrounded by four Zn (or O) ions. The Zn-O distance of the nearest atom is 1.992Å in the direction parallel to the c-axis and 1.973 Å in the other direction of the tetrahedral structure .This tetrahedral arrangement indicates the covalent bonding nature between Zn and O atoms. The covalent radii of Zn and O were reported to be 1.31 Å and 0.66 Å respectively [22].

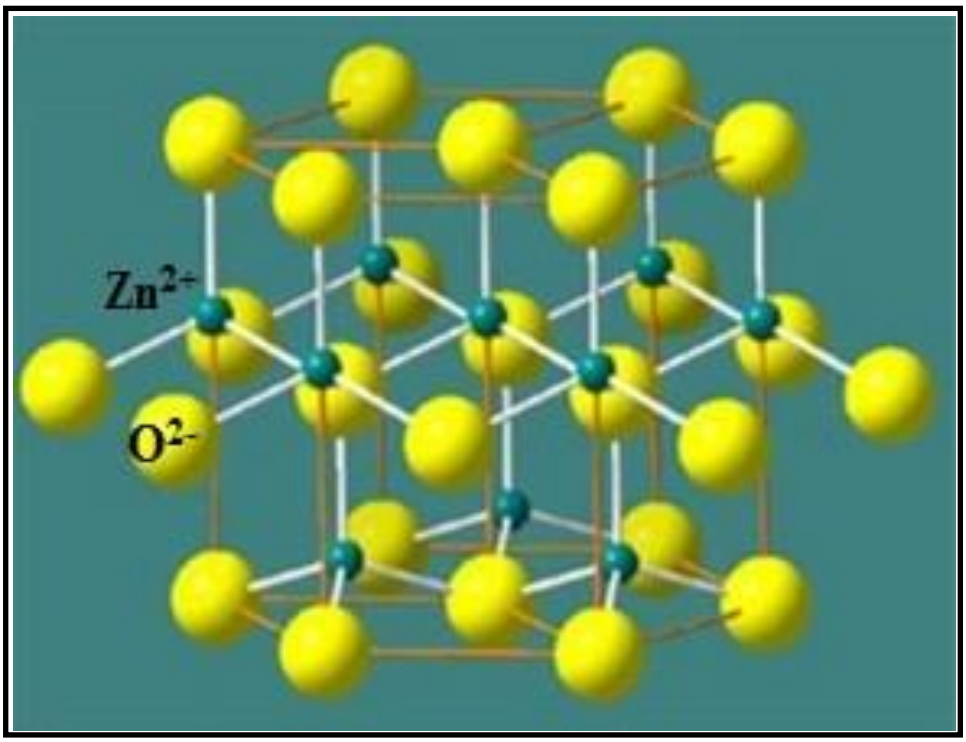

Figure I.2. Wurtzite structure model of ZnO [22].

I.4.Physical Properties of MgO , ZnO and MgO-ZnO

I.4.1. Structural Properties of MgO , ZnO and MgO-ZnO Synthesized In Different Conditions

A) Preferred Orientation

The MgO thin films were crystallized with a cubic structure that can be related to obtaining peaks in the XRD diffraction of MgO thin films. The nanostructures of MgO thin films were studied by the XRD patterns with MgO the major peaks appear in 2θ: 36.80 °, 42. 84°, 62.16°, and 78.44 correspond with the MgO plane of (111), (200), (220), and (222) plans of the MgO phase structure.[11] (JCPDS 01-075-0477)[11].

The ZnO thin films polycrystalline were crystallized with a hexagonal structure that can be detected peaks at 2θ values of 31.83°, 34.49°, 36.40°, 47.57°, and 56.65°. correspond with the plane of (100), (002), (101), (102), and (103) orientations (JCPDS card no. 00-036-1451), the predominant peak of (002) crystalline planes indicated the preferential[14].

In **(2014) S.Nisatharaju et al** [23] deposited the MgO thin films by spray pyrolysis method with 0.05 at 230 °C. Found that the (200) peak is high than other diffractions which indicating that the preferred orientation with (200) plan.

In **(2017) Abdelkader Hafdallah et al** [24]. Zinc oxide (ZnO) thin films were deposited by the pyrolysis spray technique. The effect of nozzle-substrate distance on the structural and optical properties of films was investigated. The crystallinity of all films is improved with nozzle-substrate distance. ZnO films preserve their (002) preferential orientation .

In recent years, researchers have focused more on the synthesis of nanocomposite of ZnO / MgO due to their application in advanced technologies. Various physicochemical techniques have been employed to construct nanosized ZnO/MgO nanoparticles.

Magnesium (Mg) is a suitable dopant for improvement of the band gap of ZnO films because MgO has a wide band gap of about 7.3 eV. Moreover the ionic radii of Mg^{2+}(0.57Å) and Zn^{2+}(0.60 Å) are close, so films are found to be a single phase alloy over a wide range of Mg doping levels [25].so replacement of Zn by Mg should not cause a significant change in lattice constants. By dropping suitable Mg into ZnO, it

may be possible to obtain a ternary ZnMgO alloy with a wider bandgap. However, the large crystal structure dissimilarity between wurtzite-hexgonal ZnO and rock-salt-cubic MgO can be cause unstable phase mixing[26]. (see Table I.2).

$Zn_{1-x}Mg_xO$ films of various Mg compositions (x= 0.0, 0.3, 0.5, 0.7, 0.8, 0.9) deposited at 750 °C. The XRD patterns reveal that the films with Mg content, $x \leq 0.5$, show a highly intense (002) diffraction peak along with a (101) peak which corresponds to the wurtzite ZnO phase without any impurity phase. The appearance of only (200) peak for films with higher Mg content (x= 0.9) is the sign of cubic single phase indicating deviation from wurtzite to rock-salt-cubic structure in Zn1 − xMgxO films with an increase in Mg content. The presence of (002)-wurtzite reflection along with (200)-cubic reflection at $x \geq 0.7$ indicates the coexistence of two phases. The observed deviation from the wurtzite structure with increasing Mg content is attributed to the fact that when the Mg and Zn atoms bond to the O atom, the Mg atom loses electrons more easily than the Zn atom because of the difference in Pauling electronegativities, (1.31 for Mg is smaller than that of the 1.65 for Zn). Moreover, the large angle between the nearest-neighbor Zn–O bonds and the nearest neighbor Mg–O bonds, leads to the stronger interaction between the second nearest-neighbor Mg–O bonds due to the stronger polarity of the Mg–O bonds, and hence results in deviation of crystal structure from wurtzite as the quantity of the Mg–O bond is increased. The position of (002) and (200) peaks shifted to higher diffraction angles with the increase in Mg content, which manifests itself by the c-axis compression .This shows the onset of lattice strain in the films due to the difference in ionic radii of Mg2+ (0.57 Å) and Zn2+ (0.60 Å) ions. [27].

B)The crystallite size

The crystallite size of MgO measured by various preparation processes is shown in Table 1. observe different sizes have different properties owing to temperature rate in the thermal decomposition method; conditions of gel preparation such as the heating rate for gel formation, pH, gelling agents, and temperature of gel calcination in the sol-gel method.

Table I.2: The Preferred Orientation And Thickness Of MgO ,ZnO And MgO-ZnO Synthesized In Different Conditions.

S.N.	Condition	Preferred orientation	Cristallite size D (n.m)	Ref.
MgO by SILAR technique	C=0.1 M pH =11.5 T=400 °C	(200) (200) (200) (200) (200)	*24.74nm* 23.52 nm *23.18nm* *20.68 nm* *25.00nm*	[28]
MgO by by chemical spray pyrolysis technique	Precursor:$MgCl_2$ C=0.2 mol L^{-1} Precursor:$Mg(NO_3)_2$ C=0.2 mol L^{-1} Precursor:$Mg(CH_3COO)_2$ C=0.2 mol L^{-1}	(200) (200) (200)	*30.00 nm* *16.30 nm* *37.60 nm*	[29]
ZnO by by spray pyrolysis method	C=0.2 M $Zn(CH_3C00)_2 \cdot 2H_2O$ T=400°C	(0 0 2)	40 nm	[30]
ZnO by by Sol-Gel Method	$(Zn(CH_3COO)_2 \cdot 2H_2O)$ C=0.80M T= 400 ◦C	(0 0 2)	90 nm 180 nm 360 nm	[31]
$Zn_{1-x}Mg_xO$ by sol–gel method	pure ZnO, 2 wt-% MZO, 4 wt-% MZO, 6 wt-% MZO	(1 0 0)	*21n.m* *21n.m* *15n.m* *20n.m*	[32]
Mg-doped ZnO (MZO) by by spray pyrolysis method	Dopant Mg (wt %) $[MgCl_2. (H_2O)_6]$ C=0.05 M, T= 400 °C	(0 0 2) (0 0 2) (0 0 2) (0 0 2)	13.30 42.66 43.81 40.87	[33]

C) Lattic parameter

The lattice constant (see Table I.3), or lattice parameter, refers to the physical dimension of unit cells a crystal lattice. Lattices in three dimensions generally have three lattice constants, referred to as a, b, and c. However, in the special case of cubic crystal structures, all of the constants are equal and we only refer to a. Similarly, in hexagonal crystal structures, the a and b constants are equal, and we only refer to the a and c constants. A group of lattice constants could be referred to as lattice parameters. However, the full set of lattice parameters consist of the three lattice constants and the three angles between them.

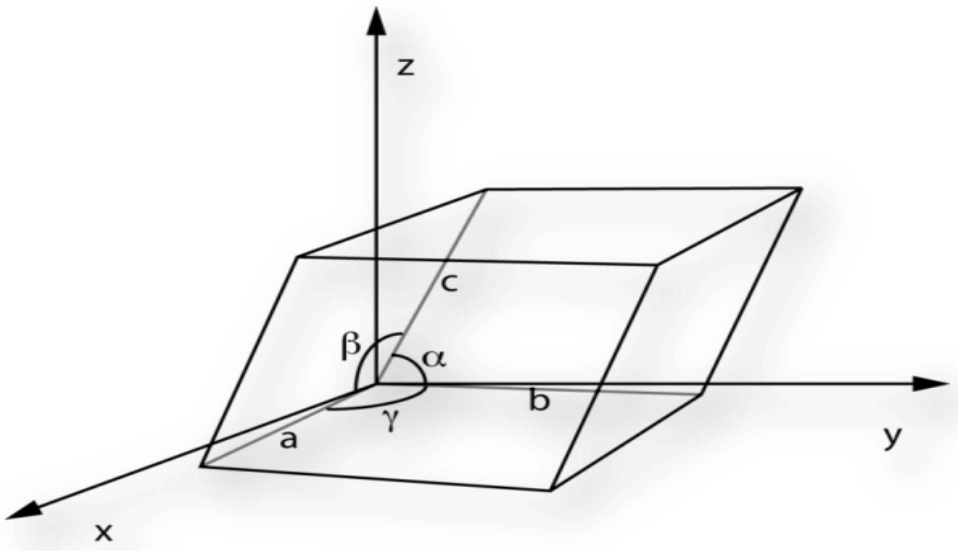

Figure I.3: Unit cell definition using parallelepiped with lengths a, b, c and angles between the sides given by α, β, γ (hk1) [34**].**

D) Strain

In general terms, the strain is a macroscopic measure of deformation. Truesdell and Toupin, in their famous Classical Field Theories review article in Handbuch der Physik, introduce the concept as "The change in length and relative direction occasioned by deformation are called, loosely strain (see Table I.3) [34].

Table I.3 Lattice Constants And Strain Of MgO, ZnO, And MgO-ZnO Synthesized In Different Conditions.

S.N.	Condition	Lattice constants (Å)		Strain ϵ ($L^{-2}m^{-4}$) (%)	Ref
MgO by by chemical spray pyrolysis technique	*T=500 °C* *T=600 °C*	*a=4.2198 A°* *a=4.2168 A°*		*1.16.10^{-3}* *0.75.10^{-3}*	[20]
ZnO Ultrasonic Spray Pyrolysis	0.1 M zinc acetate diluted in methanol and deionized T=365◦C	*a*= 3.246 *A*°	*c*=5.197*A*°	−0.171	[35]
		a= 3.240 *A*°	*c*=5.191*A*°	−0.289	
		a=3.2463*A*°	*c*=5.195*A*°	−0.204	
ZnOx%/MgO [x=30, 40 and 50 at%] Ultrasonic Spray Pyrolysis	($C_4H_6O_4Zn{\cdot}2H_2O$) Mg (CH_3COO) 5 ml of methanol 7.5 ml ethanol 12.5 ml of deionized water T=450C°	*a =b=3.246*	*a=5.186*	-3.87971X1 0–3	[36]
		a =b=3.255	*a=5.190*	−3.1691X 10–3	
		a =b=3.243	*a=5.175*	−6.0116X 10–3	

I.4.2. Optical Properties Of MgO, ZnO, And MgO-ZnO Synthesis In Different Conditions

Transparent and conductive oxide (TCO) thin films are used practically for various application fields such as transparent heaters, heat mirrors, smart windows, and optoelectronic devices; in particular, the market for transparent electrodes used in touch panels, flat panel displays, or lamps, and thin-film solar cells has been

expanding recently. Although many kinds of TCO thin-film materials have been developed. [37].

In **(2007) Moses Ezhil Raj et al [12]** investigated the dependence of the optical properties of MgO thin films deposited at different temperatures between 400 and 600°C. The MgO films deposited at 600^{o}C exhibited the highest optical transmission (>80%) , and the band gap energy was found to vary from (4.50 to 5.25 eV).

In **(2007) S.Valanarasu et** [38]. Observed the transmittance increases with the increase of annealing times, The increment of transmittance value can affect optical band gap values due to the increment of carrier concentration on the surface of the film value can affect optical band gap values due to the increment of carrier concentration on the surface of the film because in the part of optical properties, film thickness, and intercrystalline nature can contribute to the identical role.

In **(2006) C. GÜMÜ et al** [30] ZnO was prepared by the spray pyrolysis technique on a glass substrate at 400 °C; characterize thin films are Highly transparent. The film possesses high transmittance of over 90 % in the visible region and. The film has a direct band gap with an optical value of 3.27 eV .

We have managed to produce MgO and ZnO grains together inside the film matrix which, to our knowledge, is the first appearance of this kind of empirical process in the literature.

In **(2011) B .Anuradha et al** [39]. investigated the MgxZn1-xO has a band gap energy that can increase from 3.37 to 7.8 eV with the increase of the Mg concentration . Also, the experimental observations of MgZnO alloys fabricated under different techniques show that the formation of wurtzite structure for large ZnO concentrations and the formation of rock salt structure with high MgO concentrations and also phase separation may occur with an intermediate range of ZnO concentrations. It has been reported that the formation of rock salt structure by alloying ZnO as high as 50% while wurtzite for greater than 54% ZnO. [40].

In (2007) **BENHARRATS Farah et al**[41]. The crystal structure of MgxZn1-xO depend by the value of x. As a result, when x is less than 0.35, the crystal structure is hexagonal, and when x is greater than 0.8, the crystal structure is cubic and The gap is also affected by x composition. (Figure I.12).

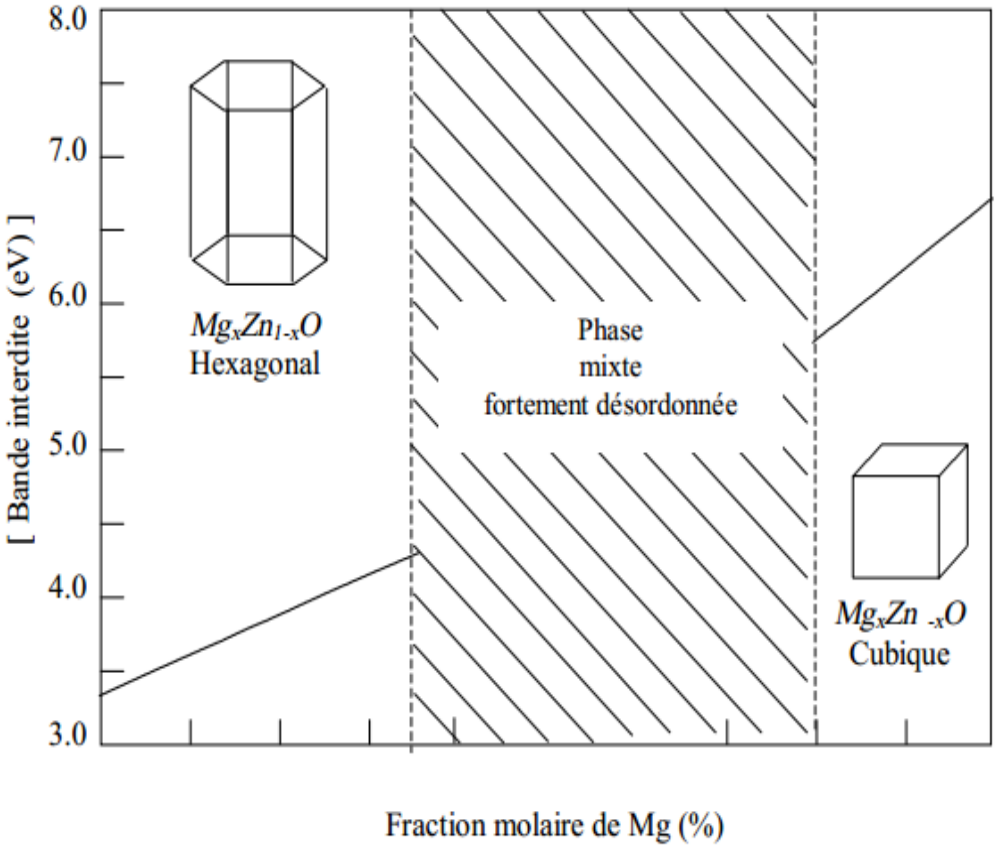

Figure I.4: variation of the gap according to the composition x (%)[41].

In **(2004) Yuantao Zhang et al** [42]. was prepared by metal-organic chemical vapor deposition (MOCVD) the $Mg_xZn_{1-x}O$ alloys ($0 \leq x \leq 0.39$) have optical band gaps that range from 3.3 to 3.95 eV. were measured between 200 and 800 nm. These films are highly transparent in the visible region from 400 to 800nm and have sharp absorption edges in the UV region. The transmittance is around 80% in the visible region for all $Mg_xZn_{1-x}O$ films. The absorption edge shifted to a short wavelength as the Mg content increased which indicates the bandgap energy of all $Mg_xZn_{1-x}O$ depends on the Mg content. Variation of the band gap of the all $Mg_xZn_{1-x}O$ function of Mg content was reported. The Eg increases almost linearly up to 3.95 eV with the increase of Mg content ($0 \leq x \leq 0.39$).

Table I.4.: Band gap energy and transmittance values Strain Of MgO, ZnO, And MgO-ZnO Synthesized In Different Conditions.

S.N.	Condition	Grain Crystallite size (nm)	Band gap energy (eV)	Transmitence (%)	Ref
MgO by Spray Pyrolysis Technique	T_S=643 K	119.5	3.57	80–90%	[43]
	T_S= 653 K	109.3	3.38		
	T_S= 663 K	109.7	3.69		
	T_S= 673 K	105.3	3.64		
	T_S= 683 K	97.6	3.68		
	T_S= 693 K	85.3	3.70		
MgO by Spray Pyrolysis Technique	Precursor of MgO			90%	[44]
	$MgCl_2$	30.00	4.10		
	$Mg(NO_3)_2$	16.30	4.09		
	$Mg(CH_3COO)_2$	37.60	4.05		
ZnO by Spray Pyrolysis Technique	Precursor of ZnO T=300°C				[45]
	Acetate	15	3.02	90%	
	Nitrate	200	3.17	80%	
	Chloride	245	3.35	30%	
ZnO by Spray Pyrolysis Technique	Zinc acetate C=0.1M Nozzle-substrate distance(cm) 15, 20, 25 and 3	29 and 31nm	3.21 and 3.26 eV	80 to 95%.	[46]

$Zn_{1-X}Mg_XO$ By Ultrasonic Spray Pyrolysis Technique	X=0.3 T=750 °C	30 nm	3.73	90%.	[47]
	X=0.9 T=750 °C	30 nm	6.06		

A)Refractive index

The optical reflectance spectra (R) have been used to determine the refractive index (n) (see table I.5) .

Table I.5.: Refractance index values Strain Of MgO, ZnO, And MgO-ZnO Synthesized In Different Conditions.

N.S	Condition	n	Ref
MgO by spray pyrolysis technique	425C 500C	1.6 1.77	[48]
MgO by electrodeposition technique	$MgSO_4.7H_2O$, Citric acid and NaOH	2.45 to 1.4	[49]
ZnO by Spray Pyrolysis Technique	0.1 M of zinc acetate dihydrate T=623 K	1.731 to 1.675	[50]
$Mg_xZn_{1-x}O$ by pulsed-laser deposition	X=0 X=0.24 X=0.36	2.60 2.37 2.27	[51]

I.4.3. Electrical Properties of MgO, ZnO, and MgO-ZnO Synthesized In Different Conditions.

As mentioned earlier, one of the promising materials belonging to the single metal oxide group is magnesium oxide. Magnesium oxide, also referred to as periclase, is an inorganic material with a molar mass of 40.31 g/mol and a density of 3.58 g/cm3 . Its empirical formula is MgO, and its lattice consists of Mg^{2+} ions and O^{2-} ions linked by an ionic bond in a $1s^2 2s^2 2p^6$ and $1s^2 2s^2 p^6$ configuration, which means that the d-orbitals are empty in this case. The magnesium oxide structure is of the rock-salt type (lattice parameter 4.21 Å)In general, it consists of two intersecting Mg and O lattices that are offset relative to each other by 0.5 of the body diagonal [52]. The electronic configuration and crystal structure are shown in **Figure I.5.**

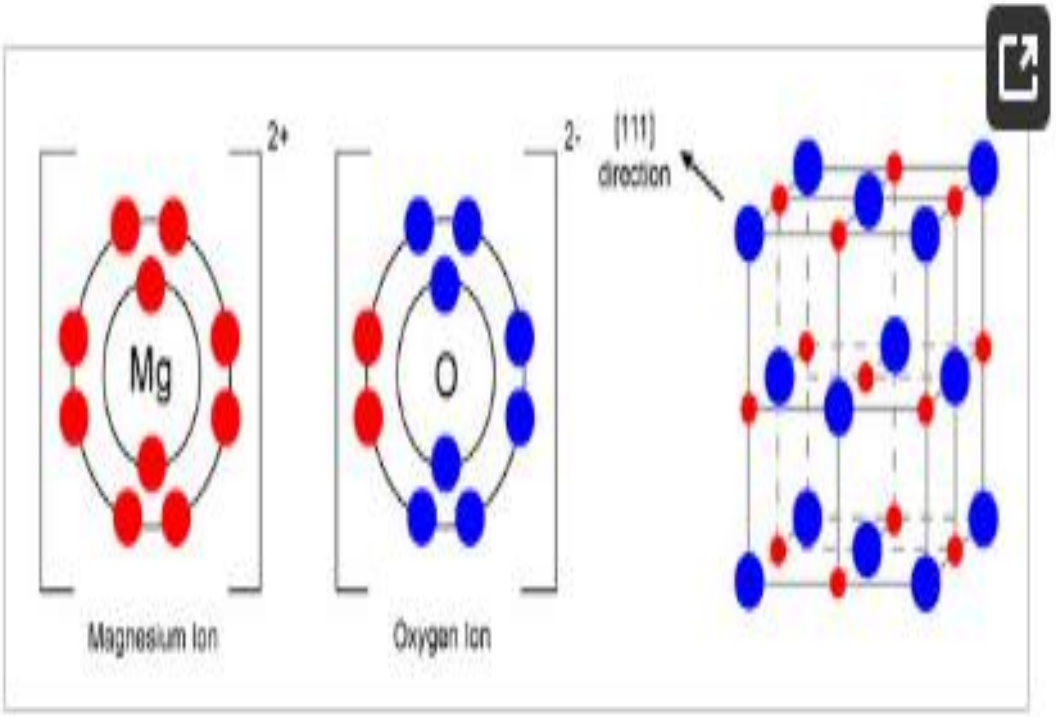

Figure I.5. Electronic configuration of Mg^{2+} and O^{2-} ions and crystal structure of MgO .

The halite structure ($Fm3^{-}m$) is assigned to MgO, which can be regarded as a cubic close packing of O ion and all the octahedral sites are filled with Mg+ ions (Fig. 1). Each O ion is surrounded by six Mg+ ions and each Mg+ ions is surrounded by six O ions to produce 1:1 co-ordination. The radius ratio falls within the range of 0.41–0.73 A˚, which is the radius ratio of stable octahedral coordination. Existing high bond strength in ionic crystals is due to the strong electrostatic forces between ions hence MgO is an ionic the crystal that exhibits hardness and high melting point, and low electrical conductivity[20].

The electronic band of the zinc oxygen are expressed as:

Zn: $1s^2\ 2s^2\ 2p^6\ 3s^2\ 3p^6\ 3d^{10}4s^2$

O : $1s^2 2s^2 2p^4$

The 2p states of oxygen form the valence band, the 4s states of zinc constitute the semi-conduction zone, so to form an ionic bond the zinc atom must yield these two electrons from the 4s orbital to an oxygen atom which will subsequently have a 2p orbital full with 6 electrons. The ZnO formation reaction is as follows: The electronic band structure shows that ZnO is a gap semiconductor direct, the minimum of the conduction band and the maximum of the valence band are.The width of the forbidden band is of the order of 3.2 eV indicates that it is a direct gap semiconductor. The high conductivity of pure ZnO oxides is due to the high concentration of carriers (electrons), since the mobility in these films is considerably lower than that in volume of the corresponding material. The strong electron concentration is attributed to deviation from stoichiometry (or flaws in the structure). [53].

MgO has a band gap of about 6.7 eV. For the purpose of changing the electrical and optical properties of ZnO, MgO was often doped into or combined with ZnO in various ways .A number of research efforts have been focused on artificial engineering of oxides and semiconductors for functional device applications [54] .

Table I.6: Electrical conductivity values of MgO, ZnO, and MgO-ZnO Synthesized In Different Conditions

N.S	Condition	Electrical Resistivity ρ ($(\Omega.cm)^{-1}$	Ref
MgO by Spray Pyrolysis	400 C° 425 C° 450 C° 475 C° 500 C°	$2.12X10^6$ Ωcm $2.08X10^6$ Ωcm $1.19X10^6$ Ωcm $9.14X\ 10^5$ Ωcm $7.56X\ 10^5$ Ωcm	[55]
ZnO by spray pyrolysis	C= 0.1 M nozzle fixed = 15cm thickness :425 nm and 650 nm	6.03×10^1 Ωcm	[50]
$Zn_{1-x}Mg_xO$ by ultrasonic spray pyrolysis technique	Wurtzite X= 0.3 Cubic X=0.9	10^3 Ωcm 10^5 Ωcm	[27]

I.5. Application of MgO And ZnO

Nanostructures of MgO are not only known for the observation of numerous phenomena as elaborated in section 1.2 but also because of significant enhancement of their applications in a variety of fields [56].

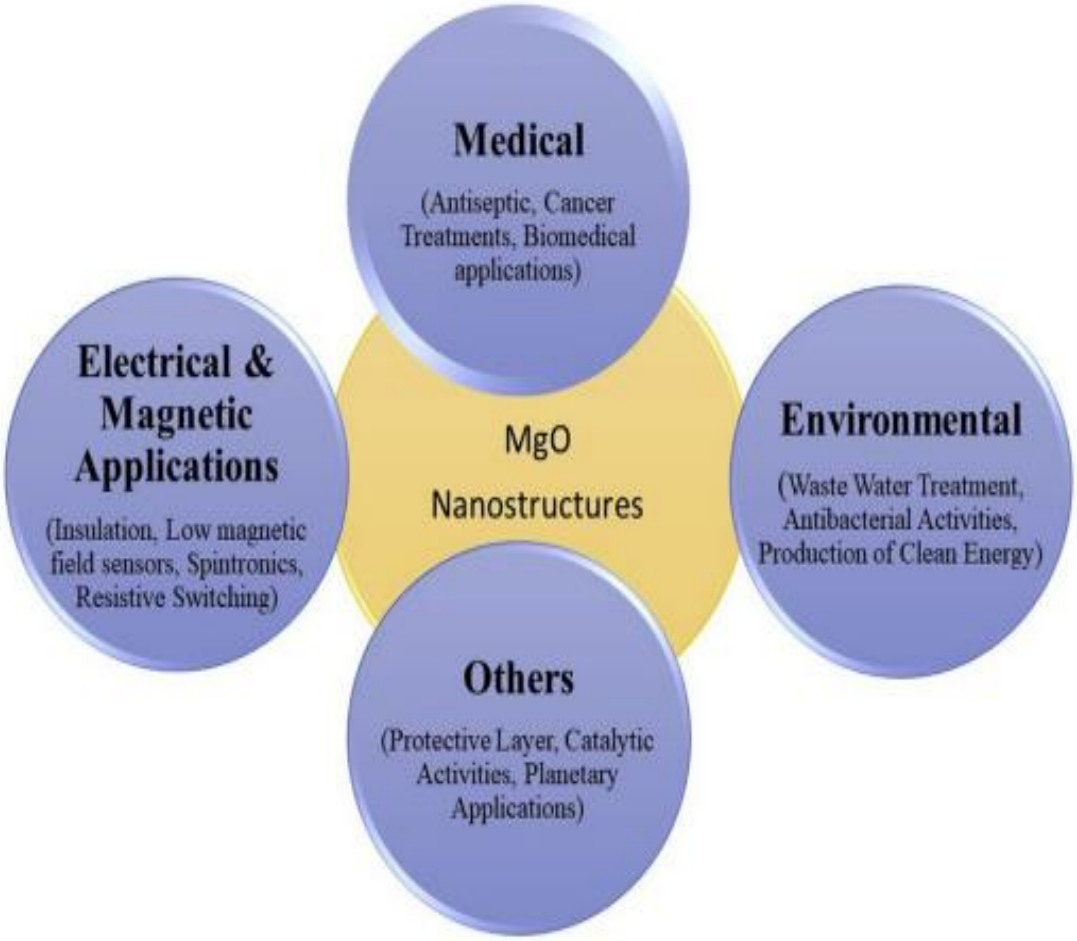

Figure I.6: The schematic is depicting the importance of MgO nanostructures in numerous field.

Because of its diverse properties, both chemical and physical, zinc oxide is widely used in many areas. It plays an important role in a very wide range of applications, ranging from tyres to ceramics, from pharmaceuticals to agriculture, and from paints to chemicals. [57].

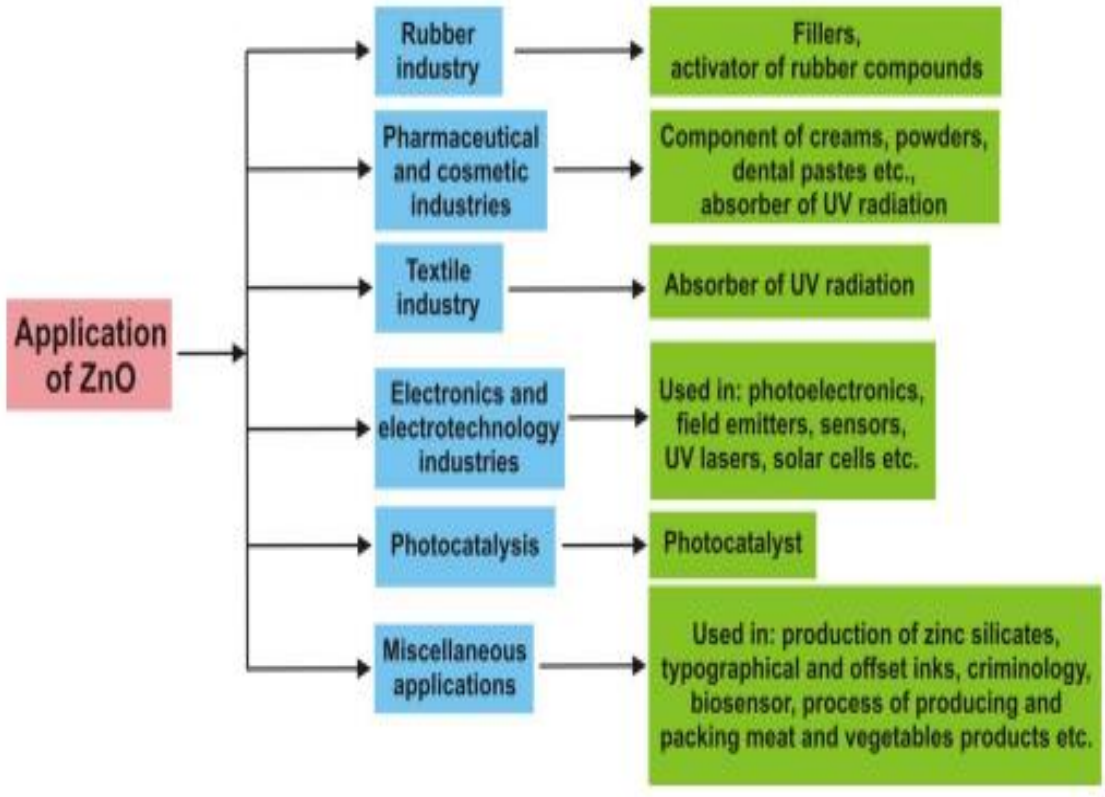

FigureI.7: The schematic is depicting the importance of ZnO nanostructures in numerous field.

In recent years, researchers have focused more on the synthesis of ZnO and MgO in composite or alloy forms of both nanoparticles due to their application in advanced technologies, such as in electronics, catalysis, ceramics, petrochemical products, coatings, and many other fields.

I.6. Conclusion

To sum up, magnesium oxide thin films, zinc oxide thin films, and doped thin films attract great interest in material science. can be used in various potential applications such as solar cells due to the n-type and p-type semiconducting, transparent diodes, transparent transistors, displays, and defrosting windows because their transparency can be used for the UV photodetectors and touch screens due to the good responsively. these oxides can be produced by several techniques such as reactive

evaporation, molecular beam epitaxy (MBE), magnetron sputtering technique, pulsed laser deposition (PLD), spray pyrolysis, sol-gel process, chemical vapor deposition, and electrochemical deposition.

References

[1] Sreekanth K Mahadeva, Magnetism in Band Gap Engineered Sputtered $Mg_xZn_{(1-x)}O$ Thin Films Effect of stabilizer on optical and structural properties of MgO thin films. Doctoral Dissertation in Material Physics 2013.

[2] B. Borca and C. Bartha, "Advances of Nanoparticles and Thin Films," *Coatings*, vol. 12, no. 8, pp. 12–14, 2022,.

[3] F. Sayılkana, M. Asilturka, N. Kirazb, E. Burunkayab, E. Arpac, Hikmet Sayılkan, Photocatalytic antibacterial performance of Sn4þ doped TiO2 thin films on glass substrate, J. Hazard. Mater. 162 (2009)1309–1316.

[4] J. Aanchal, B. Richa, P. Pankaj, Probing interaction of gram-positive andgram-negative bacterial cells with ZnO nanorods, Mater. Sci. Eng. C. 33(2013) 1247–1253.

[5] O. Akhavan, E. Ghaderi, Cu and CuO nanoparticles immobilized by silicathin films as antibacterial materials and photocatalysts, Surf. Coat.Technol. 205 (2010) 219–223.

[6] X. Bingshe, N. Meia, W. Liqiao, H. Wensheng, L. Xuguang, The structural analysis of biomacromolecule woolfiber with Ag-loading SiO2nano antibacterial agent by UV radiation, J. Photochem. Photobiol. A.Chem. 188 (2007) 98–105.

[7] C. Karunakarann, R.S. Sakthi, P. Gomathisankar, Photocatalytic and bactericidal activities of hydrothermally and sonochemically prepared Fe2O3–SnO2 nanoparticles, Mater. Sci. Semicond. Process. 16 (2013) 818–824.

[8] J. Sawai, T. Yoshikawa, Quantitative evaluation of antifungal activity of metallic oxide powders (MgO, CaO and ZnO) by an indirect conductimetric assay, J. Appl. Microbiol. 96 (2004) 803–809.

[9] D.A.L. Tellez, Y.P. Yadava, J.M. Ferreira, Supercond. Sci. Technol.12, 18 (1999).https://doi.org/10.108
8/0953-2048/12/1/005.

[10] L. Cai, J. Chen, Z. Liu, Front. Microbiol.9, 790 (2018)..

[11] O.V. Diachenko, A.S. Opanasuyk, in2016 IEEE 7th International Conference on Advanced Optoelectronics and Lasers (CAOL), pp. 31–33 (2016).

[12] A. Moses Ezhil RaA. Moses Ezhil Raj, L. C. Nehru, M. Jayachandran, and C. Sanjeeviraja, Spray pyrolysis deposition and characterization of highly (100)

oriented magnesium oxide thin films. Cryst. Res. Technol. 42, No. 9, 867 – 875 (2007).

[13] G. H. P. Casey, E. O'Connor, R. D. Long, P. K. Hurley, "Growth and characterization of thin MgO layers on Si (100) surfaces," Journal of Applied Physics: Conference Series, 2008.

[14] R. Kara, L. Mentar, A. Azizi . Synthesis and characterization of Mg-doped ZnO thin-films electrochemically grown on FTO substrates for optoelectronic applications. RSC Adv., 2020, 10, 40467.

[15] Cheyma Abed, Susana Fernández, Habib Elhouichet. Studies of optical properties of ZnO:MgO thinfilms fabricated by sputtering from home-made stable oversize targets. Optik - International Journal for Light and Electron Optics 216(2020) 164934.

[16] M. Caglar, Y. Caglar, S. Ilican, Investigation of the effect of Mg doping for improvements of optical and electrical properties, Physica B 485 (2016) .

[17] M. Rouchdi, E. Salmani, A.El Hat, N. Hassanain, A. Mzerd, Synthesis and magnetic properties of Ni-doped ZnO thinfilms: experimental and theoretical study, Surf. Rev. Lett. 24 (2017) 1750085.

[18] V. Devi, M. Kumar, R. Kumar, B.C. Joshi, Effect of substrate temperature and oxygen partial pressure on structural and optical properties of Mg doped ZnO thin films, Ceram. Int. 41 (2015) 6269.

[19] B. Khalfallah, F. Chaabouni, G. Schmerber, A. Dinia, M. Abaab, Investigation of physico-chemical properties of conductive Ga-doped ZnO thinfilms deposited on glass and silicon wafers by RF magnetron sputtering, J. Mater. Sci 28 (2016) 75.

[20] A. Moses Ezhil Raj, M. Jayachandran, C. Sanjeeviraj, Fabrication techniques and material properties of dielectric MgO thin films—A status review. CIRP Journal of Manufacturing Science and Technology 2 (2010) 92–113.

[21] Thonglem, S., Sirisoonthorn, S., & Pengpat, K. (2014). *Integrated Ferroelectrics : An Effect of Mg Doping on Optical Properties of ZnO Films by Ultrasonic Spray Pyrolysis*. *September*, 37–41.

[22] T. Royal, *Magnetism in Band Gap Engineered Sputtered Mg*. 2013.

[23] S. Nisatharaju, R. Ayyappa, D. Balamurugan. Structural, Morphological and Optical Characterization of Spray Deposited MgO Thin Film. August 2014 Asian Journal of Applied Sciences 7(8):780-785.

[24] Abdelkader Hafdallah, Abderrahman Azzedine, Hanane Belhani, Mohamed Salah Aida, Effect of the Nozzle-Substrate Distance on the Structural and Optical Properties of ZnO Thin Films Deposited by Spray Pyrolysis Technique. American Journal of Nano Research and Applications 2017; 5(6): 87-90.

[25] . Q. Shi, J. Zhang, D. Zhang, C. Wang, B. Yang, B. Zhang, and W. Wang, Red luminescent and
structural properties of Mg-doped ZnO phosphors prepared by sol–gel method.Mat Sci Eng B.177, 689–693 (2012).

[26] K. Yoshino. S. Oyama. M. Yoneta, Structural, optical and electrical characterization of undoped
ZnMgO film grown by spray pyrolysis method . J Mater Sci: Mater Electron (2008) 19:203–209.

[27] Ajay Kaushal , Dinesh Pathak , R.K. Bedi , Davinder Kaur, Structural, electrical and optical properties of transparent Zn1 − xMgxO nanocomposite thin films. Thin Solid Films 518 (2009) 1394–1398

[28] Harun Güney, Demet İskenderoğlu, Synthesis of MgO thin films grown by SILAR technique. Ceramics International (2018).

[29] Maher Tlili1,a, Neila Jebbari, Wafa Naffouti, Najoua Turki Kamoun, Effect of precursor nature on physical properties of chemically sprayed MgO thin films for optoelectronic application .Eur. Phys. J. Plus (2020) 135:68S.

[30] C. GÜMÜ , O. M. OZKENDIR, H. KAVAK, Y. UFUKTEPE, Structural and optical properties of zinc oxide thin films prepared by spray pyrolysis method. JOURNAL OF OPTOELECTRONICS AND ADVANCED MATERIALS Vol. 8, No. 1, February 2006, p. 299 .

[31] Ziaul Raza Khan , Mohd Shoeb Khan , Mohammad Zulfequar , Mohd Shahid Khan, Optical and Structural Properties of ZnO Thin Films Fabricated by Sol-Gel Method. Materials Sciences and Applications, 2011, 2, 340-345.

[32] Muhammad R. Islam & Muhammad G. Azam, Enhanced photocatalytic activity of Mgdoped ZnO thin films prepared by sol–gel method. Surface Engineering(2020) 1-9

[33] Krithika Upadhya , U.G. Deekshitha , Albin Antony , Aninamol Ani , I.V. Kityk , J. Jedryka , A. Wojciechowski , K. Ozga , P. Poornesh , Suresh . Kulkarni , N. Andrushchak ,Second and third harmonic nonlinear optical process in spray pyrolysed Mg:ZnO thin films.

[34] Chouaieb ZAOUCHE, "THE ROLE OF Ni AND Zn ON DILUTED MAGNETIC SEMICONDUCTOR Ni 1-x Zn x O THIN FILMS," 2020.

[35] E. Gungor and T. Gungor, "Effect of the Substrate Movement on the Optical Properties of ZnO Thin Films Deposited by Ultrasonic Spray Pyrolysis," vol. 2012, 2012,

[36] S. Roguai and A. Djelloul, "Photocatalytic degradation of methylene blue using sprayed Mg diluted ZnO heterostructure thin films photocatalysts," *React. Kinet. Mech. Catal.*, vol. 132, no. 2, pp. 1225–1244, 2021.

[37] T. Minami**,** Transparent Conductive Oxides for Transparent Electrode *Applications*, 1st ed., vol. 88. Elsevier Inc., 2013.

[38] S. Valanarasu, V. Dhanasekaran, M. Karunakaran, T. A. Vijayan, R. Chandramohan, and T. Mahalingam, "Microstructural, optical and electrical properties of various time annealed spin coated MgO thin films,".

[39] B. Anuradha and C. Sanjeeviraja, "Review on magnesium indium oxide thin films: Material properties and preparation techniques," *Mater. Sci. Forum*, vol. 699, pp. 39–66, 2011, doi: 10.4028/www.scientific.net/MSF.699.39.

[40] F. González et al., ``No Covariance Structure Analysis of Health-Related Indicators in the Elderly at Home Focusing on Subjective Feelings of Health," Qual. Res. Psychol., vol. 0, no. 2, pp. 47 –54, 2006.

[41] BENHARRATS Farah, ETUDE DES NANOSTRUCTURES LASER A BASE DE ZnO/MgZnO LE DIPLOME DEMAGISTER(2007).

[42] Y. Zhang *et al.*, "Structural and optical properties of MgxZn1-xO thin films grown by metal-organic chemical vapor deposition," *J. Cryst. Growth*, vol. 268, no. 1–2, pp. 140–143, 2004.

[43] O. V Diachenko, A. S. Opanasuyk, D. I. Kurbatov, and N. M. Opanasuyk, "Surface Morphology , Structural and Optical Properties of MgO Films Obtained by Spray Pyrolysis Technique," vol. 130, no. 3, 2016.

[44] M. Tlili, N. Jebbari, W. Naffouti, and N. T. Kamoun, "Effect of precursor nature on physical properties of chemically sprayed MgO thin films for optoelectronic," *Eur. Phys. J. Plus*, vol. 123, pp. 1–12, 2020.

[45] N. Lehraki, M. S. Aida, S. Abed, N. Attaf, A. Attaf, and M. Poulain, "ZnO thin fi lms deposition by spray pyrolysis : In fl uence of precursor solution properties," *Curr. Appl. Phys.*, vol. 12, no. 5, pp. 1283–1287, 2012.

[46] A. Hafdallah, "Effect of the Nozzle-Substrate Distance on the Structural and

Optical Properties of ZnO Thin Films Deposited by Spray Pyrolysis Technique," *Am. J. Nano Res. Appl.*, vol. 5, no. 6, p. 87, 2017.

[47] A. Kaushal and D. Kaur, "Effect of Substrate Temperature on Structural , Electrical and Optical Properties of Wurtzite and Cubic Zn 1-X Mg X O Thin Films Grown by Ultrasonic Spray Pyrolysis," vol. 339, 2009.

[48] R. Mahani, "INVESTIGATION OF DIELECTRIC AND OPTICAL PROPERTIES OF MGO THIN INVESTIGATION OF DIELECTRIC AND OPTICAL PROPERTIES OF MGO THIN FILMS," no. January 2014, 2016.

[49] D. State and A. State, "Optical Properties of Electrodeposited Magnesium," vol. 1, no. 2, pp. 11–18, 2019.

[50] E. Muchuweni, T. S. Sathiaraj, and H. Nyakotyo, "Synthesis and characterization of zinc oxide thin films for optoelectronic applications," *Heliyon*, vol. 3, no. 4, p. e00285, 2017.

[51] J. Muth, H. O. Everitt, and J. Narayan, "indices and absorption coefficients Refractiveof MgxZn1-xO alloys Refractive indices and absorption coefficients of Mg x Zn 1 À x O alloys," no. June 2014, 2000.

[52] J. Hornak, "Synthesis, properties and selected technical applications of magnesium oxide nanoparticles: A review," Int. J. Mol. Sci., vol. 22, no. 23, 2021.

[53] N. BENCHERIF,SYNTHESE ET CARACTERISATION DES FILMS DE ZnO PUR ET DOPE A L'INDIUM PAR LA TECHNIQUE DE SPRAY PYROLYSESULTRASONIQUE (. 2014).

[54] S. Phanichphant, "Characterization of ZnO / MgO Nanocomposites Synthesized by Flame Spray Pyrolysis," no. July 2009, 2015.

[55] Z. Habibah, L. N. Ismail, R. A. Bakar, and M. Rusop, "Influence of Heat Treatment on the Properties of MgO Thin Films as Dielectric Layer," pp. 16–19, 2011.

[56] J. Pal, V. Singh, A. Sharma, G. Pandey, and K. Hwa, "Heliyon Approaches to synthesize MgO nanostructures for diverse applications," *Heliyon*, vol. 6, no. September, p. e04882, 2020.

[57] A. Kolodziejczak-Radzimska and T. Jesionowski, "Zinc oxide-from synthesis to application: A review," Materials (Basel)., vol. 7, no. 4, pp. 2833–2881, 2014.

Chaptre II

Elaboration and Characterization Techniques

This chapter explains the spray pyrolysis techniques and describes the elaboration of thin films, The different characterization techniques used such as X-ray diffraction, UV-Vis spectroscopy, energy dispersive spectroscopy (EDS), and four points probe measurements.

II.1. Introduction

The growth of MgO and ZnO thin films have prepared by using several methods such as reported in the previous chapter. Many scientists use Spray pyrolysis to improve the properties of Magnesium oxide thin film because they can be used for a variety of things, including transparent electrodes, photovoltaic devices, solar front panel displays, surface acoustic wave devices, low emissivity layers for structural glass, various gas sensors, and heat reflectors for high-tech solar cells. The properties of thin films differ significantly from those of bulk due to surface and interface effects, and this dominates the overall behavior of the thin films. In the advancement of nanotechnology and nanoscience[1].

II.2. Thin Film Deposition Methods

Thin Film Deposition is the technology of applying a very thin film of material – between a few nanometers to about 100 micrometers, or the thickness of a few atoms – onto a "substrate" surface to be coated, or onto a previously deposited coating to form layers. Thin Film Deposition manufacturing processes are at the heart of today's semiconductor industry, solar panels, CDs, disk drives, and optical devices industries.[2]

The application of thin films in modern technology is widespread. The methods employed for thin-film deposition can be divided into two two broad categories – Chemical Deposition and Physical Vapor Deposition Coating Systems[3]. The wide classification of thin film deposition techniques is shown in **Figure II.1**. Among all these thin film deposition techniques, Spray pyrolysis deposition offers a wide range of advantages over more expensive and vacuum-based other methods of thin film deposition. Along with being a simple, inexpensive, and economic method, it has its own advantage of no wastage of material, no production of gases, it does not require very pure starting material, etc. The art and science of electrodepositing metal and metallic alloys and anodization have been developed for more than a century.

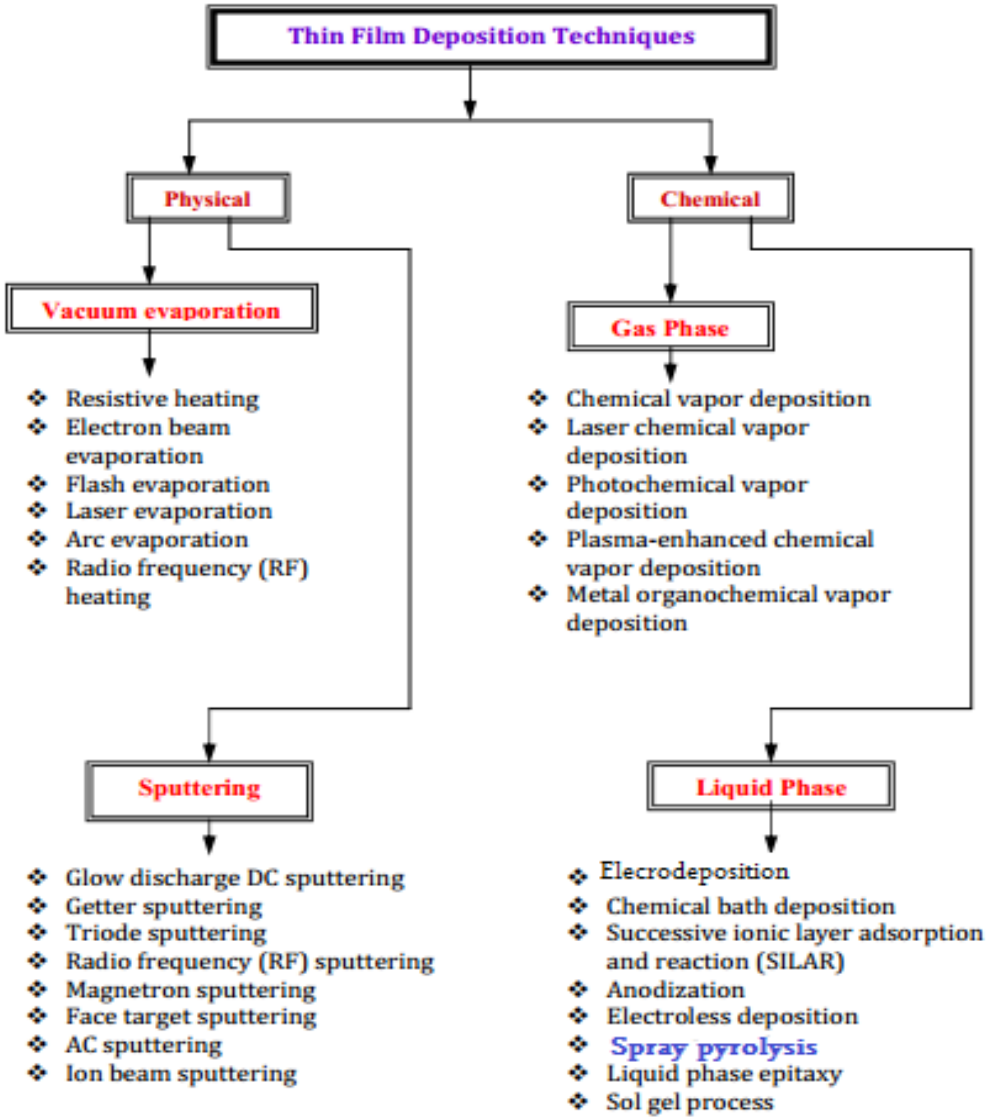

Figure II.1: Classification of thin film deposition techniques[4].

II.3. Spray Pyrolysis Technique (PS)

Spray Pyrolysis is a processing technique for preparing thin and thin films, ceramic coating, and powder The basic principle involved in the spray pyrolysis technique (SPT) is shown in **Figure II.2**. Unlike many other film depositions, this technique represents a process of simple and cost-effective processing, typical spray pyrolysis equipment where a solution is sprayed onto a heated surface, where the constituents react to generate a chemical product, leaving behind a thin film. The chemical reactants are chosen so that, at the deposition temperature, the products other than the intended molecule are volatile. The process has long been used to create a clear

electrical conductor of SnOx for glass, and it is very helpful for the deposition of oxides. Since the ground breaking paper by Chamberlin & Skarman on CdS films for solar cells in 1966, there have been various studies in this field, including a review of transparent conductors and a bibliography by Pamplin given at a conference on spray pyrolysis[5].

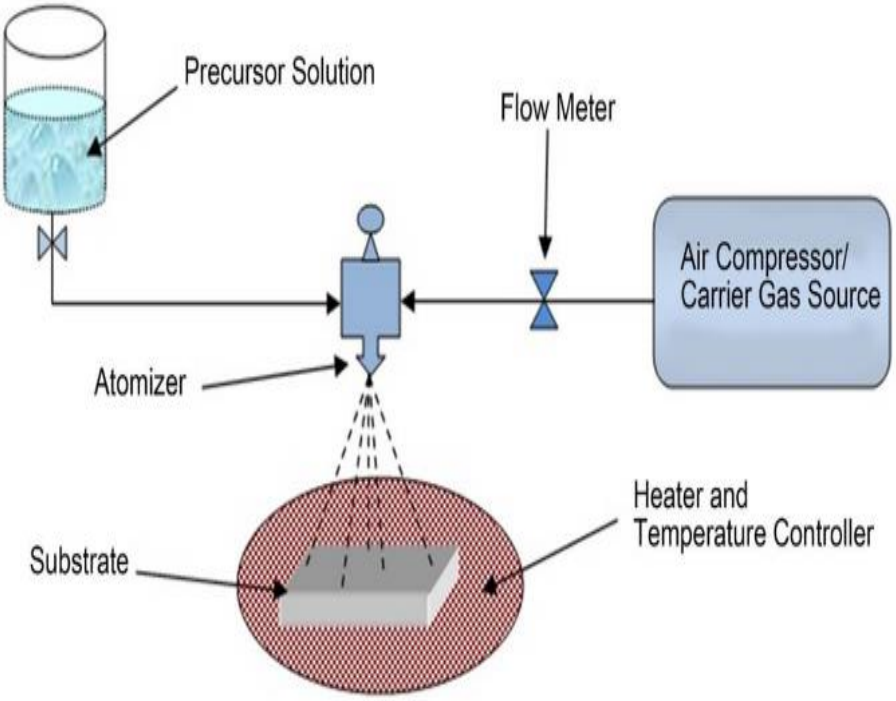

Figure II.2: General schematic of a spray pyrolysis deposition process[6].

Thin film deposition using spray pyrolysis can be divided into three main steps: atomization of the precursor solution, transportation of the resultant aerosol and decomposition of the precursor on the substrate.

- **Atomization of the precursor solution**

  The film quality and the droplet size of the aerosol are typically set by the atomization technique. The most commonly used techniques for generating droplets are:

  1) The pneumatic method (PS): a relatively pressurized air flow carry the solution that contains precursors, the atomization into droplets is composed at the nozzle orifice.

2) Ultrasonic spray method (USP): an ultrasonic wave generator atomizes the solution. The droplet size is more regular and thinner in ultrasonic spray nozzle than in pneumatic spray. In addition, comparing with the droplet speed in PS, it is low in USP; hence, this may affect the films growth in both methods.[7].

- **Transportation of the resultant aerosol**

This process occurs at the lower end of the nozzle when the solution flow comes into contact with air pressure. The type of nozzle is an important parameter of the properties of the aerosol droplets and particularly their sizes.During the transport of the aerosol, the droplets of the solution containing the precursors move towards the heated substrate. Droplets remain in the air and others evaporate turning into powder forming a thin layer deposited on the substrate.[8].

- **Decomposition of the precursor**

Depending on the substrate temperature, four different processes can occur:

1. In the low temperature regime (process A), the aerosol droplets are projected directly onto the surface of the substrate and decompose.
2. At higher temperatures (process B) the solvent evaporates completely before reaching the hot surface of the substrate. The precursor rushes and reacts on the surface. It decomposes and undergoes chemical reactions to form the layer of the desired material.
3. At even higher temperatures (process C), the solvent also evaporates before the droplet reaches the substrate. The precursor precipitates and passes into the gaseous phase in the vicinity of the hot surface. The vapor of the precursor is adsorbed on the surface, diffuses and then reacts to form the layer.
4. At high temperatures (process D) the precursor vaporizes before reaching the substrate, and therefore solid particles are formed after the chemical transformation in the vapor phase**.(see Figure II.3)**

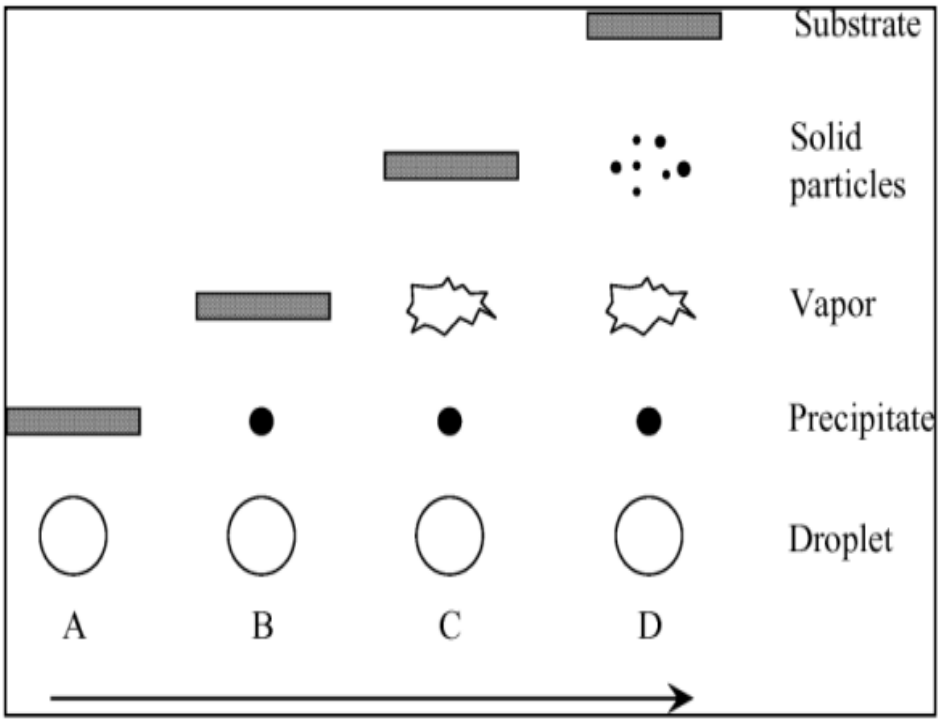

Figure II.3: Description of the deposition processes[9].

II.4.Advantages of The spray pyrolysis technique

The spray pyrolysis technique is a new emerging wonderful method in material science. It possesses many advantages, in the fabrication of thin film materials for progress numerous industrial applications[10].

- Economical technology; the fact that the used devices do not need to complex and expensive systems.
- Membranes can be deposited on a wide area, with thin films prepared with good adhesion and high stability in their physical properties over time.
- Transient sedimentation is easy to obtain for selected materials in terms of compositional, optical and electrical properties by mixing two or more substances or changing the concentrations of the elements involved in membrane composition or changing the temperature of the base.
- The preparation of membranes for a wide range of materials with high melting grades is difficult to prepare in other ways.

II.5.Disadvantage of The Spray pyrolysis technique

- It requires a lot of efforts and time to get homogeneous membranes.
- Only chemical solutions are used and the powder cannot be deposited directly.

II.6. Experimental details

The MgO and Zn-doped MgO solutions with different pH were sprayed on the heated glass substrates by spraying the pneumatic method which transforms the liquid to a formed stream with uniform and fine droplets of 25µm average diameter. The deposition was performed at a substrate temperature of 450°C with a deposition rate was 5.7 mL /min. The structural properties of MgO and Zn-doped MgO) studied by means of X-ray diffraction (XRD Bruker AXS-8D) with CuKα radiation (λ=0.15406 nm) in the scanning range of (2θ) was between 20° and 80°. The optical transmission of the deposited films was measured in the range of (200 – 1000 nm) by using an ultraviolet-visible spectrophotometer (LAMBDA 25) while Scanning electron microscopy (SEM) is applied to find surface morphology and energy dispersive X-ray (EDX) to study film elemental composition. Then the electrical resistance R was measured by four-point methods.

II.7.Study of Various Concentrations on MgO thin film

To prepare the magnesium oxide, we follow these steps.

II.7. 1.Preparation of the solution

MgO solution were prepared by dissolving 0.05, 0.1, 0.15, and 0.2 mol L^{-1} of Magnesium nitrate hexahydrate ($Mg(NO_3)_2.6H_2O$) in the solvent containing equal volumes of absolute H_2O adding drops of HCl to stabilize the solution. The mixture solution was stirred for 3 h at 40°C to get a clear and transparent solution. (**see Table II.1)**

Table II .1: The parameters of chemical products.

Chemical name	Magnesium nitrate hexahydrate	deionized water	Hydrogen chloride
Molecular formula	($Mg(NO_3)2.6H_2O$)	H2O	HCl
Volume	/	50 ml	1 ml

II.7. 2.Preparation of the films

To get good results in their properties, we deposited the films during their development on glass substrates. Slides made of soda lime glass (SLM) with

dimensions of (2.5 cm × 2.5 cm × 0.15 cm) were utilized as substrates. The glass substrate was cleaned and rinsed in preparation for deposition.The glass substrate was utilized, as shown in figure 2.3, and it was cleaned using methanol and acetone for 10 minutes, then deionized water for 5 minutes, before being dried in the air. **(** see **Figure II.4.)**

Figure II.4: Cut glass substrates using a sharp pen.

MgO samples were fabricated by dropping MgO solution in the glass substrates at 450°C by a pneumatic spray technique, which is based on the transfer of MgO solution to the heated glass substrate in air, and we fixed the distance between the heated glass substrate and the spray solution in the gun nozzle at 15 cm, and the sample size is 0.1 × 2.5 × 7.5 cm^3. The experimental conditions such as the concentration of the MgO solution, deposition rate, deposition time, substrate temperature, and final measured film thickness of MgO thin films used in this work are presented in Table I.. MgO thin films were obtained at several MgO precursor molarities in the range of .05–.2 mol L^{-1}. A pneumatic spray technique was used for technological applications because it is one of the most important techniques used for deposition and large-scale production and because of low cost**. (see Figure II.5)**

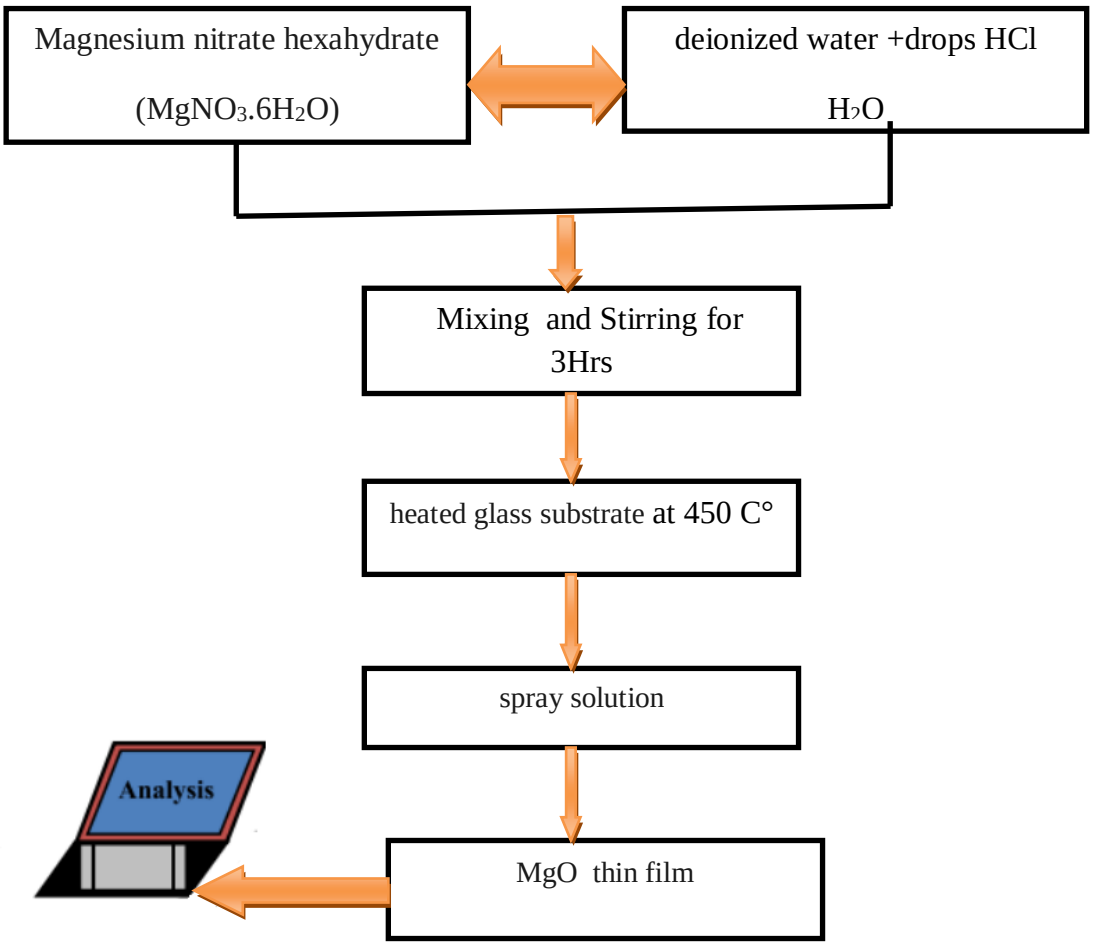

Figure II.5: Flow chart showing the schematic diagram for MgO thin films preparation.

II.7:Effect of pH solution on MgO thin film

II.7.1:Preparation of solution

Magnesium oxide MgO thin films have been synthesized by the chemical spray pyrolysis technique on glass substrates. The glass substrates were initially clean with soap solution, double distilled water, ethanol, acetone. The spraying solution used in this work was prepared by dissolving Magnesium acetate powder Mg $(CH_3COO)_2.4H_2O$ diluted in a volume distilled water see **Table II .2**. To investigate the role of the pH on the growth of the MgO, the solution was. To different pH ranging from MgO thin films deposited at different pH (2.5, 5, 6.8, 8.30, to 10). The pH values were varied by adding precise amounts of hydrochloric acid (HCl) or of

Sodium hydroxide (NaOH) to the aqueous solutions as pH controlling agents, where the sprayed precursor concentration was fixed to 0.15 M. The Mg^{2+} ions in the solution react with oxygen atoms of compressed air. The deposited films were at the temperature of 450°C and, All the pH measurements were carried out with a pH meter. as shown in **Figure II.6**.

Table II .2: The parameters of chemical products.

Chemical name	Magnesium Acetate Tetrahydrate	Deionized Water	Hydrochloric Acid	Sodium Hydroxide
Molecular formula	$Mg(CH_3COO)_2.4H_2O$	H2O	HCl	NaOH
Volume	/	20 ml	drops	drops
Concentration	0.15 M	/	1M	2M
Molecular weight	214.455 g/mol	/	/	40g/mol

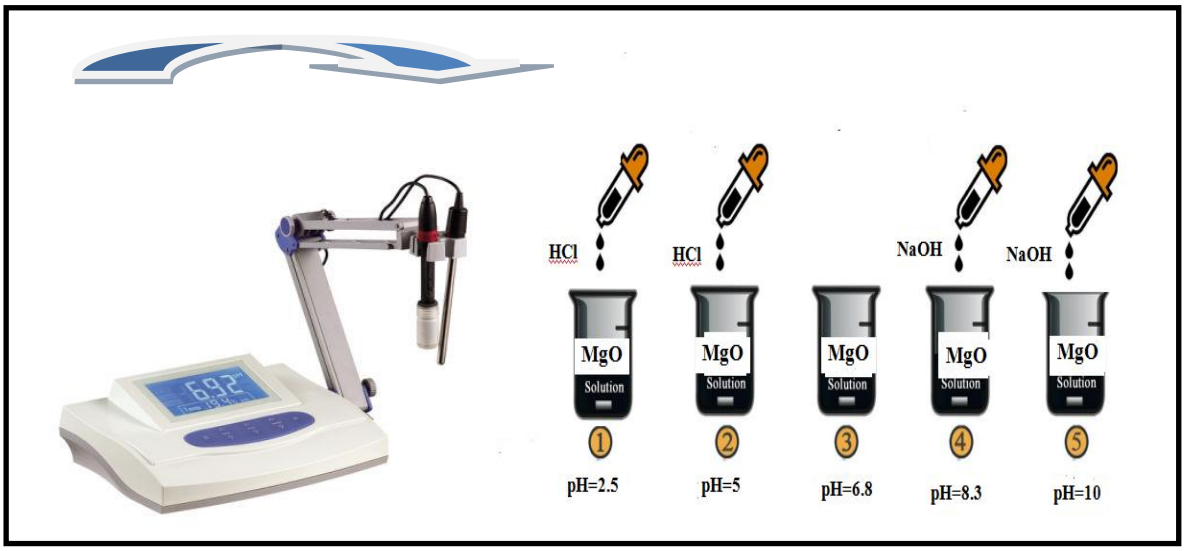

Figure II.6: Experimental procedure for the pH adjustment in the MgO solution.

II.7.2.Preparation of the films

Magnesium oxide MgO thin films have been synthesized by the chemical spray pyrolysis technique on glass substrates as shown in **Figure II.7**. The glass substrates were initially clean with soap solution, double distilled water, ethanol, acetone.

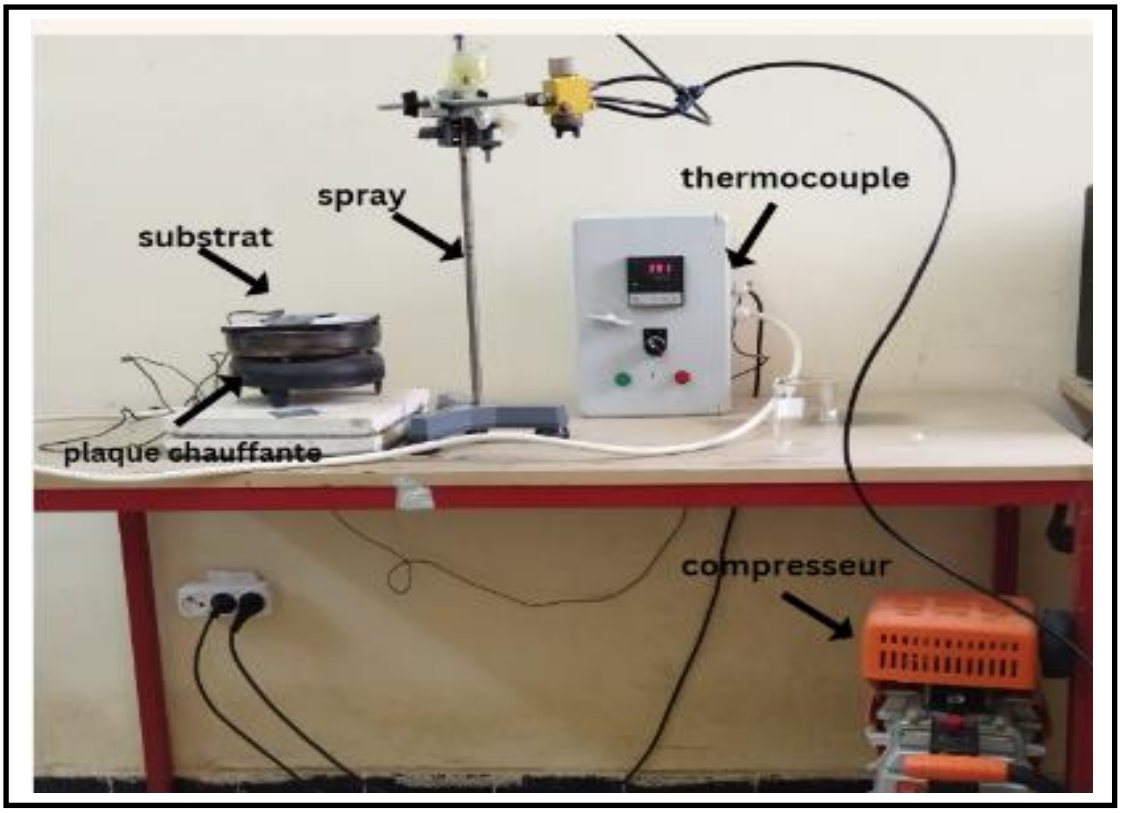

Figure II.7: the preparation of MgO thin films by spray pyrolysis.

II.8.Influence of pH solution on $Zn_{0.5}Mg_{0.5}O$ thin film

II.8.1.Preparation of solution:

The $Zn_{0.5}Mg_{0.5}O$ nanofilms were prepared by mixing two chemical solutions of 0.15 M. The solutions were prepared by dissolving Magnesium Acetate Tetrahydrate $Mg(CH_3COO)_2.4H_2O$ and Zinc Acetate Dihydrate $Zn(CH_3COO)_2.2H_2O$ in distilled water. The melange solution was stirred and mixed for 10 min . was obtained with the solution pH= 7.10. This process is repeated until the pH is changed by adding drops of hydrochloric acid (HCl) to the mixture for pH solution 2.50 .then drops of Sodium hydroxide for solution pH solution 8.30. As we mentioned before using the pH-meter technique; we obtained various of pH solutions of $Zn_{0.5}Mg_{0.5}O$ thin film (2.5, 7.10, and 8.30). (**see Table II.3).**

Table II .3: The parameters of chemical products.

Chemical name	Magnesium Acetate Tetrahydrate	Zinc Acetate Dihydrate	Deionized Water	Hydrochloric Acid	Sodium Hydroxide
Molecular formula	$Mg(CH_3COO)_2.4H_2O$	$Zn(CH_3COO)_2.2H_2O$	H_2O	HCl	NaOH
Volume	/	/	20 ml	drops	drops
Concentration	0.15 M		/	1M	2M
Molecular weight	214.455 g/mol	219.551g/mol	/	/	40g/mol

II.8.2.Preparation of the films

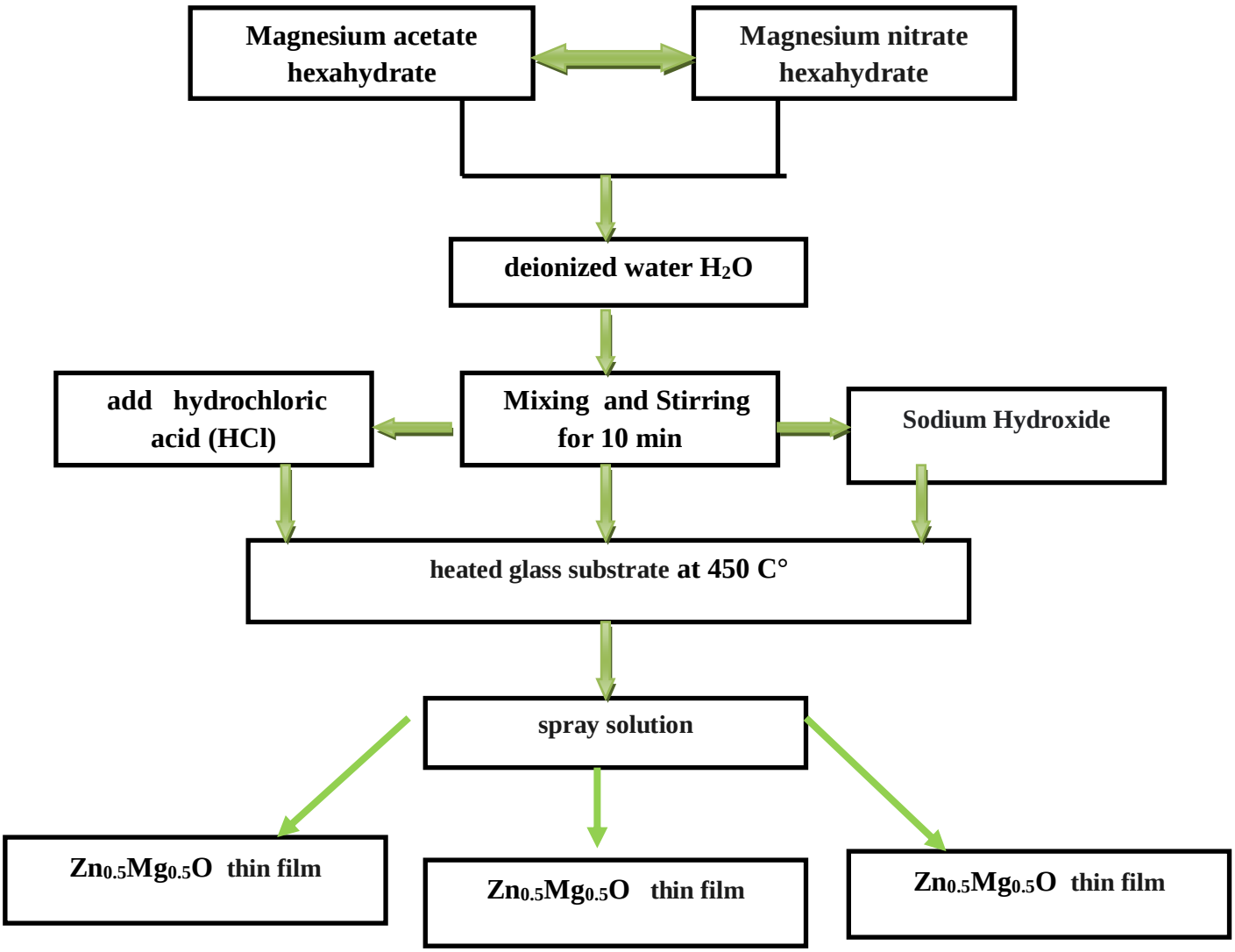

Figure II.8: Flow chart of Spray pyrolysis method for preparation of $Zn_{0.5}Mg_{0.5}O$ thin films.

II.10. Characterization Techniques

II.10.1 Structural characterization

X-ray diffraction is a tool for the investigation of the fine structure of matter. This technique had its beginnings in von Laue's discovery in 1912 that crystals diffract x-rays, the manner of the diffraction revealing the structure of the crystal[11]. At first, x-ray diffraction was used only for the determination of crystal structure. Later on, however, other uses were developed, and today the method is applied not only to structure determination, but to such diverse problems as chemical analysis and stress measurement, to the study of phase equilibria and the measurement of parti- cle size, to the determination of the orientation of one crystal or the ensemble of orientations in a polycrystalline aggregate [12].

$$n\lambda = 2d_{hkl}\sin\theta \qquad \textbf{(II.1)}$$

Where(λ) is the wave length of the X-ray beam, (d_{hkl}) is the spacing between theparallel planes in the atomic lattice, (h,k and l) are the miller indices of the corresponding lattice planes (hkl), θ is the angel between the incident ray and the scattering planes, and n is an integer. Waves that satisfy this condition interfere constructively and result in a reflected wave of significant intensity.

.

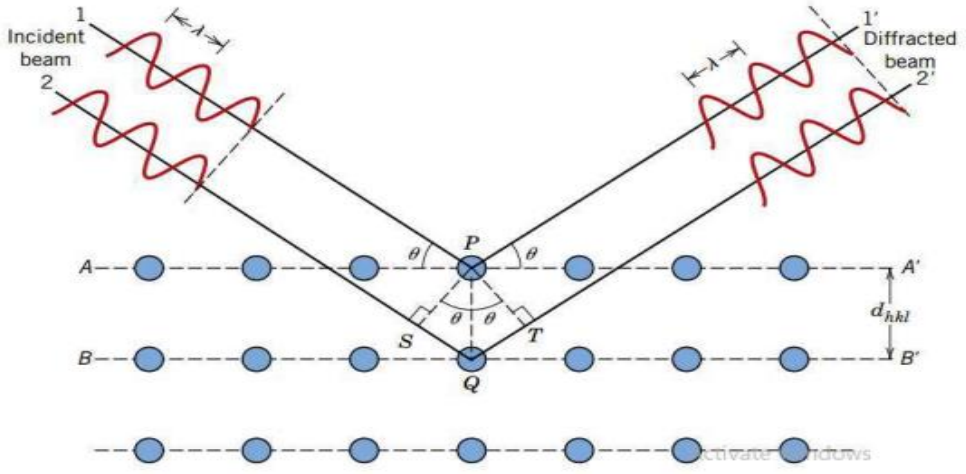

Figure II.9 . Incident and scattered X-rays in XRD analysis.

By measuring the strength of scattered waves from a sample as a function of the scattering angle, a diffraction pattern is created. The diffraction pattern exhibits extremely strong intensities known as Bragg peaks at the locations where the scattering angles meet Bragg's requirement. The average crystalline size, orientation, and crystal structure of the films may all be learned via X-ray diffraction examinations. The experimentally determined diffraction patterns from the sample are contrasted with the expected patterns of the elements and compounds it is likely to contain. Conclusions concerning the sample's crystal structure and orientation can be made on the basis of this comparison (**See Figure II.9)** [13].

II.10.1.a. Analysis of XRD Data

After the XRD pattern forms, the value of 2θ is estimated for each diffraction peak, and the d-spacing (dhkl) values are computed from 2 values using Bragg's equation. These numbers are utilized to derive thin-film crystallographic parameters such as phase identification, crystallite size determination, lattice parameter determination, etc.

II.10.1.b.Identification of phases

Phases of various materials can be identified in the usual way: The observed values (interplanar spacing) for the same material synthesized using a standard chemical process are compared to normative d values from an ASTM (international American Standard for Testing of Materials) standard data file or a JCPDS (Joint Committee for Powder Diffraction Standards) data file[14]. This study displays the many phases that are present in the sample as well as the atomic planes' miller indices (h, k, and l). The absence of reflection peaks suggests that the sample is amorphous. Epitaxial growth is shown by a single reflection peak, whereas polycrystalline (heteroepitaxial) development is indicated by various reflection peaks. is small, there is no more complete destructive interference at $\theta \pm d\theta$, which broadens the peak corresponding to diffracted beam in proportion to the size of the tiny crystal[15]. Moreover, the XRD approach can also afford precise results for lattice parameters, unit cell volume, constituents of the coatings, and crystal symmetry with atom positions.

II.10.1.c.Determination of Crystallite Size from XRD Data

From the X-ray diffraction pattern, the width generated in a peak which knownas full width at half maximum (FWHM) (**See Figure II.10**),The crystallite size was calculated using the relation given by Scherrer and formulated as,[16]

$$\mathbf{D_{hkl} = 0.9\lambda/\beta_{hkl}\cos(\theta_{hkl})} \qquad \mathbf{(II.2)}$$

Where,

D_{hkl} - Crystallite size size, ([D] = nm) .

θ_{hkl} - is the diffraction angle in degrees.

λ - is the wavelength of the X-rays beam (A °).

β- line broadening at Full Width at Half Maxima (FWHM).

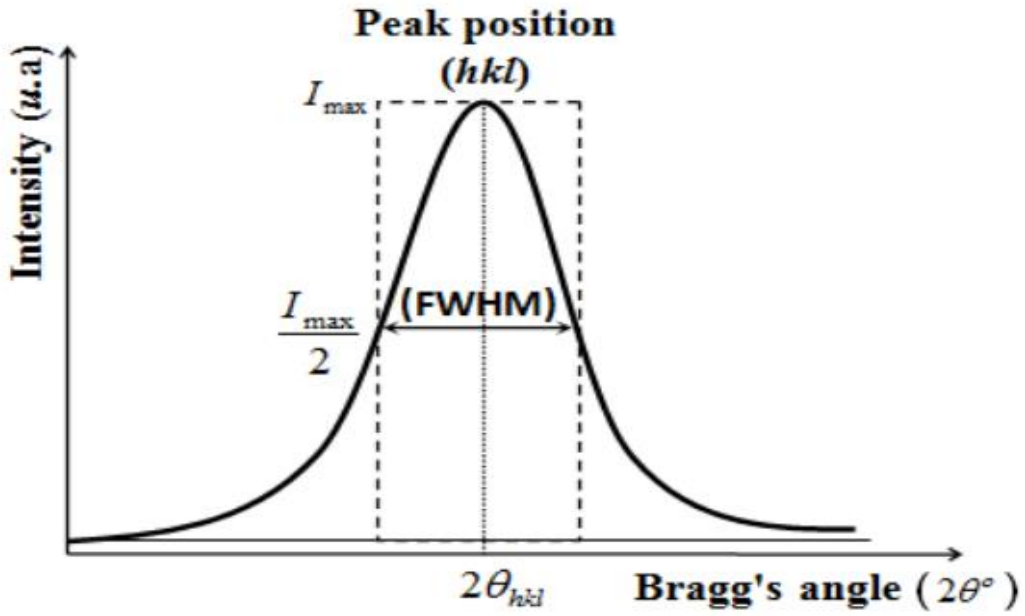

Figure II.10: Full width at half maximum (FWHM) of an arbitrary peak.

II.10.1.d.Determination of Lattice Parameter

By applying Bragg's law to determine the dhkl value, the standard Bravias lattice relation for a cubic structure(a = b = c), and Miller indices (hkl) related to the reflection orientation as follows, it is simple to derive the lattice parameters of a crystal structure have been determined by equation:

$$\mathbf{a = d(h^2 + k^2 + l^2)^{1/2}} \qquad \textbf{(II.3)}$$

Two main factors that are present in metal oxide films affect the mechanical strain in the films. The first one is the variation in the substrate's and the expanding film's coefficients of thermal expansion. The creation of strain in the film lattice is caused by the second factor, which is the distortion of the developing film composition from stoichiometry. Additionally, the microstrain in the films exhibits a relation with (FWHM) by[17].

$$\mathbf{\varepsilon = \beta/4\tan\theta} \qquad \textbf{(II.4)}$$

A dislocation is a flaw in a crystal that results from the lattice in one portion of the crystal being misregistered with that in another. Dislocations, in contrast to vacancies and interstitial atoms,are not equilibrium flaws; hence, thermodynamic considerations are insufficient to explain the importance of including dislocations.Using the formula, the dislocation density is calculated as the number of dislocation lines per unit area of the crystal[18].

$$\mathbf{\delta = 1/\ D2\ (Lines\ /\ m^2)} \qquad \textbf{(II.5)}$$

II.10.2. Optical characterization

The UV-Visible spectrophotometry technique tells us about certain optical properties of the material such as the optical absorption threshold, the absorption coefficient, the gap optics, Urbach energy, and the refractive index. It can also inform us in some cases about the thickness of the sample.

Ultraviolet-visible spectroscopy or ultraviolet-visible spectrophotometry (UV-Vis or UV/Vis) refers to absorption spectroscopy or reflectance spectroscopy in the ultraviolet visible spectral region. The absorption or reflectance in the visible range directly affects the perceived color of the chemicals involved, it measures the intensity of light passing through a sample I and compares it to the intensity of light before it passes through the reference I0. The ratio (I/I0)is called the transmittance and it is usually expressed as a percentage (T %). The absorbance, A is based on the transmittance[19]**.**

$$\boldsymbol{A = -\log(\frac{T}{100}\%)} \qquad \textbf{(II.6)}$$

The UV-visible spectrophotometer can be also configured to measure reflectance. In this case, the spectrophotometer measures the intensity of light reflected from a sample (I), and compares it to the intensity of light reflected from a reference material (I0) (such as a white tile). The ratio (I I0) is called the reflectance, and is usually expressed as a percentage (R %) (**See Figure II.11**).

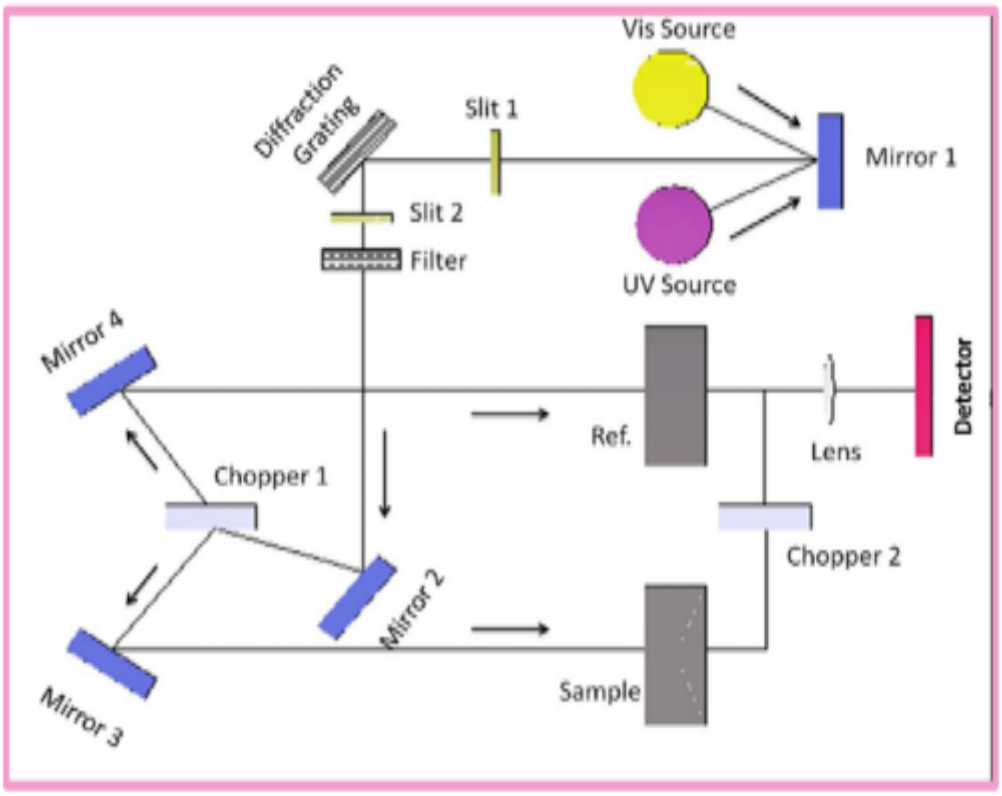

Figure .II.11: Schematic spectrometer of UV-Vis .

II.10.2.1. Band Gap Calculations

Transmission data can be used to determine thin film optical band gap energy. Jan Tauc reported that the transmittance data of a thin film coating can be used to calculate the absorption coefficient (α) of a coating along the entire wavelength. Plotting (αhυ) 1/n versus photon energy results in a Tauc plot, which shows the linear drop of the absorption edge. The value of n depends on the type of electron transition whether it is direct (n = 1/2) or indirect (n = 2). By extrapolating the linear part of Tauc plot toward X-axis, the optical band gap energy is obtained. **Figure II.12** shows a typical Tauc plot for estimating the band gap energy[20]**.**

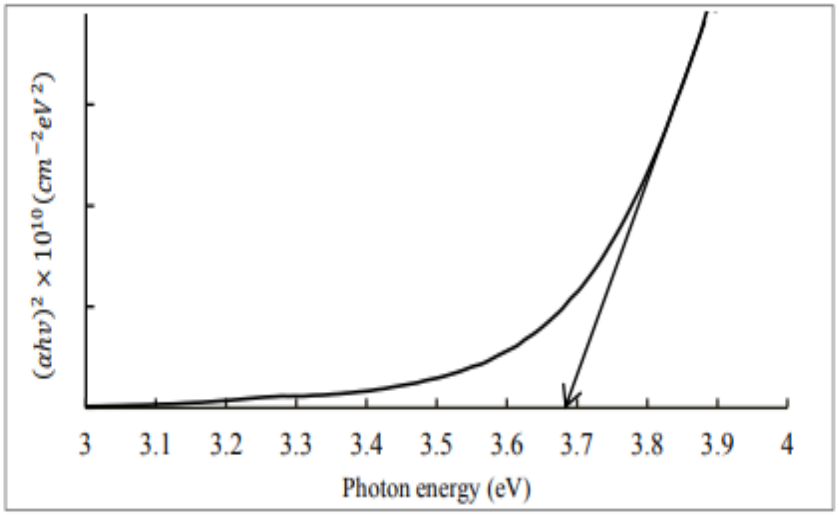

Figure II.12: Typical Tauc plot for estimating the band gap energy of a thin film

II.10.2.2. Disorder calculating (Urbach Energy)

We observe localized states formed band tails border of the band gap in the valence band and conduction. For energies above and below Ev, Ec is the extended state, this difference is known as the disorder or Urbach Energy; According to Urbach law, Indeed, the absorption coefficient, according to the law of Urbach, is given by the relation[21]. **(See Figure II.13)**

$$\alpha(h\nu) = \alpha_0 \exp\left(\frac{h\nu}{E_u}\right) \qquad \textbf{(II.7)}$$

Where :

α_0: Constant

E_{Urb}: Energy of Urbach(eV)

By plotting ln(α) as a function of hν, we can access the value of E_{Urb}

$$\ln \alpha = \left[\frac{1}{E_{Urb}}\right] h\upsilon + \ln \alpha_0 \qquad \text{(II.8)}$$

The parameter E_{Urb} is the width of the tail of the band which characterizes the disorder

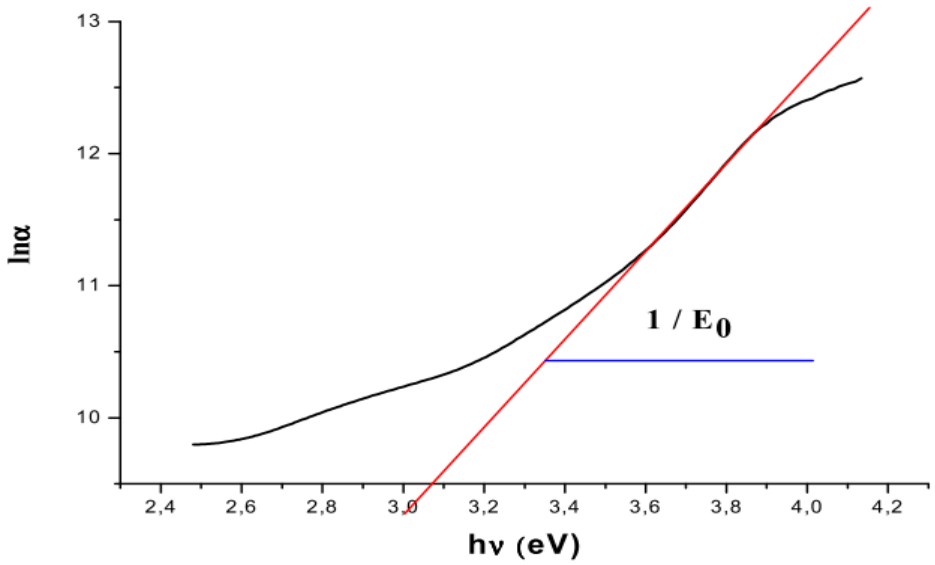

Figure II.13: Example of the determination of the Urbach parameter from the Variation of lnα as a function of hυ.

II.10.3 Morphological characterization

II.10.3.1. Scanning electron microscope coupled with microanalysis (SEM/EDX):

Scanning Electron Microscop SEM is a technique that can provide information on the morphology of a solid sample. It is based on the principle of electron-matter interactions. For this, a cannon produces a beam of electrons thanks to a tungsten filament heated by the Joule effect in a second vacuum chamber. This beam is accelerated by a high voltage created between the filament and the anode. It is then focused on the sample and scans the surface line by line, either by a mechanical or electromechanical movement[22]. The sample must be conductive, otherwise, it must be covered with a thin film of metal (Au, Ag, Cu, etc.) or carbon to allow the electron

beam to pass. The interaction of the electron beam with the material produces electrons (secondary and backscattered) and X-rays. The analysis of these electrons makes it possible to deduce the topography of the sample.

Energy dispersive spectrometry (EDX) coupled with SEM allows the determination of the chemical composition of the examined surface. It consists in analyzing the X-rays generated by a sample placed under the kls electron beam of the scanning electron microscope (SEM). The radiation emitted during the interaction between the x-rays and the material of the sample is transcribed in the form of a spectrum, where peaks of variable intensity appear, characteristic of the metallic or mineral elements present (**See Figure .II.14)**

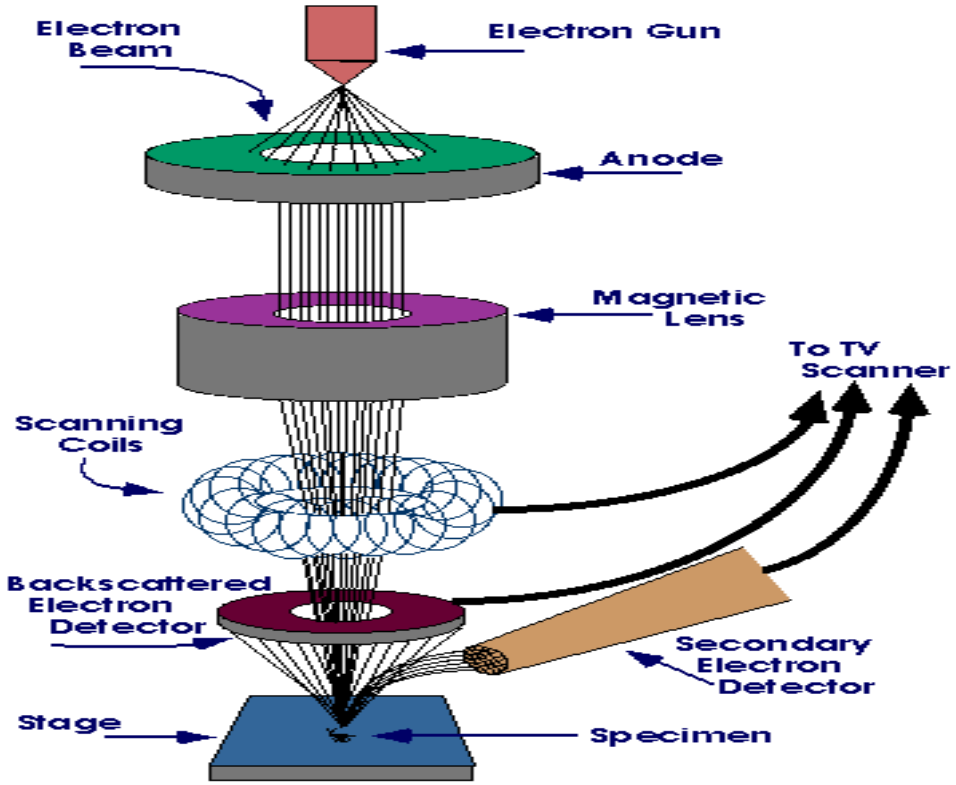

Figure .II.14:Ray diagram of scanning electron microscopy.

II.10.4. Fourier transforms infrared spectroscopy (FTIR)

Electromagnetic radiations in which wavelength extend in the range of 1micron to 1 mm are termed infrared, which lie between the visible and microwave region. Usually, the wavelength used in IR spectroscopy ranged from 2.5-25 microns or 4000 to 400 wave numbers (waves per cm)[23]. FTIR is mostly used to identify chemicals

that are either organic or inorganic. We can also use it to get information on some compounds of an unknown mixture. The FTIR can be applied to the analysis of solids, liquids, and gases. Today, the FTIR is computerized and it has become more sensitive than the other dispersive instruments. The FTIR not only identifies chemicals but also identifies the types of chemical bonds (functional groups). To get the absorption spectrum of material it absorbs the wavelength of light. By interpreting the IR absorption spectrum, we can able to determine the chemical bonds in the molecule. We can obtain unique FTIR spectra of pure compounds like a molecular fingerprint. The spectrum of unknown materials can be identified by comparison to a library of known compounds[24]. West coast analytical service (WCAS) has several IR spectral libraries including online computer libraries. The technique is founded upon the simple fact that a chemical material shows famous selective absorption in the IR region, a diagram of the components of a typical spectrophotometer is shown in **Figure II.15.**

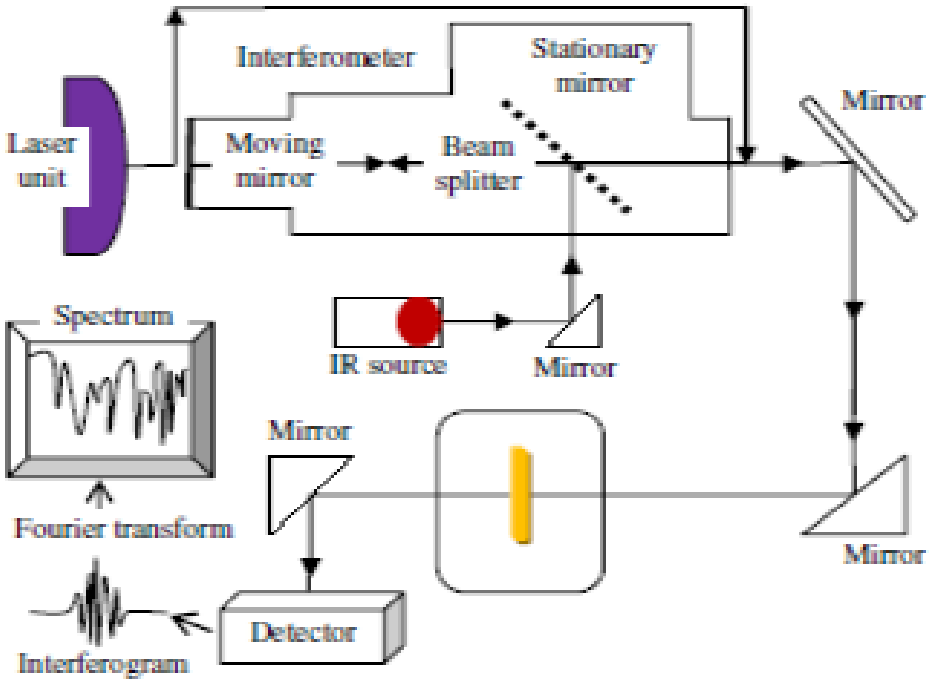

Figure II.15: Schematic diagram of a Fourier transform infrared spectrometer [23].

II.10.5. Electrical characterization

Four-Point Probes Measurements

A 4-point probe system is a powerful tool commonly used to measure the electrical resistivity and sheet resistance of semiconductor materials. Compared to a traditional 2-point probe, a 4-point probe gives more accurate results of material resistivity because it eliminates the contact and probe resistance. Typically, this instrument has four regularly spaced probes that are arranged in a linear pattern (**see Figure.II.16**). Each pair of adjacent probes is separated by 1 mm. As long as the thickness is known, the film resistivity can be measured by applying an electric current through the two outside probes and recording the voltage from the two circular probes. The following relationship determines the electrical resistivity[25]:

$$\rho = \left[\frac{\pi}{\ln 2}\ \frac{U}{I}\right] d = R_S \mathrm{d} \qquad \textbf{(II.9)}$$

where,d is the film thickness, V is the voltage across the inner two probes and I is the current passed through the outer two probes. For accurate resistivity measurements, the four probes must perfectly attached the film surface and the contact diameter should be smaller than the spaces between the probes.[10]

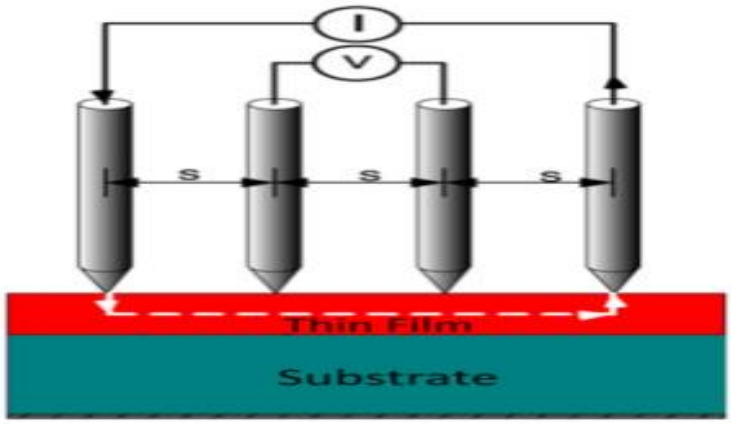

Figure :II.16: Schematic of in-line four-point probe configuration

II.11. Conclusion

In this chapter, We have explained the spray pneumatic method, in addition, have also we have described the preparation of MgO thin films and Zn-MgO, and determined the experimental conditions. Finally, we used various characterization methods such as XRD, UV-VIS spectroscopy, Fourier transforms infrared (FTIR) spectroscopic analysis, and electrical characterizations (the four points technique).

References

[1] T. Justin Kunene, L. Kwanda Tartibu, K. Ukoba, and T. C. Jen, "Review of atomic layer deposition process, application and modeling tools," *Mater. Today Proc.*, vol. 62, pp. S95–S109, 2022.

[2] A. Chala, A. Attaf, H. B. E. N. Temam, and S. Rahmane, "SYNTHESIS AND CHARACTERIZATION OF ZINC OXIDE THIN FILMS FOR THE OPTIMIZATION OF A SPRAY DEPOSITION SYSTEM," 2012.

[3] D. Perednis and L. J. Gauckler, "Thin film deposition using spray pyrolysis," *J. Electroceramics*, vol. 14, no. 2, pp. 103–111, 2005.

[4] N. Boukhenoufa, "Contribution à l ' étude des propriétés des films minces à base de ZnO," *Doctorat*, 2017.

[5] J. B. Mooney and S. B. Radding, "Spray Pyrolysis Processing.," *Annu. Rev. Mater. Sci.*, vol. 12, pp. 81–101, 1982.

[6] O. J. Ilegbusi, S. M. N. Khatami, and L. I. Trakhtenberg, "Spray Pyrolysis Deposition of Single and Mixed Oxide Thin Films," pp. 153–169, 2017.

[7] O. Malik, F. J. D. La Hidalga-Wade, and R. R. Amador, "Spray Pyrolysis Processing for Optoelectronic Applications," *Pyrolysis*, 2017.

[8] Dellaoui, "Memoire de magister de biologie," pp. 1–128, 2016.

[9] B. Youcef, " Elaboration and characterization of thin layers of zinc oxide (ZnO) deposited by ultrasonic spray for photovoltaic and optoelectronic applications ", thesis, University Mohamed Khider of Biskra, 2019.

[10] ZAOUCHE Chouaieb, "THE ROLE OF Ni AND Zn ON DILUTED MAGNETIC SEMICONDUCTOR Ni 1-x Zn x O THIN FILMS," 2020.

[11] G. Hildebrandt, "The Discovery of the Diffraction of X-rays in Crystals — A Historical Review," *Cryst. Res. Technol.*, vol. 28, no. 6, pp. 747–766, 1993
.

[12] A. Engstrom, Reduction Annealing Synthesis of Nanostructured. 2014.

[13] B. Fultz and J. M. Howe, Diffraction and the X-Ray Powder Diffractometer. 2002.

[14] E. Sup, R. S. Universit, M. Khider, B. Facult, and S. Rahmane, " caractérisation des couches minces de ZnO dopées cobalt et indium "

[15] M. Radhia, " Elaboration and characterization of undoped and doped titanium dioxide thin layers by sol gel (spin coating) for photocatalytic applications". Doctoral thesis, Université de mohamed kheider biskra.," 2021.

[16] "THEME Elaboration and characterization of nanostructuring NiO thin films for gas sensing applications."

[17] Rahil AZIZI," The effect of doping on the properties of thin films of Indium oxide(In_2O_3) deposited by ultrasonic spray for optoelectronic application"2020.

[18] F. Székely, I. Groma, and J. Lendvai, "Characterization of self-similar dislocation patterns by x-ray diffraction," *Phys. Rev. B - Condens. Matter Mater. Phys.*, vol. 62, no. 5, pp. 3093–3098, 2000.

[19] K. Chafia, "Presented to obtain the Degree of Tin dioxide SnO 2 thin films deposited by ultrasonic spray technique: Properties and Applications Speciality: thin films," 2018.

[20] H. Taha, "Optoelectronic and Mechanical Properties of Sol-Gel Derived Multi-Layer ITO Thin Films Improved by Elemental Doping, Carbon Nanotubes and

Nanoparticles," 2018.
[21] "Aicha CHENNOUFI."L'effet de la molarite et de température du substrat sur les propriété des couches minces d'oxyde d'indium déposées par spray Ultrasonique".2012.
[22] BENAMEUR Khedidja, "Elaboration et caractérisation des couches minces chalcopyrites CuIn1-xMxSe2 (M = Ga, Zn, Fe …) pour application photovoltaïque", 2022.
[23] S. Benhamida, "Caractérisation Des Couches Minces D'oxyde De Nickel (Ni O) Elaboré Par Spray Pyrolyse,". November 2018, 2020.
[24] Yahia Anouar ,"Optimization of indium oxide thin films properties prepared by sol gel spin coating process for optoelectronic applications". 2020
[25] P. O. F. T. H. E. I-r-e, "Resistivity Measurements on Germanium for Transistors*," *Proc. IRE*, vol. 29, pp. 1429–1434, 1952.

Chaptre III

Study physical properties of the MgO thin films by various concentrations

III.1. INTRODUCTION

In the latest research, for the important subjects in the field of materials science, the synthesis of thin films from a metal oxide (semiconductor), the magnesium oxide (MgO) was used in microelectronic and optoelectronic devices due to the good dielectric constant (~ 9.8) and high breakdown field (12 $MV.cm^{-1}$) with compared to the layer of silicon dioxide (SiO_2) [1,2]. On the other hand, MgO is an important semiconductor material due to the good electrical resistance as well as excellent optical and thermodynamic stabilities [1,2]. MgO was slightly crystallized at any temperature to the cubic of NaCl structure with lattice parameter a = 0.421 nm [1-3], The optical bandgap of MgO thin films varied between 5.6 to 7 eV [1-4] and high stability that are similar to ZnO [4]. In addition, MgO was used in a variety of sciences and technology such as optoelectronic devices due to the good structure crystallinity and high transparent in the visible region [5,6]. Moreover, the MgO thin films can be used in various applications due to the simplicity of synthesis such as solar cells, chemical sensors, photodetectors, organic light-emitting diodes, infrared window material, ferromagnetic thin films, ferromagnetic thin films, and protective layer in AC-plasma display panels [1-9].

The MgO thin films can be obtained by various deposition techniques likely reactive evaporation, electrochemical deposition, technique of magnetron sputtering, molecular beam epitaxy (MBE), pulsed laser deposition, sol-gel process, chemical vapor deposition, and spray pyrolysis [5–12]. The aim of this work, we have used pneumatic spray technique to fabricate the magnesium oxide (MgO) thin films, which it studied at several MgO precursor molarites (0.05; 0.10; 0.15 and 0.20 $mol.l^{-1}$). The optical, electrical and structural characterizations of magnesium oxide (MgO) thin films.

III.2. Results and discussion

III.2.1.Study structural properties

The effect of MgO concentration on the crystal structure and preferred orientations of the sprayed MgO thin films was characterized by the XRD technique. Figure.**III.1** shows the XRD patterns of MgO thin films deposited with various concentrations of 0.05, 0.10, 0.15 and 0.2 $mol.l^{-1}$. As the first result, All the films exhibited two diffraction peaks at 2θ = 22 and 31° related to (002) and (220) planes of MgO phase, indicating MgO thin films are polycrystalline cubic structure. The good crystal structure showed for a strong peak, which corresponded to the (002) plane of the MgO cubic structure. It can be seen that the intensity of the (002) peak of sprayed MgO thin film with 0.15M has a good crystallinity, which confirmed the improvement of the crystalline quality and the reduction of defects

in the crystal structure. The lattice parameter *a* of MgO thin films was found in order to 0.421 nm, which it agreed with obtained by [18-21].

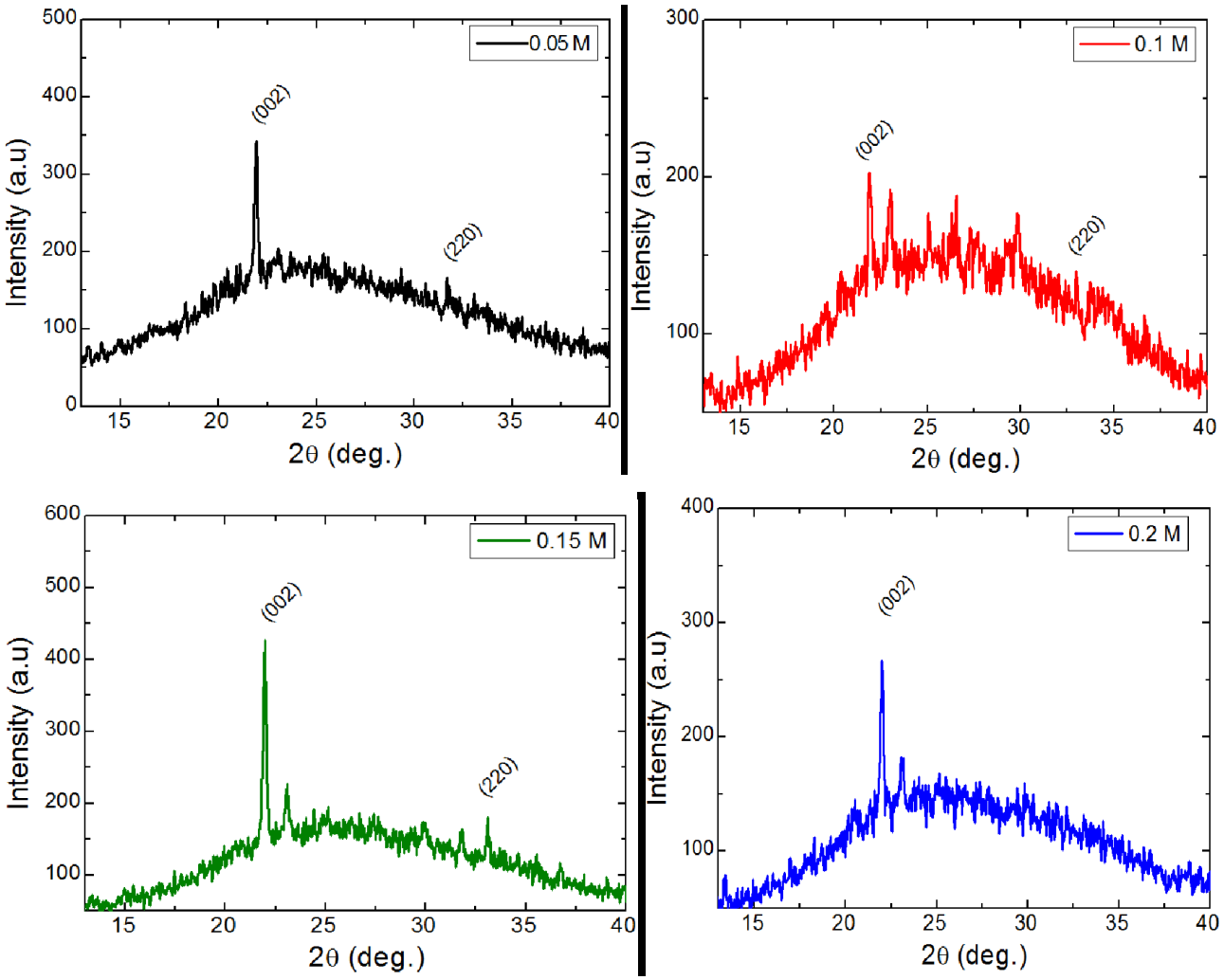

Figure. III.1: XRD spectra of MgO thin film doposited with different molarities.

The crystallite size G of (002) diffraction peak of the MgO thin films was calculated using the Scherer's equation [23]:

$$G = \frac{0.9\,\lambda}{\beta \cos\theta} \qquad (1)$$

where G is the crystallite size, λ is the wavelength of X-ray (λ = 1.5418 A°), β is the full width at half-maximum (FWHM), and θ is the angle of diffraction peak. Figure. **III.2** shows the variations of the crystallite size of the (002) diffraction peak as a function of MgO concentration. It can be seen, the crystallite size increased with increasing the MgO concentration from 12.1 nm for 0.05 to 21.4 nm for 0.20 mol.l^{-1}, which may be due to the improvement of the crystalline quality of MgO.

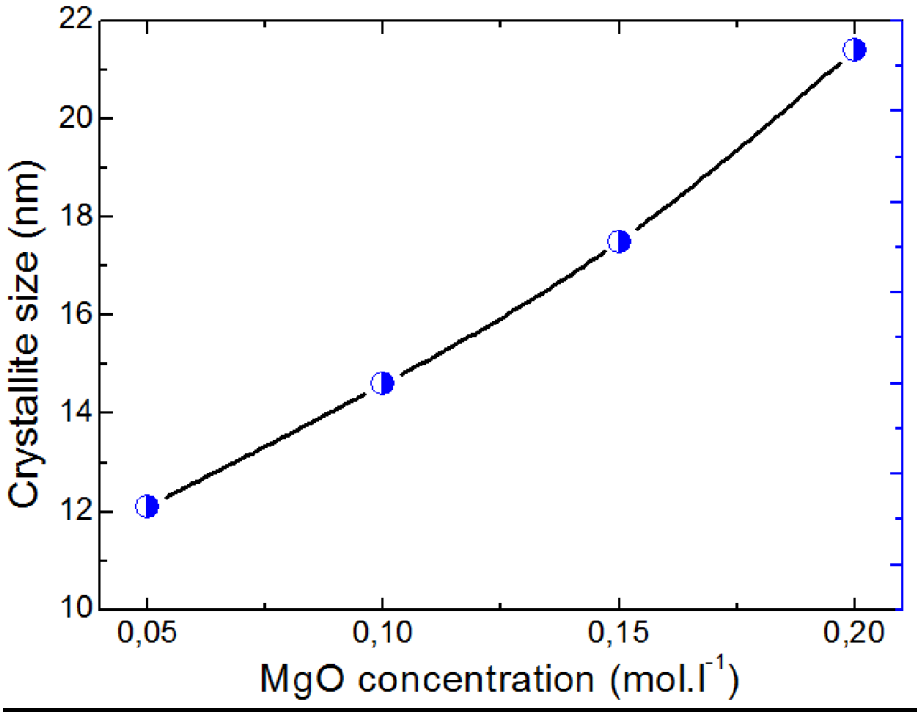

Figure. III.2: the variation of crystallite size of MgO thin film doposited with different molarities.

III.2.2. Study Optical properties

Figure. **III.3** shows the relation between transmission and wavelength in the range of (300- 1000 nm) for magnesium oxide thin films. The transmission for all thin films increases as the wavelength increases in the range of (300- 1000 nm) (see Table **III.1**), which it is corresponds the region between the valence band and conduction band. The spectrum shows high transmission in the visible and infrared regions, and low in the ultraviolet region. The transmission of MgO thin films decreases with increasing of MgO precursor molarity from 0.05 to 0.2M in all deposited films due to the increase film thickness (see Table**. III.1**). On the other hand, the region of the transition (absorption edge) between the valence band and the conduction band it is observed between 300–330 nm, this attribution can be explain to find low optical band gap energy. Płóciennik et al. [13] have found that the absorption edge of MgO films which is of about 160 nm. We concluded that the effect of MgO precursor molarity on optical property was observed.

Reflectance *R* can be obtained from absorption and transmission spectrum in accordance to the law of conservation of energy by the relation [14]:

$$A+T+R=1 \qquad (2)$$

where R is the reflectance, T is the transmission of the films and A is the absorption. Figure. **III.4**, it have been noticed that all the prepared thin films have a different absorption in visible range of the spectrum, which shows the relation between the absorption (A) with Transmission (T). The high absorption edge value can be find with 0.2M because the increases in the film thickness.

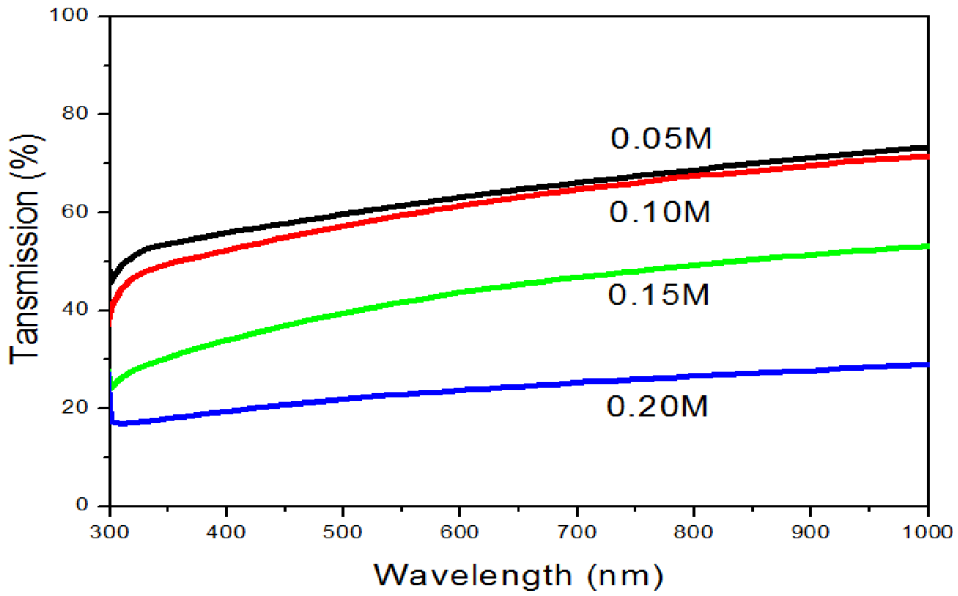

Figure. III.3: Variation of transmittance spectra (T) with wavelength (λ) of MgO thin film doposited with different molarities.

Table III.1. Variation of film transmission of MgO as a function of molarity.

Molarity (mol.l^{-1})	0.05	0.1	0.15	0.2
TRANSMISSION (%) BETWEEN 400 AND 800 *NM*	*62*	*59*	*41*	*22*

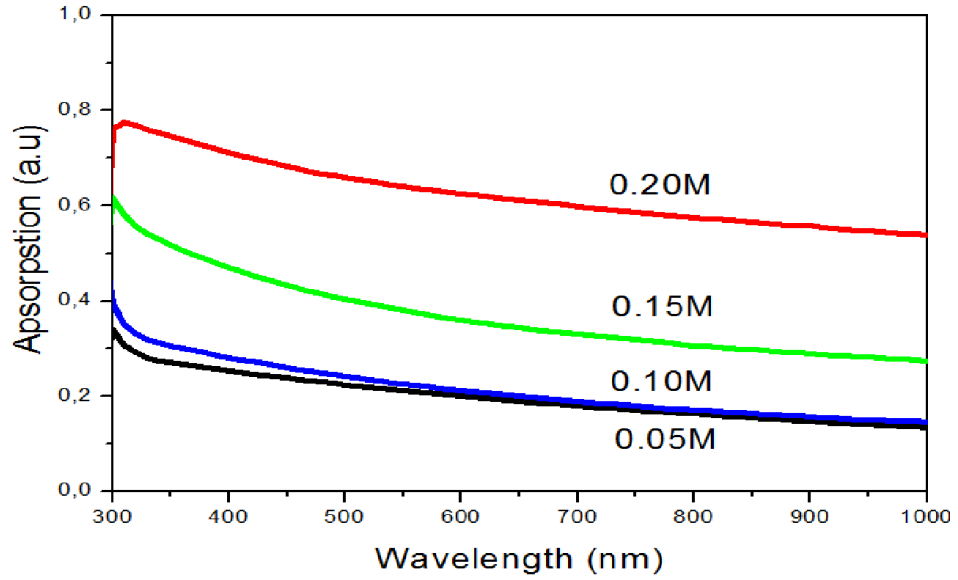

Figure. III.4: The relation between absorption and wavelength of deposited MgO thin films.

The optical energy gap (E_g) was derived assuming allowed direct transitions between the edge of the valence and conduction band. For MgO thin films, we can calculated using Tauc's equation [15]

$$(\alpha h\upsilon) = C(h\upsilon - E_g)^n \tag{3}$$

where α is the absorption coefficient, C is a constant, $h\nu$ is the energy of incident photon and n depends on the quantum selection rules for different materials which may be equals to 1/2 for direct and 2 for indirect band gap. In our case, we have used n=1/2 because it gives an excellent linear fit curve in the band-edge region [16].

The absorbance **($\alpha d=2.303A$)** has been used to determine the band gap of the evolving MgO film by measuring the absorption coefficient as a function of the incident photon energy **($h\nu$)**.

The graphs of **$(\alpha h\nu)^2$** versus **($h\nu$)** plots of MgO films fabricated at different molarities were obtained. It can be measured by the extrapolation of linear portion of the graph to the energy axis at α= 0 [15] in the range between 300–330 nm gives band gap energy E_g is shown in Table **III.2**.

In the addition of we have used the tail width, which can be calculated using the Urbach rule for the absorption coefficient at lower photon energy [17].

$$\alpha = \alpha_0 \exp\left(\frac{h\upsilon}{E_u}\right) \tag{4}$$

gives as the values of E_g and E_u at different concentrations of molarities to MgO solution. In the other hand, Figure. **III.5** shows the variation of optical band gap and Urbach energy of MgO thin films as a function molarity. As can be seen, that the band gap energy E_g and Urbach energy E_u are dependent to the change in MgO solution, it is clear that the values of E_g are agreements to E_u variation. However, can be observe that the band gap energy of MgO thin films decreased slowly with incrassating the MgO molarity, this result can be explained by the increase of oxygen with the film preparation. As mentioned above, As a result, both a decrease in the optical gap and a broadening of the Urbach tail occurred. Similar to our findings, El-Gamal and l Sayed [18] they obtained that the optical gap energy of PAM/PVA-loaded MgO NPs was varied between 4.4 to 5.3 eV. However, Fuad T. Ibrahim [19] have a highest value of Urbach energy that was found in the range of 1.8-4.2 eV.

Refractive index (n) of MgO thin films was calculated by using the following formula [20]:

$$n = \frac{(1+R)}{(1-R)} + \sqrt{\frac{4R}{(1-R)^2} - K^2} \tag{5}$$

where R is the reflectance and K is the extinction coefficient of MgO thin films. The extinction coefficient was determined from λ is the wavelength and α is the absorption coefficient by the following relation [20].

$$k = \frac{\alpha\lambda}{4\pi} \quad (6)$$

The refractive index n is presented in Table 3, we have observed that the value is smeller then the 2.4. Mousa et al. [21] they found that the deposited MgO thin film at 450 °C has a refractive index of about 3.1.

Table III.2: Variation of the optical band gap energy Eg and the Urbach energy of MgO thin films with different molarities.

Molarity (mol.l-1)	Optical gap E_g (eV)	Urbach energy E_u (meV).	Refractive index (n)
0.05	4.77	519	1.8
0.10	4.48	465	1.9
0.15	4.42	420	2.2
0.20	4.28	375	2.4

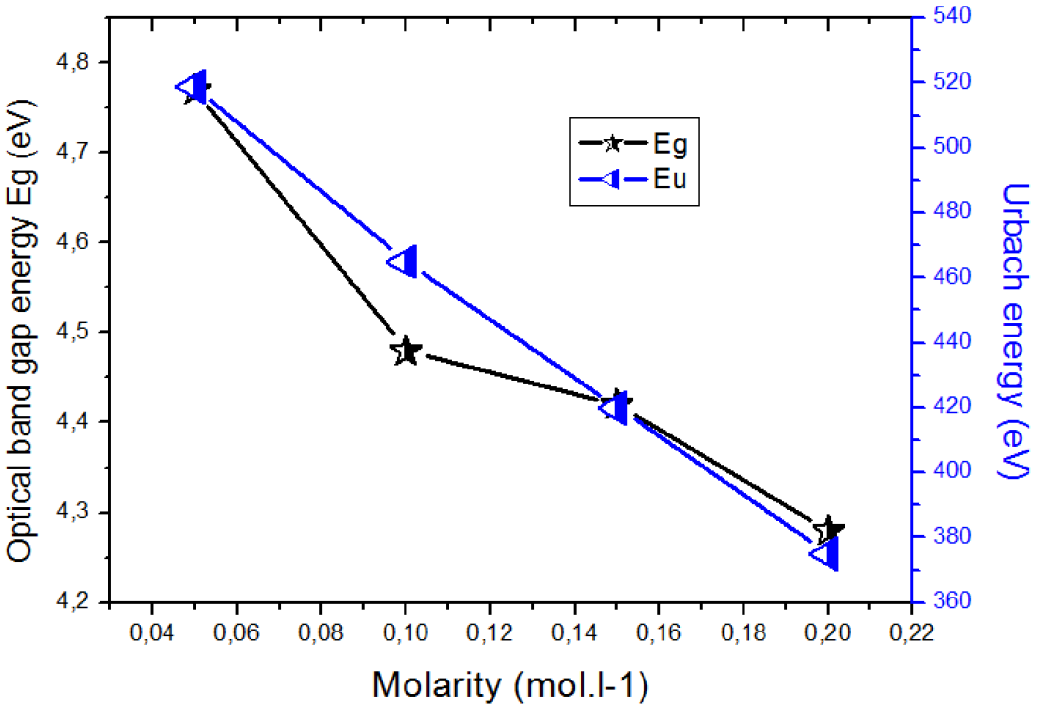

Figure. III.5: The variation of optical band gap and Urbache energy of MgO thin films as a function molarity.

III.2.3. Study electrical properties

The four-point probe is required to measure the sheet resistance of the films. Since negligible contact and spreading resistance are associated with the voltage probes, the sheet resistance (R_{Sh}) can be estimated, when the film thickness less than the spacing between the probes, using the following relation [22]:

$$R_{sh} = \frac{\pi}{\ln 2}\frac{V}{I} \qquad (7)$$

where I is the applied currant and V is the measurement voltage.

Table **III.3** and Figure. **III.6** gives the R_{sh} values of MgO thin films as a function of concentration molarity. As can be seen that the R_{sh} was found decreases with increasing the concentration molarity. The decrease of the resistance can be explain by the increase in the films thickness of the deposited MgO thin films with molarity.

Table III.3. The electrical resistance of of MgO thin films with different molarities.

Molarity (mol.l^{-1})	0.05	0.10	0.15	0.20
I (A)*10^{-6}	0.5	0.5	0.5	0.5
V_1 (V)	0.0712	0.0542	0.0473	0.0325
V_1 (V)	0.0290	0.0473	0.0277	0.398
V_3 (V)	0.0640	0.0521	0.0455	0.217
R_{SH} (Ω) *10^7	2.18	2.11	1.87	1.68

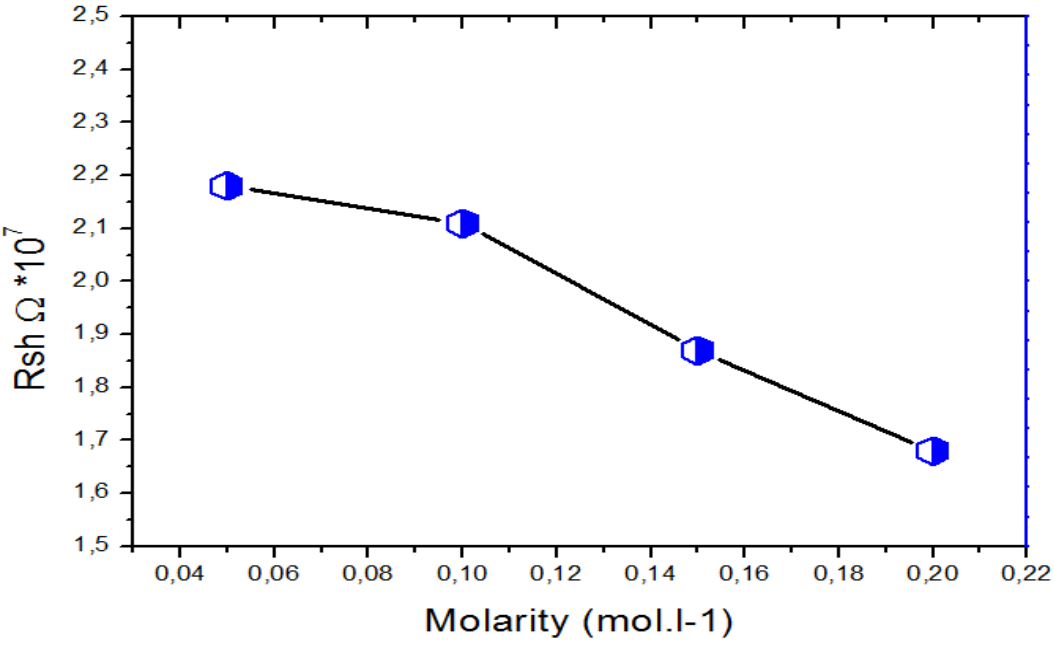

Figure. III.6. The electrical resistivity variations with different molarities of MgO thin films.

III.3. CONCLUSION

In this study Magnesium Oxide thin films were deposited on galas substrate by pneumatic technique. The effects of concentration molarity (0.05; 0.1; 0.15 and 0.2M) were successfully investigated. The high transmission was found in the deposited MgO thin film with lowest molarity. The transmittance of MgO thin films decreases rapidly as the wavelength increases in the range of (300-400) nm, and then increases slowly at higher wavelengths. The band gap of MgO thin films decreases as the molarity increases and the band gap values range between 4.8-4.3 eV. The Urbach energy values range between 375-519 meV. The electrical resistance of our films in the order $2*10^{7}\Omega$. Polycrystalline MgO films with a cubic structure with a strong (002) preferred orientation were observed at all sprayed films with maximum crystallite size of 21.4 nm was attained of sprayed film at 0.2 $mol.l^{-1}$. The good transmission was found in the deposited MgO thin film with lowest molarity.

REFERENCES

[1] P. Maiti, P.S. Das, M. Bhattacharya, S. Mukherjee, B. Saha, A.K. Mullick, A.K. Mukhopadhyay, ''Transparent Al^{+3} doped MgO thin films for functional applications,'' Materials Research Express, Vol. 4, p. 086405, 2017.

[2] Z. Bazhan, F.E. Ghodsi, J. Mazloom,'' Effect of stabilizer on optical and structural properties of MgO thin filmsprepared by sol–gel method,'' Bulletin of Materials Science, Vol. 36, pp. 899–905, 2013.

[3] D. K. Fork, F. A. Ponce, J. C. Tiramontana, T. H. Geballe, '' Epitaxial MgO on Si(OO1) for Y-Ba4U0 thin-fil growth by pulsed laser deposition, '' Applied Physics Letters, Vol. 58, pp. 2294–2296, 1991.

[4] S.G. Khalil, M.M. Mutter, Z.K. Mohammed, G. Salem, ''Fabrication and Characterization of Gas Sensor from ZrO2: MgO Nanostructure Thin Films by R.F. Magnetron Sputtering Technique,'' Baghdad Science Journal, Vol. 16, pp. 199-208, 2019.

[5] S. Iacobucci, F. Offi, P. Torelli, L. Petaccia, ''Effective attenuation lengths of low energy electrons in MgO thin films,'' Journal of Electron Spectroscopy and Related Phenomena, Vol. 233, pp. 1-4, 2019.

[6] G. Suárez-Campos, D. Cabrera-German, J.A. García-Valenzuela et al. ''Controlled synthesis of Mg(OH)2 thin films by chemical solution deposition and their thermal transformation to MgO thin films,'' Ceramics International, Vol. 45, pp. 10356-10363, 2019.

[7] Z. Mohammed, S. Khalil, M. Mutter, ''Synthesis and characterization of ZrO2: MgO thinfilms by plasma of R.F. magnetron sputtering,'' Karbala International Journal of Modern Science, Vol. 5(1), A3, 2019.

[8] İ.A. Kariper, İ.A. Kariperab, F. MeydaneriTezel, ''UV region supercapacitor: Bi-doped natural MgO rock salt thin film,'' Ceramics International, Vol. 45, pp. 9219-9224, 2019.

[9] S. Tigunta, P. Khlikhum, P. Kidkhunthod, N. Chanlek, L. Supadee, S. pojprapai, ''Dissolution behavior of MgO thin film-barrier magnetic tunneling junctions,'' Journal of Materials Science: Materials in Electronics, Vol. 30, pp. 6718–6724, 2019.

[10] T. Komori, A. Anzai, T. Gushi, K. Toko, T. Suemasu, ''Molecular beam epitaxy growth of Mn4−xNixN thin films on MgO(0 0 1) substrates and their magnetic properties,'' Journal of Crystal Growth, Vol. 507, pp. 163-167, 2019.

[11] I. Cora, Z. Baji, Z. Fogarassy, Z.Szabó, B. Pécz, ''Structural study of MgO and Mg-doped ZnO thin films grown by atomic layer deposition,'' Materials Science in Semiconductor Processing, Vol. 93, pp. 6-11, 2019.

[12] H. Güney, D. İskenderoğlu, ‘’Synthesis of MgO thin films grown by SILAR technique,’’ Ceramics International, Vol. 44, pp. 7788-7793, 2018.

[13] P. Płóciennik, D. GuichaouaA. ZawadzkaA. KorcalaJ. StrzeleckiP. TrzaskaB. Sahraoui, ‘’ Optical properties of MgO thin films grown by laser ablation technique,’’ Optical and Quantum Electronics, Vol. 48, p. 277, 2016.

[14] Y. P. Santos, E. Valença, R. Machado, M. A. Macêdo, ‘’A novel structure ZnO-Fe-ZnO thin film memristor,’’ Materials Science in Semiconductor Processing, Vol. 86, pp. 43-48, 2018.

[15] S. Benramache, B. Benhaoua, N. Khechai and F. Chabane, ‘’Elaboration and characterisation of ZnO thin films,’’ Matériaux & Techniques, Vol. 100, pp. 573–580, 2012.

[16] Y. Aoun, M. Marrakchi, S. Benramache, B. Benhaoua, S. Lakel, A. Cheraf, ‘’Preparation and Characterizations of Monocrystalline Na Doped NiO Thin Films,’’ Materials Research, Vol. 21, p. e20170681, 2018.

[17] A. Diha, S. Benramache, L. Fellah, ‘’The Crystalline Structure, Optical and Conductivity Properties of Fluorine Doped ZnO Nanoparticles,’’ Journal of Nano and Electronics Physics, Vol. 11, p. 03002, 2019.

[18] S El-Gamal, Adel M El Sayed, ‘’ Physical properties of the organicpolymeric blend (PVA/PAM)modified with MgO nanofillers,’’ Journal of Composite Materials, Vol. 53, pp. 831–2847, 2019.

[19] F.T. Ibrahim, ‘’ Characterization of Pulsed-Laser Deposited CuO-Doped MgO Thin Filmsfor Gas Sensing Applications,’’ Iraqi Journal of Applied Physics, Vol. 13, pp. 13-17, 2017.

[20] S. Gupta, A. Paliwal, V. Gupta, M. Tomar, ‘’ Surface Plasmon Resonance assisted optical analysis of Strontium BariumNiobate thinfilms,’’ Applied Surface Science, Vol. 501, p .144178, 2020.

[21] A.O. Mousa, N.A. Nema, S.H. Trier, ‘’ Study of structural and optical properties for MgO films prepared by using chemical spray pyrolysis technique,’’ Materials Science: An Indian Journal, Vol. 14, pp. 426-434, 2016.

[22] A. Rahal, A. Benhaoua, C. Bouzidi, B. Benhaoua, B. Gasmi, ‘’Effect of antimony doping on the structural, optical and electrical properties of SnO2 thin films prepared by spray ultrasonic,’’ Superlattices and Microstructures, Vol. 76, pp. 105-114, 2014.

[23] K. Kandpal, N. Gupta, ‘’Study of structural and electrical properties of ZnO thin film for Thin Film Transistor (TFT) applications,’’ Journal of Materials Science: Materials in Electronics, Vol. 28, pp. 16013–16020, 2017.

CHAPTER IV

Effect of pH on the characterization of MgO Thin Films

IV .1. Introduction

Magnesium oxide thin films are very important scientific and commercial materials [1-5]. Nowadays, oxide materials are widely used in the producing of integrated circuits, Opto-, acousto- and microelectronics, solar energy, and other areas of modern industry [2,3]. MgO is a highly ionic crystalline solid, which crystallizes into a rock salt structure. It has FCC $Mg^{+2}$and O^{-2} sublattices, with a lattice parameter of (a=b=c=4.21) Å [3-8] and low energy neutral (100) cleavage planes [4-6] also MgO is a p-type semiconducting material , Moreover, MgO material possesses direct energy ,It is attracting much interest owing to its unique properties such as a high dielectric constant (≈9.8) , and a high break down field of 12 MV/cm [5-7]. Furthermore, MgO has a direct energy band gap in the region of 3.5–5.67 eV [5, 9-11]. It is characterized by high transmission values in the visible range near to 90% [6, 10-13]. In this chapter we have prepared the MgO thin films on glass substrate. The effects of pH on structural, morphological, optical and electrical properties were investigated.

IV .2. Results and discussion

IV.2.1. Structural properties of MgO thin films

The X-ray diffraction (XRD) spectrum of the deposit MgO thin film by spray pyrolysis was presented in **Figure IV.1**. The MgO thin films were prepared at different pH values varied from 2.5 to 10. It was seen that XRD patterns changed with the pH values. We have observed that all diffraction peaks of MgO thin films were observed at the diffraction angle of $10°<2\theta<90°$ on the XRD spectrum. These diffraction patterns have cubic (MgO) structures in the (200) and (220) plane at pH: 2.5, (111), (200) and (220) at pH: 5, (200) and (220) at pH: 6.8, (200) and (220) at pH: 8.30, (111) (200) and (220), at pH: 10. The XRD spectrum of sprayed MgO thin films has matched the structure of MgO thin films is cubic structure. It clearly exhibits the peaks at angles, 36.93°, 42.90°, 62.29°, 74.67° ,and 78.61° correspond to (1 1 1), (2 0 0), (2 2 0), (3 1 1), and (2 2 2) planes (JCPDS No. 01-078-0430), planes and no diffraction peaks of other compounds were observed. The diffraction peaks were strong and sharp which indicated that the prepared samples had good crystallinity. A strong peak observed at 42.92° with the reflection plane of (200) confirms the magnesium oxide phase. The XRD result (**See Figure IV.1**.) revealed that the MgO thin film deposited in the acidic medium and neutral medium was also in the basic medium, which it's indicating that the crystallinity of MgO thin films were improved. It

can be seen that the crystal structure of the films was affected strongly by the pH values. These values are shown in.**Table IV.1.**

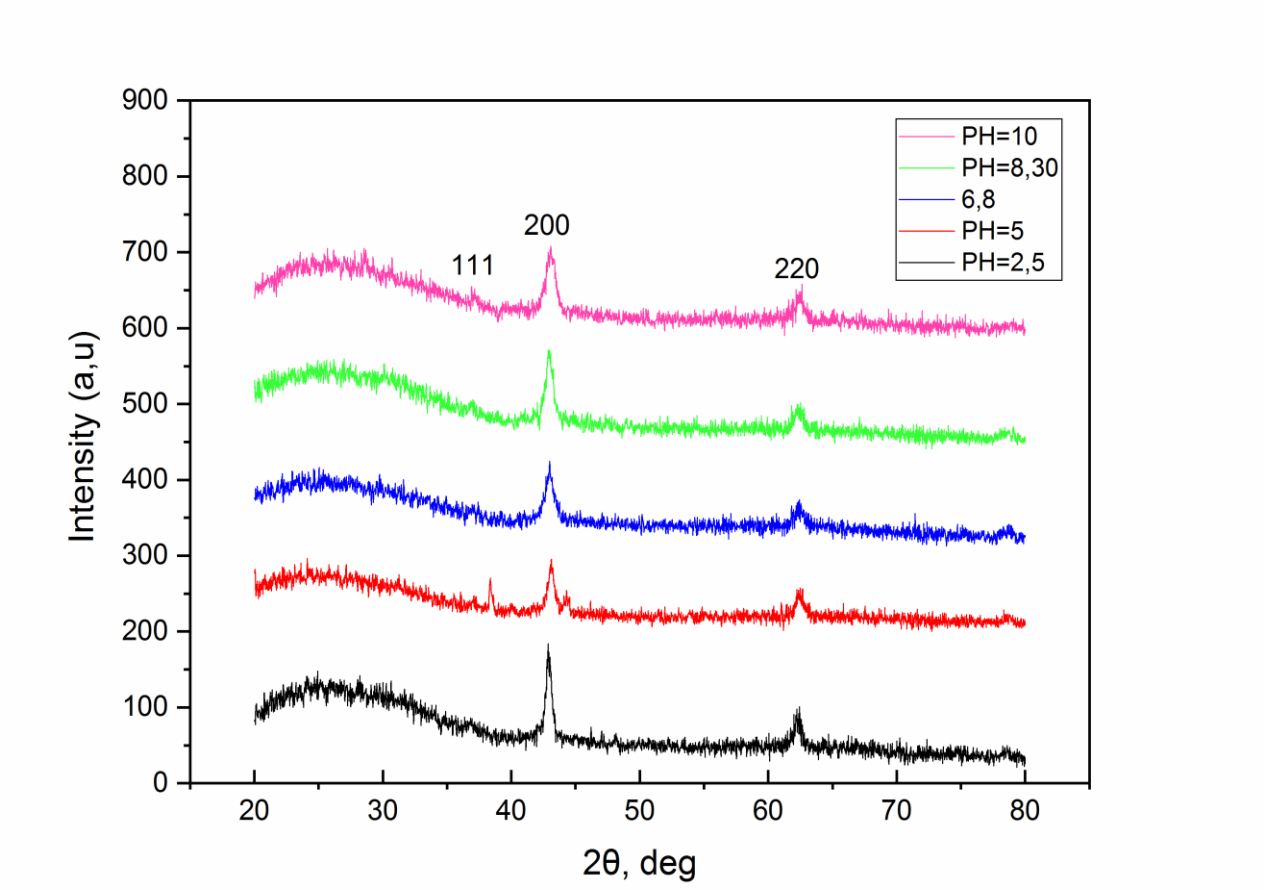

Figure IV.1:XRD patterns of MgO thin films deposited on glass substrates at different solution pH.

Table IV.1. The structural parameters of MgO films corresponding to (200) plane.

pH	Preferred Plane (hkl)	Standard 2θ (°)	The Observed 2θ (°)	Standard d (Å)	The Observed d_{hkl} (Å)	JCPDS Card No. 01-078-0430
2.5	200		42.88		2,10731	
5	200		43,06		2,09897	
6.8	200	42 ,90	42,94	2,10615	2,10594	061325
8.30	200		42,92		2,10044	
10	200		43,03		2,09951	

The crystallite size (D) was estimated from the FWHM of the high intense peaks, namely the one corresponding to (200) crystallographic plane, using the Debye–Scherer formula : [14]

$$D_{(hkl)} = \frac{0.9\lambda}{\beta \cos\theta} \qquad \textbf{(IV.1)}$$

Where 'θ' is Bragg diffraction angle, 'λ' is X-ray wavelength (λ=1.5406 Å); 'k' is shape factor (0.9); 'β' is the width of half maximum of the diffraction peak.

The pH meters have an influence on both the crystallite size and the crystallinity of the nanoparticles. From these calculations, it is observed that the crystallite size is decreased from 16.73 nm to 9.92 nm by increasing the pH level of the solution due to the increase of the FWHM value. These values are shown in **Table IV.2.**

Table IV.2: Crystallite sizes, dislocation density and strain values of MgO thin films extracted from XRD analysis.

pH	FWHM (β°)	D (n.m)	Lattic a	Strain ($\varepsilon x10^{-3}$)	Dislocation density (δ x10^{15})
2.5	0.51	16,73	4,21	2,07	3,57
5	0,53	16,10	4,19	2,15	3,85
6.8	0,81	10,53	4,20	3.29	9,01
8.30	0,67	12,73	4,21	2.7	6.17
10	0,86	9,924	4,20	3.49	10.1

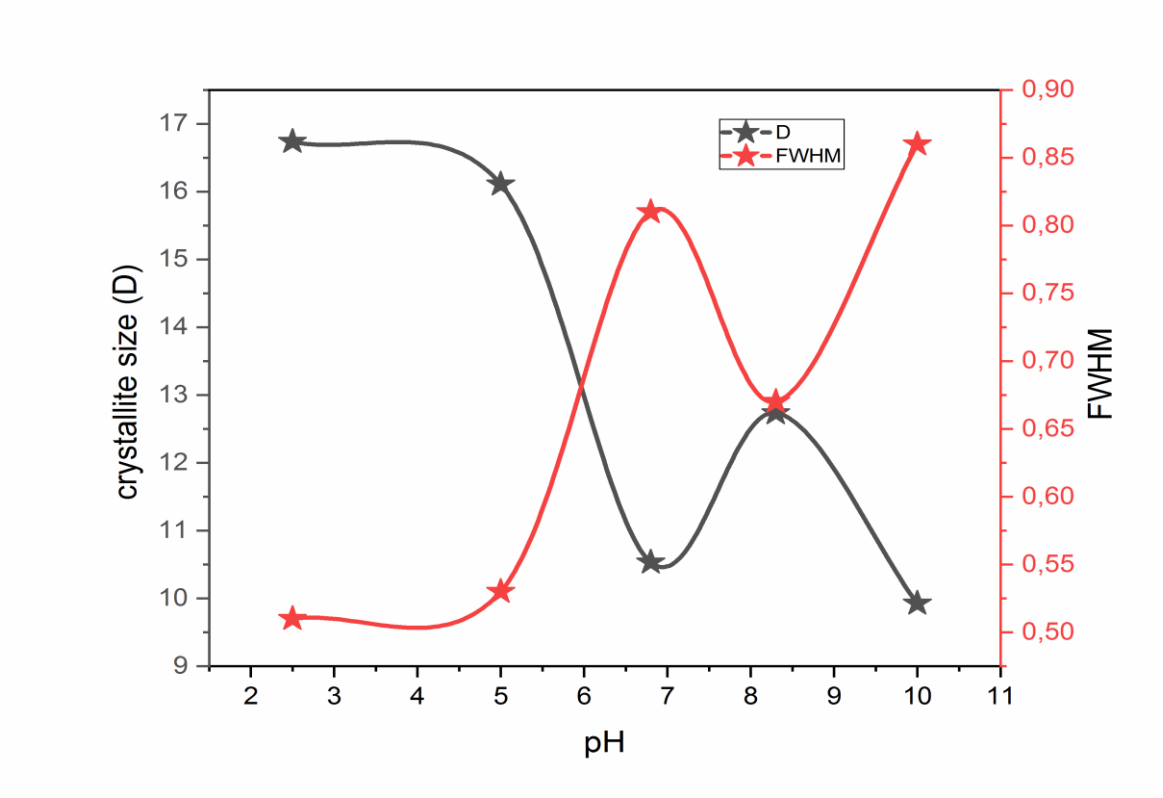

Figure IV.2: Crystallite size and FWHM of MgO thin film as a function of the different solution pH.

The pH of the solution is responsible for controlling the supersaturating and eventually the crystallite size of the crystallizing species. The solution may become supersaturated when increasing the pH of the solution. Supersaturating is critical because it is a driving force for crystal nucleation and growth. At higher supersaturating, crystal nucleation dominates crystal growth, ultimately resulting in smaller crystals. This result has a good agreement with another researcher [15].

Elsewhere the crystal lattice parameters for the cubic structure along the (200) at pH: 2.5, (200) at pH: 5, (200) at pH: 6.8, (200) at pH: 8.30 and (200) at pH: 10, (200) plane were calculated by using the formulas given below, and calculated lattice parameter (a) compared with the standard values. It can be seen from **Table IV.2** that lattice constant a change according to pH from 4.21 Å to 4.19 Å, while the diffraction angle 2θ shifted to higher angles with increasing pH values from 2.5 to 10 [16].

$$d^2 = \frac{a^2}{h^2+k^2=+l^2} \quad (\text{ Cubic Structure}) \qquad \textbf{(IV.2)}$$

where, d_{hal} is the interplanar spacing was calculated by Bragg's law ($_{hkl}$ $n\lambda = 2d_{hkl} \sin(\theta_{hkl})$),[17] (h, k, l) is the Miller indices. We have an according to the preferred direction of crystal growth is recorded in **Table IV.1**, where it is clear that they are close to the values of the JCPDS card and calculated lattice parameter a compared with the standard values are listed in **Table IV.2**. It is found that the lattice parameters were slightly different, the change that occurs in interplanar spacing, and this means that d_{hkl}. They are not equal, which in turn leads to the displacement of the atoms from their original position, and thus expansion or compression occurs, that is strain (ε) induced in powders as a result of the crystal defects and distortion was estimated using the relation. (**See Table IV.2**).

$$\varepsilon = \beta/4\tan\theta \text{ [18]} \qquad \textbf{(IV.3)}$$

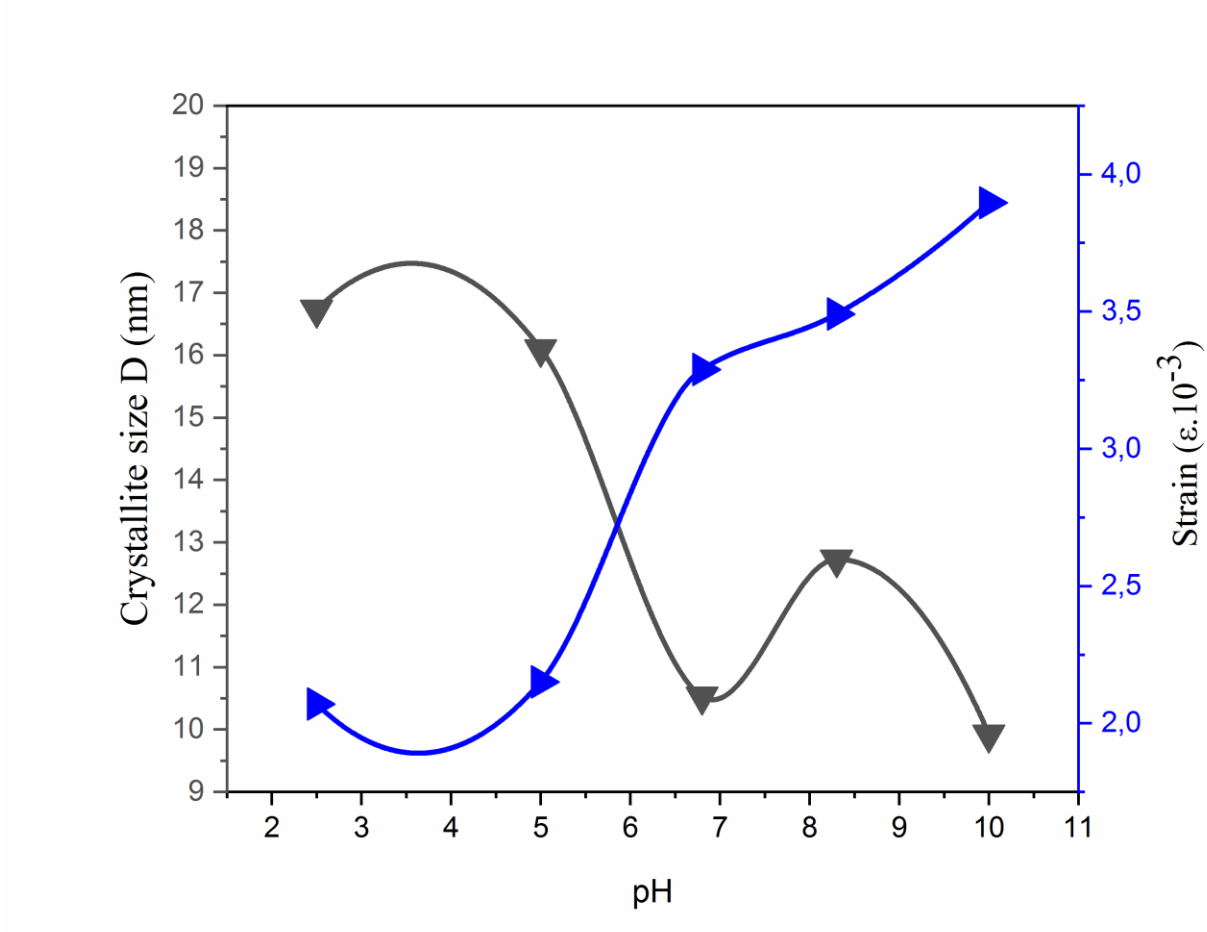

Figure IV.3: Crystallite size and the strain as a function solution pH

where β is the FWHM and θ is the diffraction angle. From these calculations, it is observed that the lattice strain is increased by increasing the solution pH due to the decrease of crystallite size of the nanoparticles.

The dislocation density (δ) is the dislocation lines per unit area of the crystal can be evaluated from the crystallite size (D) using the following formula [19].

$$\delta = 1/\ D2\ (\text{Lines} / m^2) \qquad \textbf{(IV.4)}$$

It is clear that the dislocation densities increased by increasing the pH values of the chemical solution, As a consequence, crystal defects are increased.

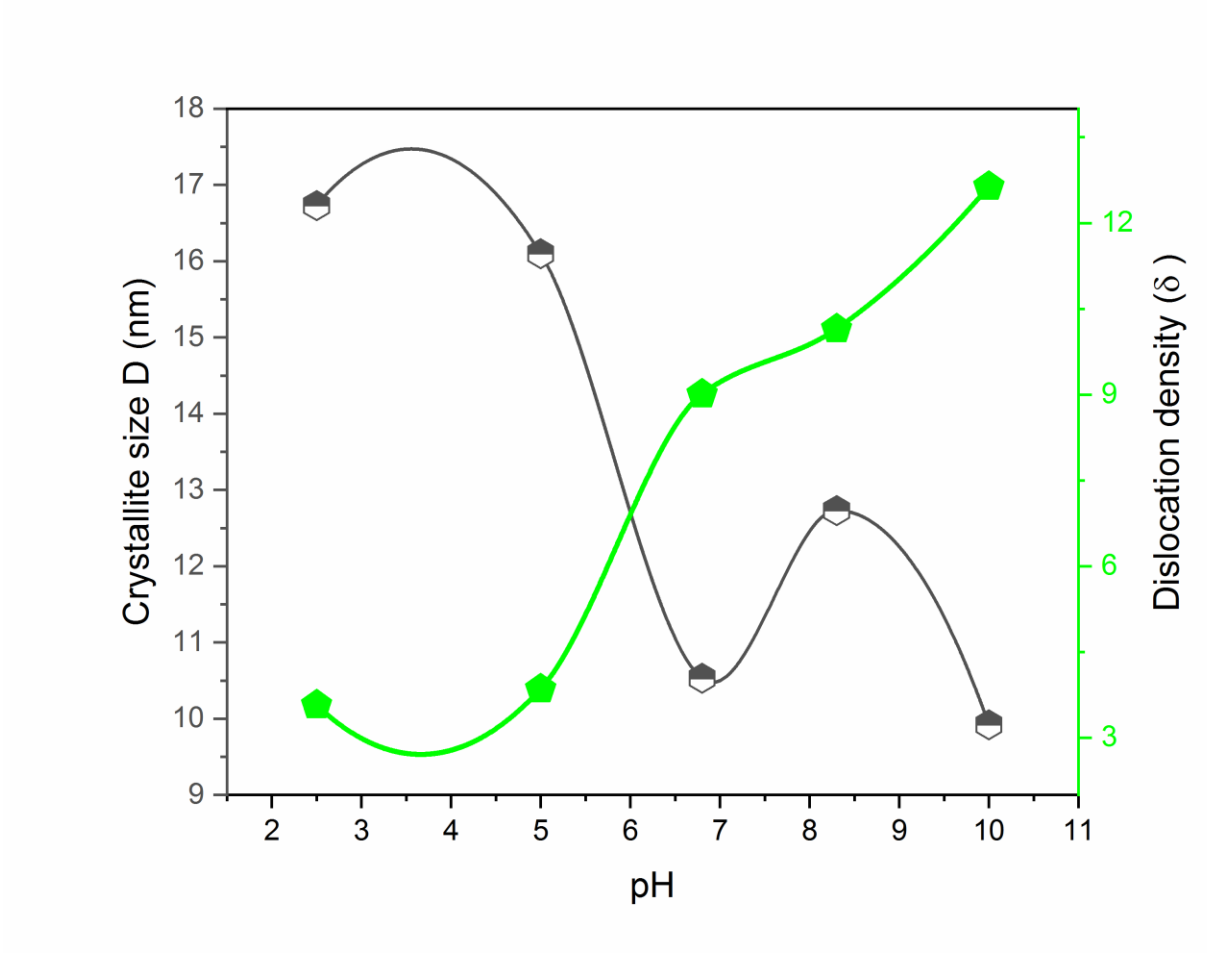

Figure IV.4 : Crystallite size and the strain as function of solution pH.

IV.2.2. Optical properties of MgO thin films

The transmission spectra of the MgO thin films were deposited at different solution pH values. The transmission of the films has studied the relationship between transmittance and wavelength in the range of (300- 1000 nm), it are shown in **Figure IV.5.**The transmittance for all thin films

increases with increasing wavelength in the ultraviolet - visible region. The spectrum shows high transmittance in the visible and low in the ultraviolet region. All deposited films exhibited a average transmittance between 25 % and 78% in the visible region, it is found by various works of literature the in the range 55 to 90 [20,21]. The fundamental absorption edge in the range of 300–350 nm , is probably due to the excitation and the migration of electron transition from the valence band to the conduction band. It can be seen that transmission improved with the increase in pH values (2.5, 8.30, to 10). Conversely the transmittance was decreased wit pH values increased from (5 to 6.80). The absorption edge shifts were clearly visible at wavelengths lower than 400 nm when the variation of absorbance data of MgO thin films was observed. The optical property of MgO thin films is affected by the pH of the solution, as can be shown in **Figure IV.6.** However the optical gap energy was amount of energy necessary to move an electron from the valence band to the conduction band.

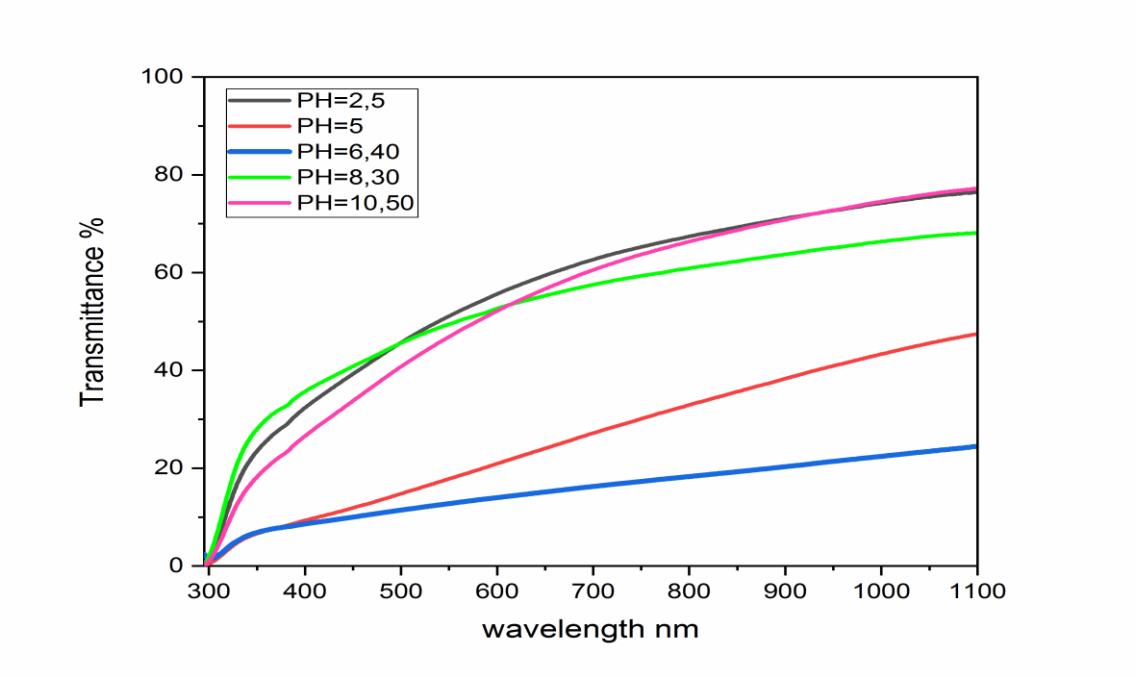

Figure IV.5:Transmittance spectra of MgO thin films with different soltion pH.

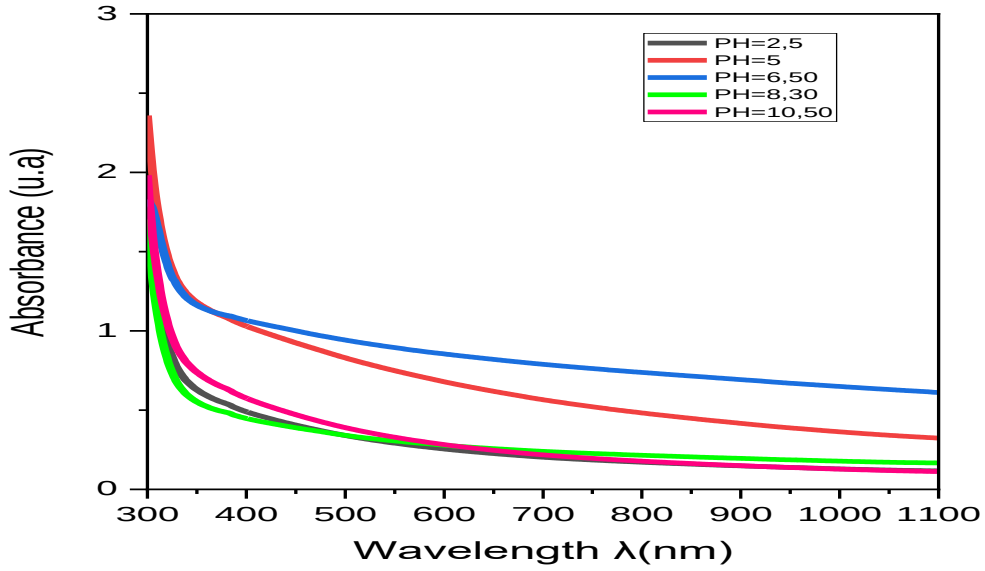

Figure IV.6: Absorbance spectra of MgO thin films with different solutions of pH values.

The optical bandgap Eg is measured by the amount of energy necessary to move an electron from the valence band to the conduction band. It was found using the classical method by extrapolating of the curve at A = 0, Adjust the linear portion of the plot $(Ahv)^2$ against (hv)(**See Figure IV.7**) [22], according to the following equations:

$$A = \alpha\, d = -\ln T \qquad \textbf{(IV.5)}$$

$$(Ah\upsilon)^2 = C(h\upsilon - Eg) \qquad \textbf{(IV.6)}$$

Where A is the absorbance, d is the film thickness; T is the transmission spectra of thin films; α is the absorption coefficient values; C is a constant, hυ is the photon energy and Eg is the band gap energy of MgO thin films (see Table 3). While whereas, the disorder in the MgO thin films was characterized by the Urbach energy (Eu) has been calculated by the following expression[23]:

$$A = A_0 \exp^{(h\upsilon / Eu)} \qquad \textbf{(IV.7)}$$

Where A_0 is a constant hυ is the photon energy and Eu is the Urbach energy, where A_0 a constant hυ is the photon energy. **Figure IV.8** shows the drawn of LnA as a function of photon energy hυ for deducing the Urbach energy.

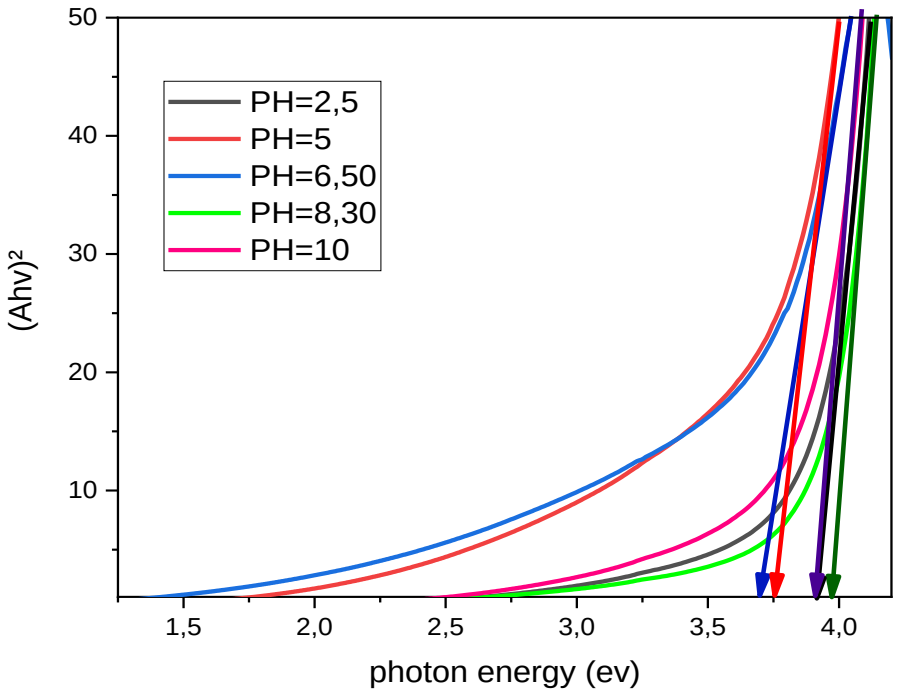

Figure IV.7: Plots of (Ahν) ^{2} versus photon energy of MgO thin films deposited at different solution pH.

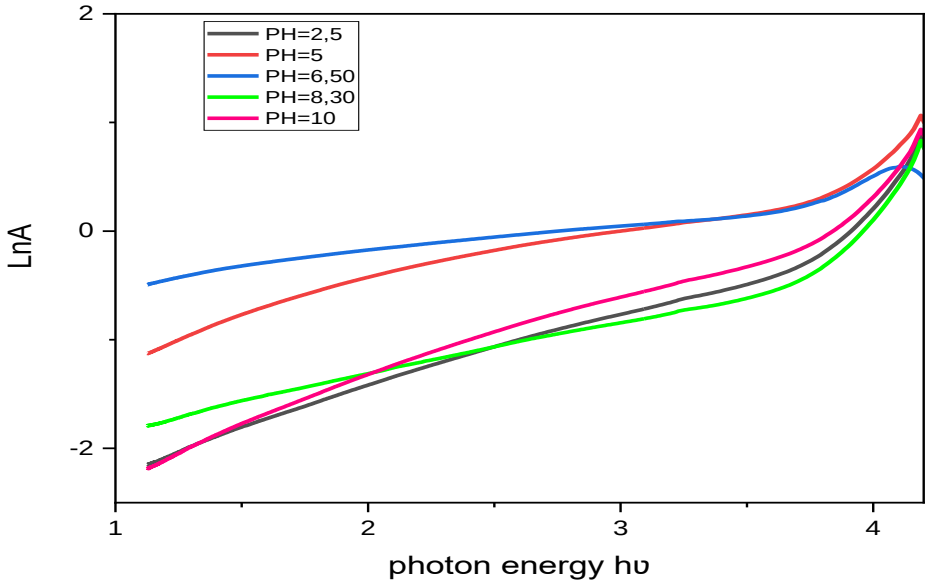

Figure IV.8: Plots of LnA versus photon energy (hν) of MgO thin films deposited at different solution pH.

Table IV.3. Summarizes the calculated optical band gap energy and Urbach energy for pH=2.5, 5, 6.8, 8.3,10. The energy (Eg) decreases between 3.9 to 3.70 eV, on the other hand, also the Urbach energy increases from 398 to 400 with increasing the pH of MgO thin films. except for the pH of solution 8.3 The bandgaps obtained are higher than the reported values, The higher bandgaps could be attributed to quantum effects caused by the orderly arrangement of the MgO structure[24]. Even so the decrease in the band gap can be due to the influence of various factors such as grain size, structural parameters, carrier concentration, presence of impurities, and lattice strain [25].

Table IV.3. The variation of the band gap energy Eg and the Urbach energy Eu of MgO thin film at various pH values.

pH of solution	Energy band gap (eV)Eg	Urbach energy Eu
2.5	3.91	0.398
5	3.76	0.505
6.80	3.70	0.953
8.30	3.97	0.396
10	3.89	0.472

IV.2.3. The Morphology Properties of MgO Thin Films

The SEM characterization was used to examine the surface morphology and overall grains distribution of the samples. Figure 9 (a-e) shows the SEM images, and **Figure IV.9** displays the EDX spectra of MgO films deposited at (a) pH = 2.5, (b) 5, (c) 6.8, (d) 8.30, and (e) 10, respectively. Through many experimental and theoretical studies the nucleation kinetics over films governed by random nucleation and process growth, as well as the extent of agglomeration, Affect the distribution and grain size of nanocrystals. The size, shape, also morphology of MgO thin films are strongly influenced by the pH of the precursor solution, as can be seen, the growth of elaborated films changes with the pH of the solution[15]. At pH = 2.5, a diversity of agglomerated grains shapes as a surface was found, illustrating that our film's surface is porous and rough. Were observed at PH= 5 and 6.80 the grains become nearly spherical and bigger. Otherwise, the pH increased to pH =10, showing spherical grains and smaller.

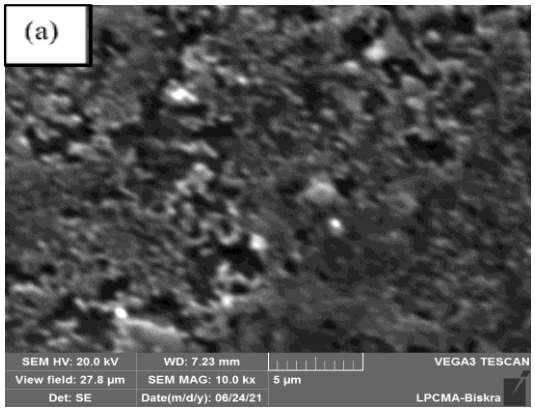
(a)
SEM HV: 20.0 kV
WD: 7.23 mm
VEGA3 TESCAN
View field: 27.8 µm
SEM MAG: 10.0 kx
5 µm
Det: SE
Date(m/d/y): 06/24/21
LPCMA-Biskra

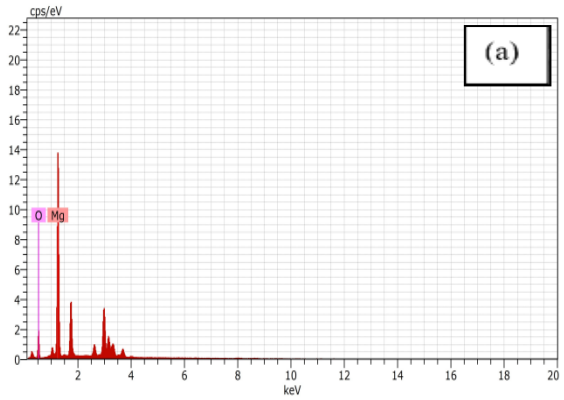
cps/eV
(a)
O
Mg
keV

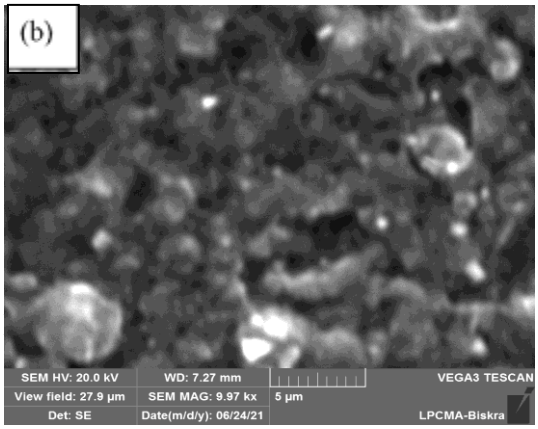
(b)
SEM HV: 20.0 kV
WD: 7.27 mm
VEGA3 TESCAN
View field: 27.9 µm
SEM MAG: 9.97 kx
5 µm
Det: SE
Date(m/d/y): 06/24/21
LPCMA-Biskra

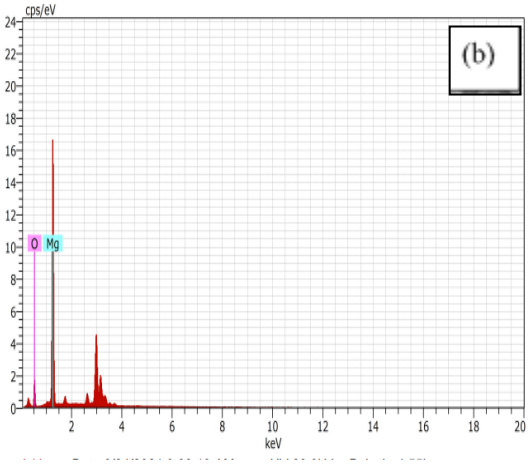
cps/eV
(b)
O
Mg
keV

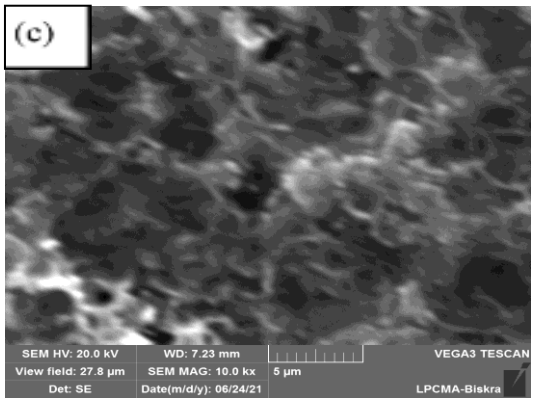
(c)
SEM HV: 20.0 kV
WD: 7.23 mm
VEGA3 TESCAN
View field: 27.8 µm
SEM MAG: 10.0 kx
5 µm
Det: SE
Date(m/d/y): 06/24/21
LPCMA-Biskra

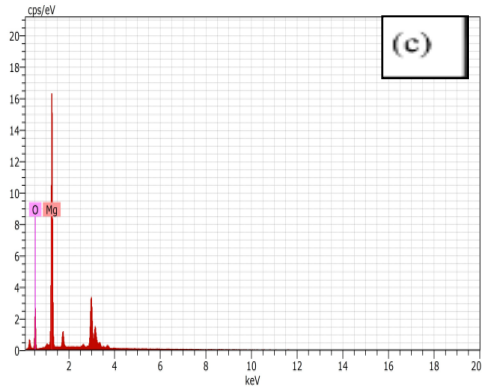
cps/eV
(c)
O
Mg
keV

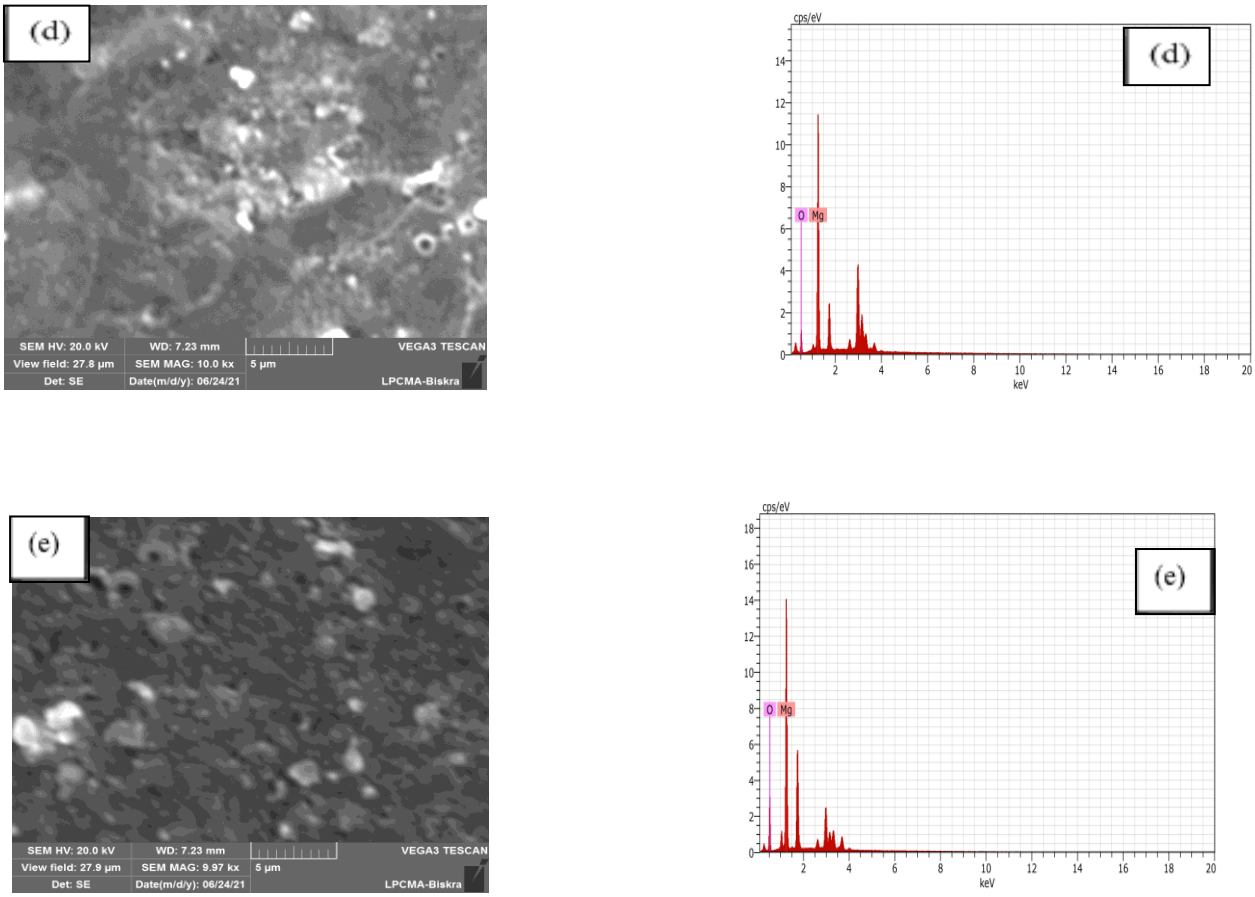

Figure IV.9: SEM images and EDX spectra of MgO thin films prepared at (a) pH = 2.5, (b) 5.0, (c) 6.80, (d) 8.30 and (e)10.

All EDX spectra identify the presence of Magnesium and Oxygen in the deposited films. Also the analyses the atomic percentage of the Mg and O compounds are presented in **Table IV.4**. As can be seen, the atomic percentages of Mg and O elements vary with solution pH.

Table IV.4: The results of quantitative elemental analysis of MgO thin films.

pH values	**Elements**	**Atomic percentage**
2.5	Mg O	63.52 36.48
5	Mg O	68.40 31.60
6.80	Mg O	59.94 40.06

8.30	Mg O	69.73 30.27
10	Mg O	54.49 45.51

IV.2.4: The Electrical Properties of MgO Thin Films

The electrical properties of the obtained MgO thin films was measured as a function of pH values by using four-probe techniques at room temperature. For measurement of sheet resistance (Rsh); the current (I) is applied between the outer two leads and the potential difference (V) is measured across the inner two probes [17]. Since negligible contact and spreading resistance are associated with the voltage probes, one can obtain a fairly accurate estimation of Rsh using the following relation:

$$R_{SH} = \frac{\pi \quad V}{\ln(2) I} \qquad \textbf{(IV.8)}$$

Where, V is the voltage and I is the current.

Table IV.5 and **Figure IV .10** give the Rsh values of MgO thin films as a function of the pH solution. As can be seen that the sheet resistance of MgO thin films were found in increases with increasing the pH solutions from 2 to 10. The resistance low at pH=2.5 may be attributed to the presence of more ions Mg in a solution because increases the solubility of increases in the acidic solution, therefore, the degree of crystallinity increased for magnesium oxide thin films. However, with the increase in pH solution for 8.30 to 10.30 (after addition of NaOH into the prepared solution of magnesium oxide), the solubility is decreased in a more basic solution, and the resistance rises which leads to an increase in vacancy defects[26].

Table IV.5: The variation Resistance Sheet as function pH solution for Mgnesium oxide thin films.

pH	2	5	6.80	8.30	10
Resistance Sheet (ohm/sheet)	1,27E+03	1,04E+04	7,44E+03	1,24E+04	1,69E+04

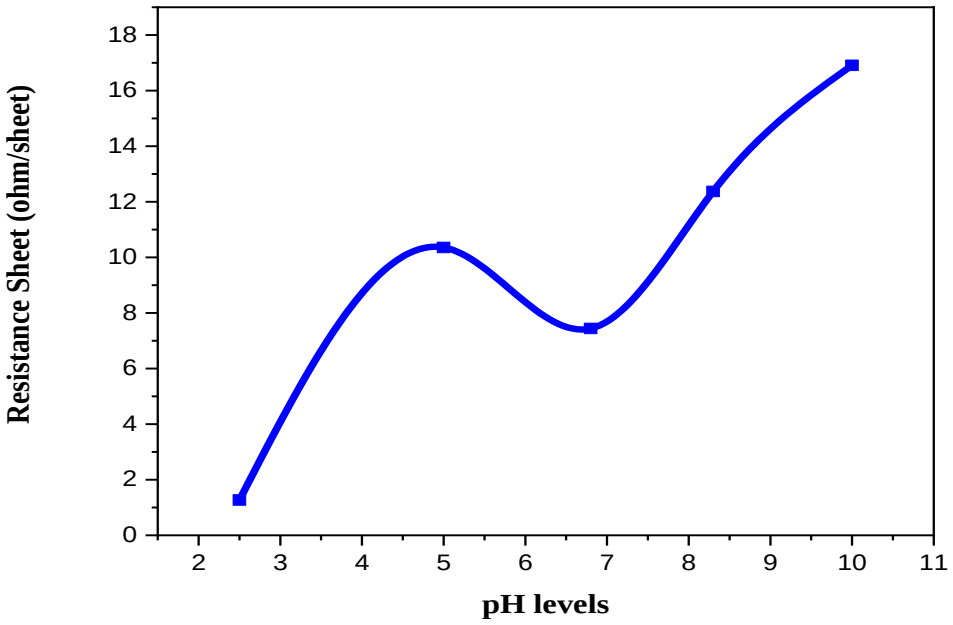

Figure IV.10: The variation Resistance Sheet as function pH solution for Mgnesium oxide thin films.

IV.3.Conclution

We concluded that the MgO Thin Films have been grown on glass substrates at 450°C by various pH solution values (2.5; 5; 8.3 and 10 of pH). The MgO thin films have a strong preferential crystallinity with a cubic structure for a high (200) phase, the minimum value of crystallite size 9.9 nm is attained of deposit MgO thin film at 450 °C with 10 of pH. The optical transmission spectra showed all the sprayed MgO thin films are transparency within the visible wavelength region. The band gap of MgO thin films decreases from 3.91 to 3.7 eV as the pH increases from 2.5 to 6.8, and the urbach energy was increased. The surface morphology by SEM

was indicated that the MgO prepared with pH= 5 and 6.80 the grains become nearly spherical and bigger, and for the pH increased to pH =10, showing spherical grains and smaller, this may be when coalescence occurs. The thin film obtained with 2.5 of pH has a lower electrical resistance.

References

[1] Z. Bazhan, F. E. Ghodsi, and J. Mazloom, "Effect of stabilizer on optical and structural properties of MgO thin films prepared by sol – gel method," vol. 36, no. 5, pp. 899–905, 2013.

[2] O. Diachenko and D. Kurbatov, "Structural Properties of Magnesium Oxide Thin Films Deposited by Spray Pyrolysis Technique," no. January, 2018.

[3] H. Zulkefle, L. N. Ismail, R. A. Bakar, and M. R. Mahmood, "Molar Concentration Effect on MgO Thin Films Properties," pp. 468–471, 2011.

[4] A. M. E. Raj, L. C. Nehru, M. Jayachandran, and C. Sanjeeviraja, "Spray pyrolysis deposition and characterization of highly (100) oriented magnesium oxide thin films," vol. 875, no. 9, pp. 867–875, 2007.

[5] O. V Diachenko, A. S. Opanasuyk, D. I. Kurbatov, and N. M. Opanasuyk, "Surface Morphology , Structural and Optical Properties of MgO Films Obtained by Spray Pyrolysis Technique," vol. 130, no. 3, 2016.

[6] M. Tlili *et al.*, "Synthesis and characterization of mgo thin films obtained by spray technique for optoelectronic applications," *Nanomaterials*, vol. 11, no. 11, pp. 1–14, 2021.

[7] N. F. Chayed, N. Badar, R. Rusdi, and N. Kamarulzaman, "Optical Band Gap Energies of Magnesium Oxide (MgO) Thin Film and Spherical Optical Band Gap Energies of Magnesium Oxide (MgO) Thin Film and Spherical Nanostructures," no. March 2016, 2011.

[8] Z. Tang and L. Shi, "Preparation of nano-MgO using ultrasonic method and its characteristics," vol. 33, pp. 15–20, 2008.

[9] G. Balakrishnan, R. Velavan, K. Mujasam Batoo, and E. H. Raslan, "Microstructure, optical and photocatalytic properties of MgO nanoparticles," *Results Phys.*, vol. 16, p. 103013, 2020.

[10] S. Valanarasu, V. Dhanasekaran, M. Karunakaran, T. A. Vijayan, R. Chandramohan, and T. Mahalingam, "Microstructural, optical and electrical properties of various time annealed spin coated MgO thin films,".

[11] D. Guichaoua, A. Zawadzka, A. Korcala, J. Strzelecki, P. Trzaska, and B. Sahraoui, "Optical properties of MgO thin films grown by laser ablation technique," pp. 1–12, 2016.

[12] Y. Wu, X. Yang, J. Li, K. V Rao, and L. Belova, "Solution processed room temperature ferromagnetic MgO thin films printed by inkjet technique," vol. 196, pp. 388–391, 2017.

[13] H. Cui, X. Wu, Y. Chen, and R. I. Boughton, "Synthesis and characterization of mesoporous MgO by template-free hydrothermal method," *Mater. Res. Bull.*, vol. 50, pp. 307–311, 2014.

[14] A. Pandey, S. Dalal, S. Dutta, and A. Dixit, "Structural characterization of polycrystalline thin films by X-ray diffraction techniques," *J. Mater. Sci. Mater. Electron.*, vol. 32, no. 2, pp. 1341–1368, 2021.

[15] A. G. Habte, F. G. Hone, and F. B. Dejene, "Effect of solution pH on structural, optical and morphological properties of SnO2 nanoparticles," *Phys. B Condens. Matter*, vol. 580, 2020.

[16] F. M. Tezel and I. A. Kariper, "Effect of pH on optic and structural characterization of chemical deposited AgI thin films," *Mater. Res.*, vol. 20, no. 6, pp. 1563–1570, 2017.

[17] V. G. Krishnan, P. Elango, V. Ganesan, and P. Sathish, "pH deeds on structural, optical, electrical and gas sensing performance of TiO2 nanofilms by automated nebulizer spray pyrolysis technique," *Optik (Stuttg).*, vol. 127, no. 23, pp. 11102–11110, 2016.

[18] E. Sup, R. S. Universit, M. Khider, B. Facult, and S. Rahmane, " Elaboration et caractérisation des couches minces de ZnO dopées cobalt et indium .

[19] A. Kariper, E. Güneri, F. Göde, and C. Gümüş, "Effect of pH on the physical properties of CdS thin films deposited by CBD," *Chalcogenide Lett.*, vol. 9, no. 1, pp. 27–40, 2012.

[20] O. V. Diachenko, A. S. Opanasuyk, D. I. Kurbatov, and H. Cheong, "Investigation of optical properties of magnesium oxide films obtained by spray pyrolysis technique," *Proc. Int. Conf. Adv. Optoelectron. Lasers, CAOL*, pp. 31–33, 2016.

[21] J. Bian, X. Li, X. Gao, and W. Yu, "Growth and Characterization of High Quality MgO Thin Films by Ultrasonic Spray Pyrolysis," vol. 283, no. 2005, pp. 1171–1174, 2007,

[22] Y. Aoun, R. Meneceur, S. Benramache, and B. Maaoui, "Sprayed NiO-Doped p-Type

Transparent ZnO Thin Films Suitable for Gas-Sensing Devices," *Phys. Solid State*, vol. 62, no. 1, pp. 131–136, 2020.

[23] E. Procedure, "The Crystalline Structure, Optical and Conductivity Properties of Fluorine Doped ZnO Nanoparticles A. Diha 1,* , S. Benramache 2 , L. Fellah 3 2," vol. 11, no. 3, pp. 5–9, 2019.

[24] P. E. Agbo, P. A. Nwofe, R. A. Chikwenze, and D. A. Famuyibo, "Effect of pH on Properties of CoSe Thin Films Deposited by Chemical Bath Technique ," vol. 8, no. 3, pp. 152–156, 2016.

[25] B. Kavitha and M. Dhanam, "The effect of pH adjustments on the structural and optical properties of CIAS thin films," vol. 13, pp. 603–612, 2010.

[26] Rahima Nouadji, " Elaboration and characterization of undoped and doped indium oxide thin layers elaborated by sol gel process for photonic and photovoltaic applications," University Mohamed Khider of Biskra 2022.

CHAPTER V

Influence Of pH On The Properties $Zn_{0.5}Mg_{0.5}O$ Thin Films

V.1. Introduction

The oxide semiconductor has attracted a lot of attention for solar cells, liquid crystal displays, and optical devices [1]. Recently, metal oxide nanoparticles like ZnO and MgO have been studied in nanotechnologies due nanocomposites are great candidates for use in a variety of industrial applications due to their superior mechanical qualities, including their high melting point, low density, low coefficient of thermal expansion, high thermal conductivity, high hardness, and strong chemical stability [2]. The doping of ZnO with magnesium (Mg) to obtain the ternary thin films ZnMgO has been reported. In recent years, ZnMgO with a smaller band gap than MgO has achieved much interest owing to its significant uses in deep ultraviolet optoelectronic detectors [3]. Between the rocksalt structure MgO (7.77 eV) and the wurtzite structure ZnO (3.37 eV), there is a significant band-gap variance in thin films[4,5]. However, the ionic radii of Mg^{+2} (0.57 Å) and Zn^{+2} (0.60 Å) are fairly similar and might alloy if they were to change places in the matrix. In this work we have studied a new materials based on the enhancement of the $Zn_{0.5}Mg_{0.5}O$ thin films, which were synthesized by chemical spray pyrolysis technique on glass using different solution pH values. The structural, optical and Electrical properties have been investigated.

V.2. Results and discussion

V.2.1. Influence of pH on structural properties of $Zn_{0.5}Mg_{0.5}O$ thin films

The XRD spectrum of elaborated $Mg_{0.5}Zn_{0.5}O$ thin films on glass substrates, which are deposited at 450C ° using the Spray pneumatic method formed at various solution pH levels, is presented in **Figure V.1**. The thin films have been prepared at various pH levels of 2.5, 7.10, and 8.30. specifically, there are highly intense peaks corresponding to (2 0 0) and (2 2 0) planes of phase cubic structure for the MgO in all films [6]. On the other hand, for the prepared thin film at a solution of pH=2.5 show up the peaks corresponding to (1 0 0) and (1 0 1) planes accord to the structure wurtzite hexagonal of phase oxide ZnO but are very weaker intense than phase MgO peaks. Because Mg atoms are more active than Zn atoms in reacting with oxygen, phase separation of MgO and ZnO [7] explains Pauling electronegativities of the Mg and Zn atoms to differ (1.31 for Mg is lower than 1.65 for Zn), the Mg atom loses electrons more readily than the Zn atom [8]. That is indicating the two phases living together and that the peaks do not affect each other's position. This process seemed to be a new route to attain various hybrid thin films that can be used in the optoelectronics industry [9]. Conversely, The film deposited at pH values of 7.10 and 8.30 No diffraction peaks of the ZnO

phase is observed, demonstrating that Zn^{2+} ions have successfully entered the MgO lattice [3]. Nevertheless, As the solution pH increased the diffraction peak intensity considering the (2 0 0) plane decreased in indicating that the crystallinity was improved. It can be seen that the crystal structure of the films was affected strongly by the solution pH values of the deposited solution.is caused due to the competition substitution of Zn^{2+} ions into Mg^{+2} ion sites in order to capture more O atoms.

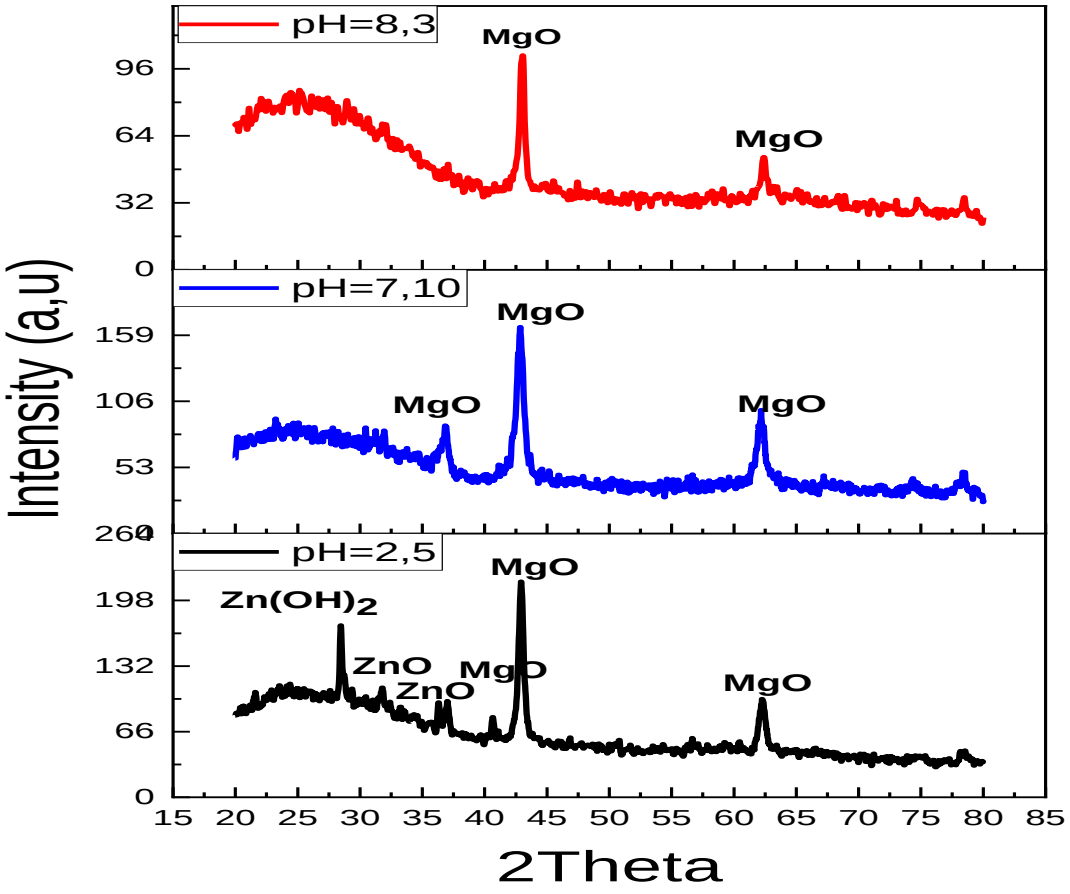

Figure V.1: The XDR of $Zn_{0.5}Mg_{0.5}O$ thin film deposited film deposited at various pH levels.

The crystallite information of the prepare $Zn_{0.5}Mg_{0.5}O$ thin films such as diffraction angle 2**θ**, diffraction picks (h k l), FWHM, the interplanar spacing value d, Lattice constant, crystallite size D, Strain , and Dislocation density was measured as a function of pH levels, it's presented in **Table V.1**. The intensity of the prominent peaks and d spacing values are found to decrease slightly with the rise in pH of $Zn_{0.5}Mg_{0.5}O$ thin films. Also, the calculated

crystallite size of prepared films of the preferred plane (200) by the Debye–Scherer formula [10].

$$D_{(hkl)} = \frac{0.9\lambda}{\beta \cos\theta} \qquad \textbf{(V.1)}$$

These results are tabulated in **Table V.1**, here, the crystalline size crystallite size decreased from 30.98 nm to 18.061 nm of solution pH = 2.5 to 7.10 and then increased to a maximal value of 72.28 for solution pH=8.30. The increased in the crystallite size due to the fact that small crystallites are consumed during crystallization this result has good agreement with another researcher [11] In addition to estimate of the lattice parameter (a) for the $Zn_{0.5}Mg_{0.5}O$ thin films synthesized at various solution pH, can be seen from **Table V.1** that the lattice constant (a) decreases from 4.21 A to 4.20 A. whereas the diffraction angle 2θ changed to higher angles with increasing solution pH values from 2.5 to 8.30.

Table V.1: The crystallite size D, FWHM, Strain and Dislocation density for $Zn_{0.5}Mg_{0.5}O$ thin films prepared at different pH solution.

pH levels	2**θ**	hkl	FWHM	d-spacing(Å)	Lattice parameter (Å)	Crystallite size D(nm)	Dislocation density ***δ*** (lines /m^2)	strain ***ε***
2.5	28.44	(201)	0.1181	3.13758	-	-	-	-
	31.71	(100)	0.4723	2,82155	-	-	-	-
	36.29	(101)	0.1968	2.47538	-	-	-	-
	36.97	(111)	0.2362	2.43106	-	-	-	-
	42.92	(200)	0.2755	2.10692	4.21	30.98	1.04E-03	3.06E-03
	6228	(22 0)	0.3936	1.49073	-	-	-	-
7.10	36.85	(111)	0.4774	2.44254	-	-	-	-
	42.84	(200)	0.4723	2.11079	4.22	18.06	3.07E-03	5.26E-03
	62.20	(220)	0.5510	1.49232	-	-	-	-
8.30	43.07	(20 0)	0.1181	1.10008	4.20	72.28	1. 91E-04	1.31E-03
	62.38	(220)	0.2362	2.48856	-	-	-	-

The strain and dislocation density δ of the films are calculated from the following relation[12].

$$\varepsilon = \beta/4\tan\theta \qquad \textbf{(V.2)}$$

$$\delta = 1/ D2 \ (\text{Lines} / m^2) \qquad \textbf{(V.3)}$$

The estimated values of strain and dislocation density are shown in **Table V.1** and their variations are depicted in **Figure V.2**. According to the result, there is an increasing in the strain and dislocation density at solution pH= 2.5 and 7.10, then showing a decrease at pH= equal to 8.3. Maybe that decrease causes the release of stress in the film due to there being a strong interaction between the substrate and depositing atoms at various pH levels [13], causing dropped inserting atoms Zn in MgO.

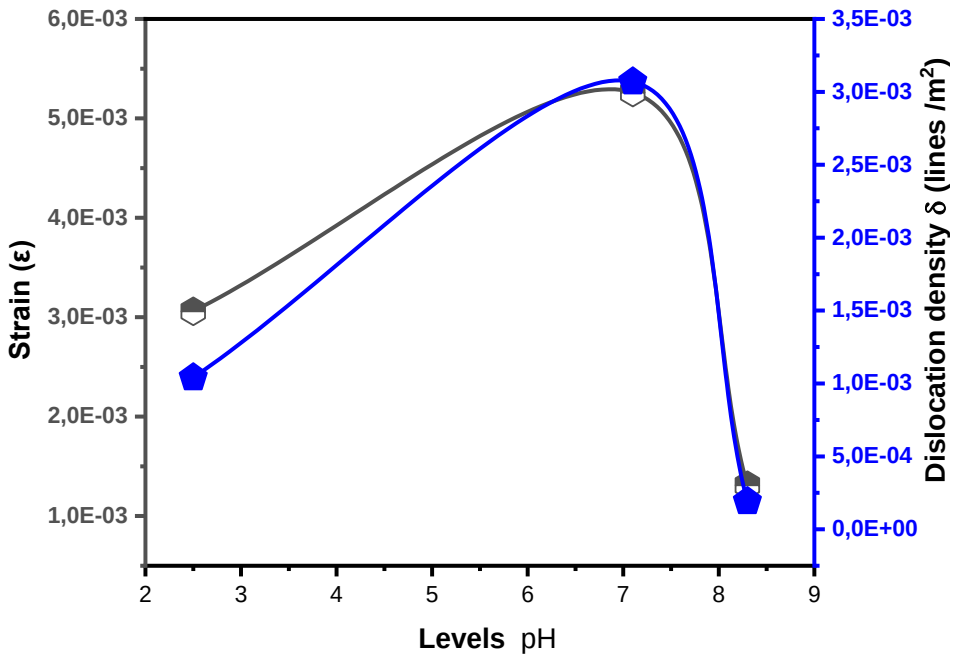

a

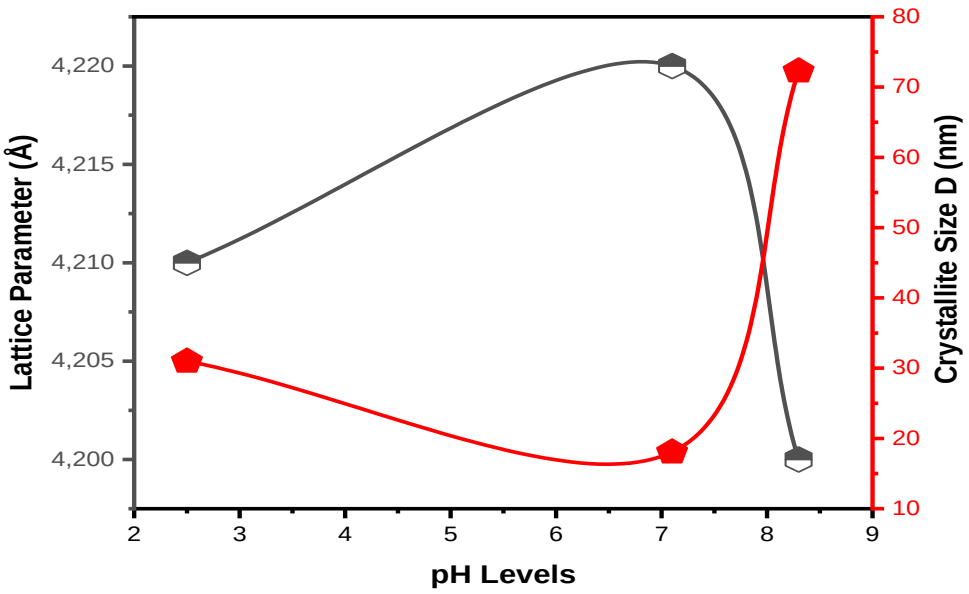

b

Figure V.2: The variation a function of pH levels for Zn $_{0.5}$Mg $_{0.5}$O thin films, a): the dislocation density and Strain, b): the lattice parameters and crystallite size.

V.2.2. Influence of pH on optical properties Zn $_{0.5}$Mg $_{0.5}$O thin films

Figure V.3 presents the transmittance (T) of the deposits fabricated on glass substrates at the temperature 450 C in the range of (300–1100 nm). The optical properties of the $Mg_{0.5}Zn_{0.5}O$ thin films at different pH levels presented various information. The optical transmission was the largest at 55% at pH= 8.30. In the visible region, the transmission values decreased to 22 and 39, at pH = 2.5 and 7.10 (**see Figure V.3**). Clearly, The absence of oxygen, the surface's roughness (surface scattering with the incorporation of Zn^{2+} in MgO affects the transmission, which in turn relies on the crystalline size and shape), and the impurity centers are likely to have an impact on the thin film's transmittance [14].

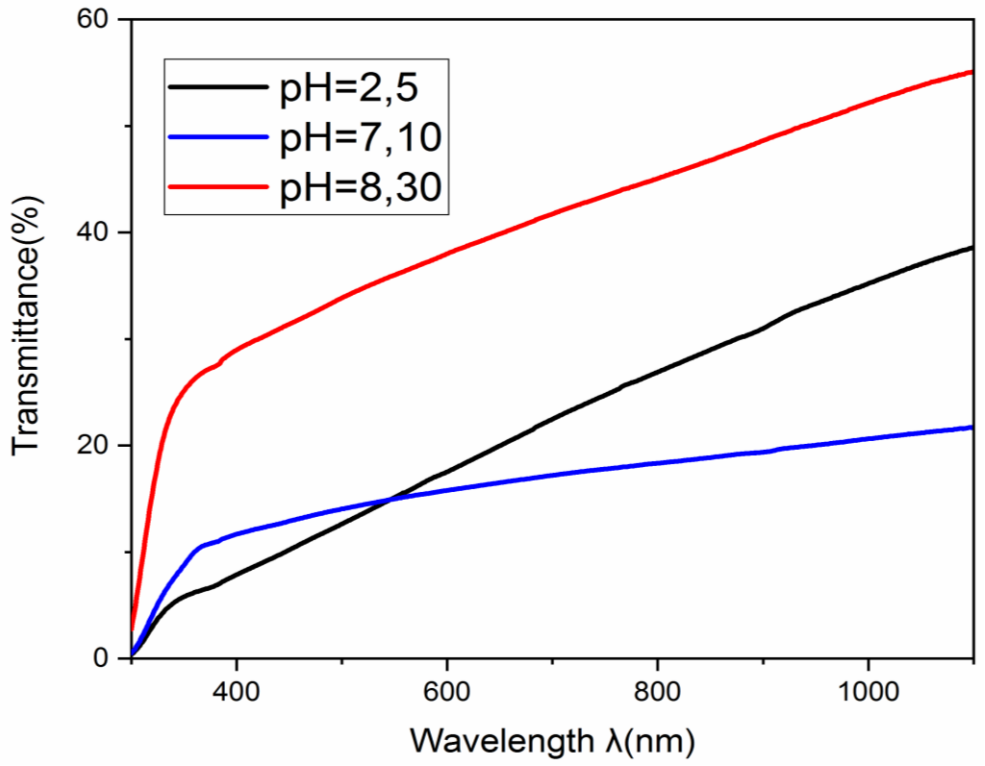

Figure V.3: the variation of transmittance spectra (T) with wavelength (λ) of $Zn_{0.5}Mg_{0.5}O$ thin films at different pH solution.

The optical absorption of the prepared thin films measured for the transmittance, which is dependent on photon energy and the existence of an absorption edge for the wavelength interval of 200–1100 nm. In the visible region, the values of absorption were obtained in the range of 0.25–0.66. The high photo-absorption is evident in the visible light area between 348 and 385 nm and for all pH values. The absorption with respect to the wavelength of films is shown in **Figure V.4**. As a result in the case of high pH film more porous structures in films, where precursor may have a high solubility in the water owing to the pH affecting Mg and Zn ions dissolution and precipitation[15].it can be seen Mg it have oxidation than Zn ions apparently that the absorption value drops as the films pH rises.

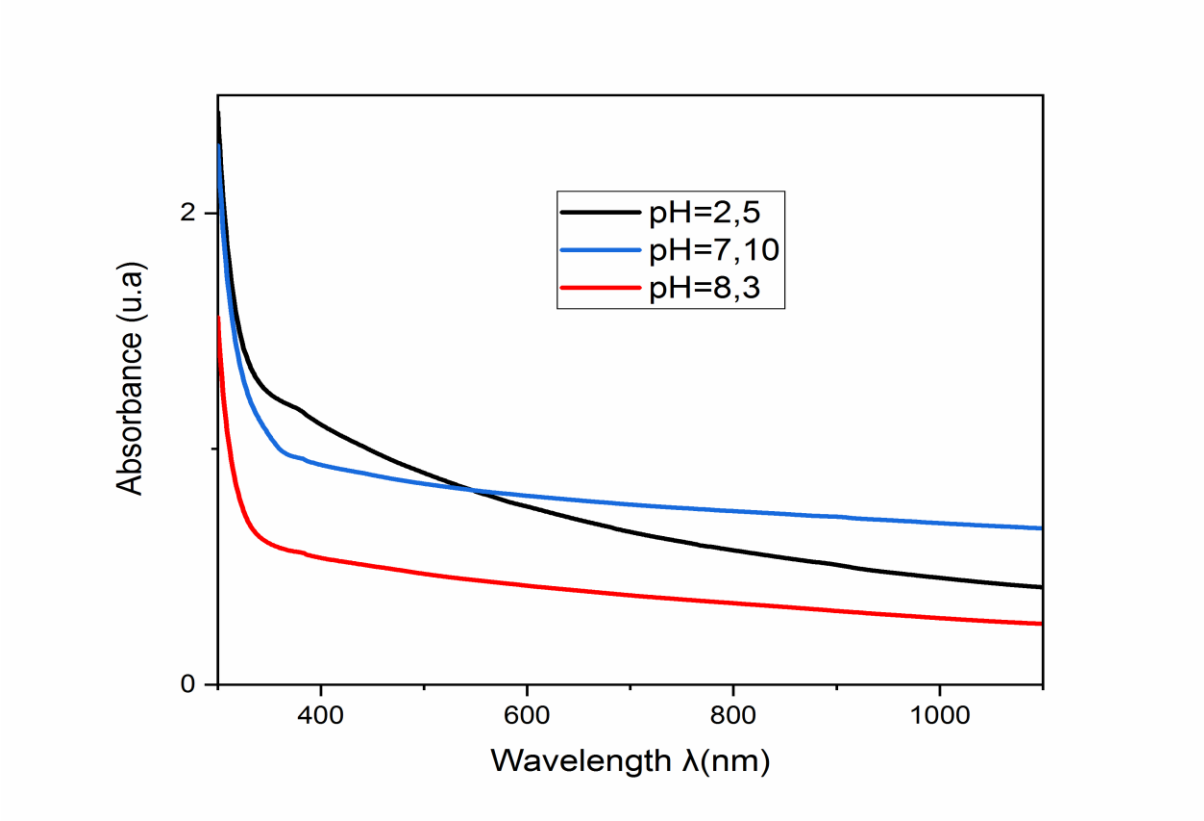

Figure V.4: The relation between absorption and wavelength of deposited $Zn_{0.5}Mg_{0.5}O$ thin films at different pH solution.

V.2.2. a.Energy gap (Eg)

The optical band gap Eg mainly depends on the wave vector and is a critical characteristic of semiconductor thin films. Additionally, optoelectronic devices require it. The fundamental absorption edge, which is also used to determine the optical band gap of the film, permitted electrons to migrate from the valance band to the conduction band [16].

The measurement optical properties such as band gap energy and Urbach energy were affected by the absorbance, which it's presented as a function of photo energy. Starting with the extrapolation of the curve that indicates the variation of $(Ah)^2$ as a function of h, one may measure the optical gap (Eg). The Eg is obtained when the linear region and the h- axis meet. The values of the optical band gap Eg were noticed to increase from 3.77 eV to 4.09 eV while the solution pH rises from 2.50 to 8.30. The literature demonstrates that the crystallite size is related to the change in band gap value, as can be seen well in **Figure V.5**.This evidenced by the Roth effect.

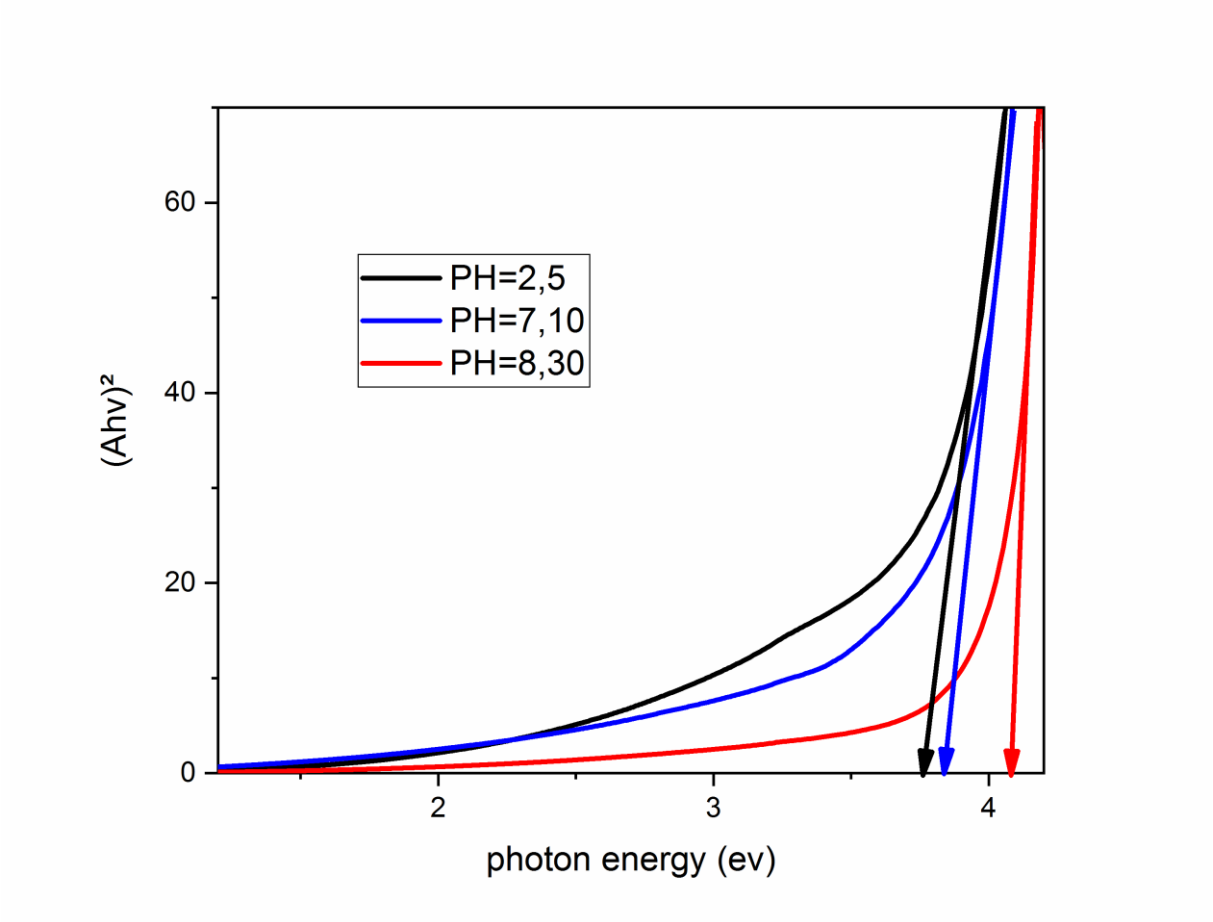

Figure V.5: Plot of $(Ah\nu)^2$ versus $(h\nu)$ of $Zn_{0.5}Mg_{0.5}O$ thin film at different pH solution.

V.2.2. b.Urbach energy

Besides, the presence of a structural defect was calculated as illustrated in the given relation [7]:

$$A = A_0 \exp\left(\frac{h\nu}{E_u}\right) \qquad \textbf{(V.4)}$$

Where A_0 is a constant $h\nu$ is the photon energy and Eu is the Urbach energy. **Figure V.6** shows the drawing of LnA as a function of photon energy hυ for deducing the Urbach energy. We observe a decrease in linear in the Urbach energy Eu from 397 to 321 with an increase in levels of pH.

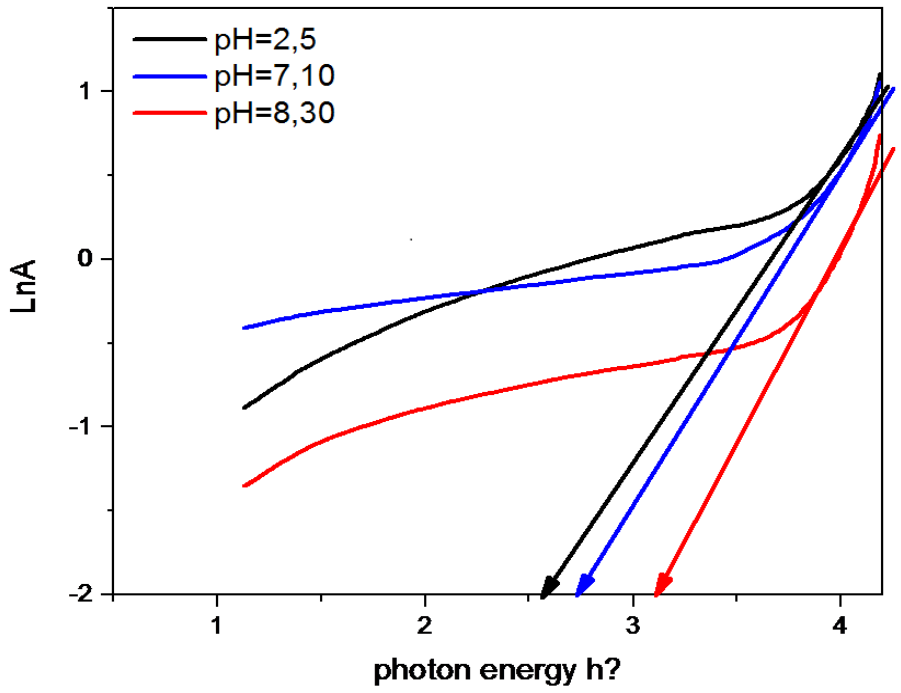

Figure V.6: Plot of (LnA) versus (hν) of $Zn_{0.5}Mg_{0.5}O$ thin films at different pH solution.

The values of Eg and Eu at various pH solutions for the $Zn_{0.5}Mg_{0.5}O$ are listed in **Table** V.2 and Figure V.7 illustrates how pH influences the optical band gap and Urbach energy of thin films the $Zn_{0.5}Mg_{0.5}O$. Moreover, it has been discovered that $Zn_{0.5}Mg_{0.5}O$ thin films' band gap energy gradually rose as the pH solution increased; this result may be attributed to compositional changes that occurred in $Zn_{0.5}Mg_{0.5}O$ thin films, this led to a narrowing of the Urbach tail width[17].

Table V.2: Variation of the optical band gap energy Eg and the Urbach energy of $Zn_{0.5}Mg_{0.5}O$ thin films at different pH solution.

.

PH	Optical gap energy E_g(eV)	Urbach energy E_u (meV)
2.5	3.77	397
7.10	3.83	366
8.30	4.09	321

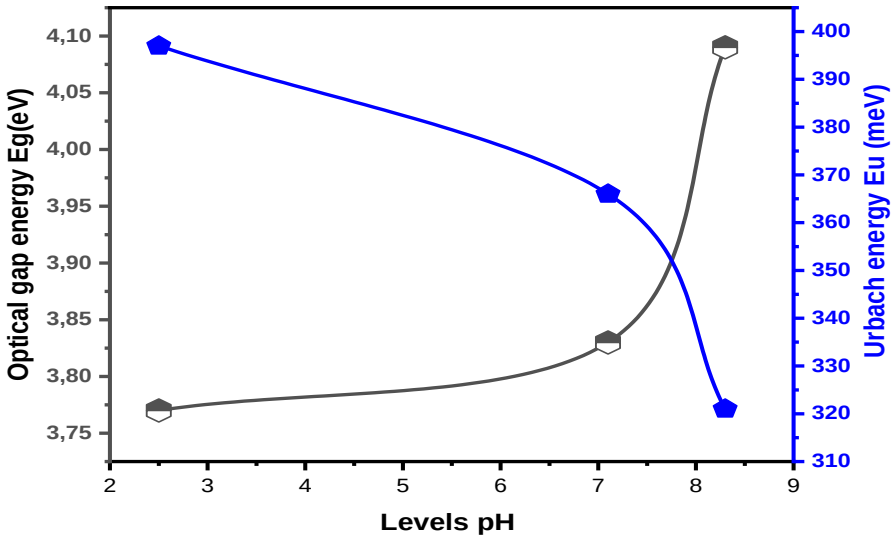

Figure V.7: Variation of the optical band gap energy Eg and the Urbach energy of $Zn_{0.5}Mg_{0.5}O$ thin films at different pH solution.

V.2. 3. FTIR spectrum Of $Zn_{0.5}Mg_{0.5}O$ thin films

Figure V.8 illustrated that FTIR spectroscopy is used to analyze changes in chemical components, impurity content, and interaction between various samples. Fig. 8 shows the FTIR spectra of $Zn_{0.5}Mg_{0.5}O$ thin films synthesized by a pneumatic spray technique recorded in the range of 400-4000 cm-1.T Generally speaking , the metal oxides give absorption bands below 1000 cm–1[18], arising due to the inter-atomic vibrations. he bands at 427 cm−1 correspond to the absorption peaks of the Zn–O bond and verifies the presence of ZnO ,[19] After that, the formation of MgO crystallite is cubic since the absorbance peak is between 1000 and 500 cm^{-1}.[20]. Here, the strong bands located at 768 and 914cm−1 indicate the stretching vibration mode of Mg–O. peaks observed in the spectra at 2923,1588 and 2858 cm−1 are the stretching and bending vibrations of – OH groups[18], which are associated with the adsorbed water on the surface of the ZnO/MgO particles. In the range of 1500–3000 cm–1 the bands due to adsorbed water and hydroxyl groups can be observed in all of the spectra. The intensity gradually decreases as the solution pH increases. It is noted that, this band absorption of pH=2.5 and 8.3 is weaker than pH=7.10 because of the neutral medium. According to the data listed above, a strongly basic medium at pH=8.3 results in the finding of surface hydroxyl groups, which are known to be important to the photocatalytic process.

The active hydroxyl radicals are created when the hydroxyl groups capture holes in activated photocatalysts and then oxidize the adsorbed molecules[21].

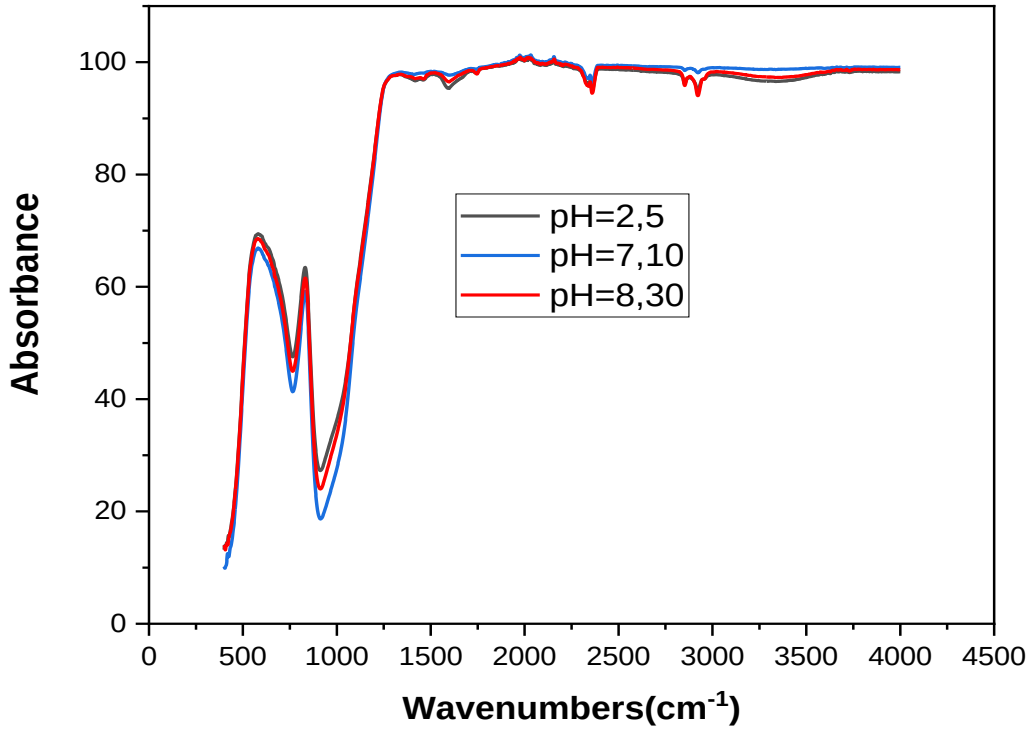

Figure V.8. FTIR absorbance spectra of of Zn $_{0.5}$Mg $_{0.5}$O thin films at different pH solutions.

V.2.4. Influence of pH on Morphological properties Zn $_{0.5}$Mg $_{0.5}$O thin films

The surface morphology of the $Mg_{0.5}Zn_{0.5}O$ thin films prepared using different solutions of pH was studied using the SEM technique, A series of changes in the morphology of the film with different values of pH is observed, that obtained shown in Figure 4 at pH=2.5, Mostly are composed of big grains appear form sphere and rod-like. Otherwise, the film at pH=7.20 has small grains with uniform distribution and is dense which is in good agreement with the decrease in crystallite size (18.06 nm).On the other hand, for the value of pH=8.30, the grains become nearly spherical and bigger and The distributions of grains are of irregular shape throughout all the regions. Small dark areas represent porous in the film and the presence of it will increase the electrical resistivity[22].

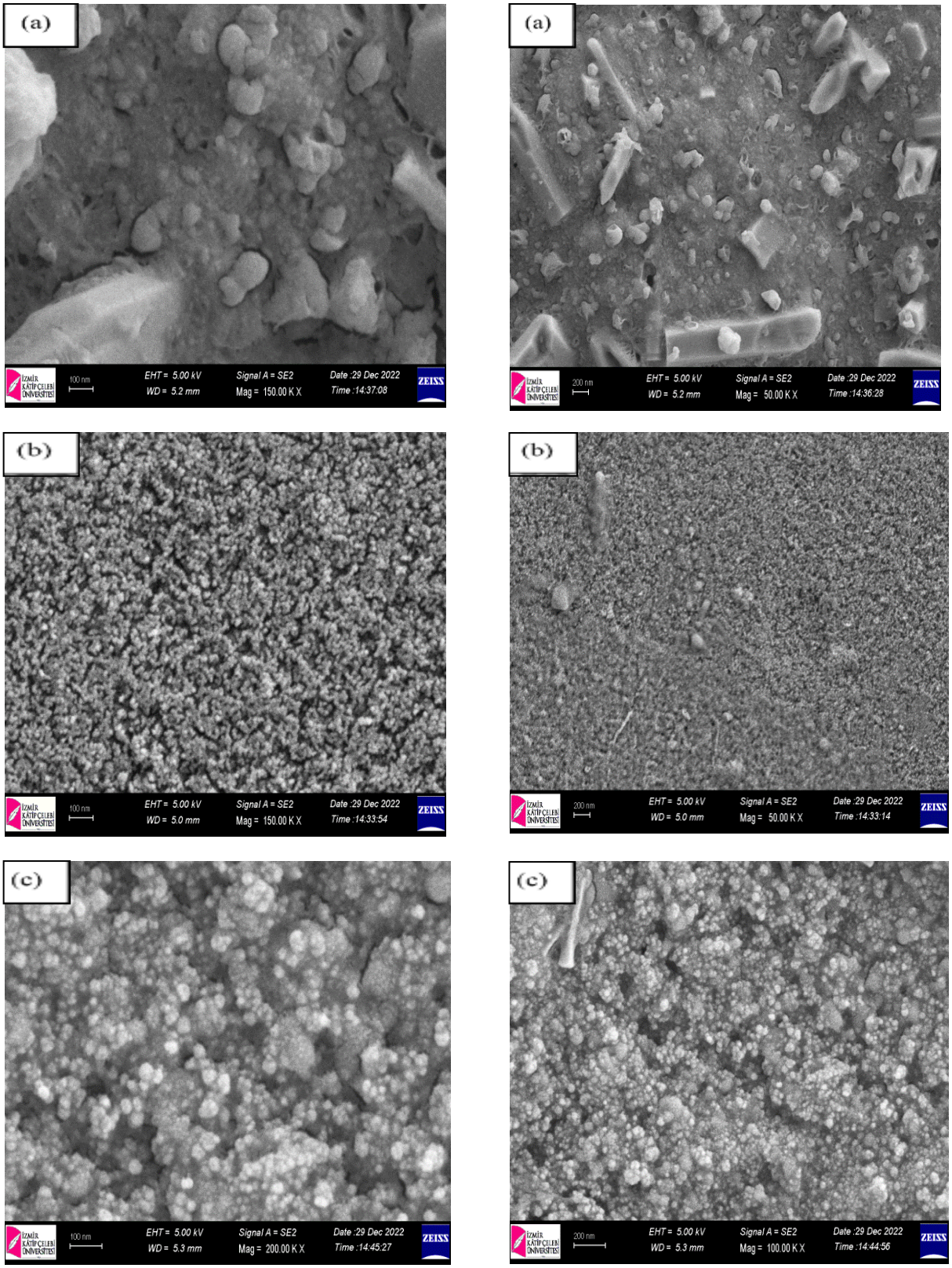

Figure IV.9: SEM images of $Zn_{0.5}Mg_{0.5}O$ thin films prepared at (a) pH = 2.5, (b) 6.80, (c) 8.30.

V.2.2. Influence of pH on Electrical properties Zn $_{0.5}$Mg $_{0.5}$O thin films

Figure 6 shows the variation of the resistance Sheet of the $Mg_{0.5}Zn_{0.5}O$ thin films as a function of solution pH. As can be seen, the resistance Sheet value decreases slightly (1,28E+06 to 1,22E+06 ohm/sheet) at pH =2.5 to pH= 7.10. on the other side at pH=8.30 the resistance Sheet value increase (2,31E+06 ohm /sheet).can be explained by results in an increase in oxygen vacancies and electrons due to a decrease in the ions Mg^{2+} and Zn^{+2} , special last caused by the presence of ions ^{-}OH in solution. in solution, a consequent band gap widening (3.77 to 4.09) As shown in the **Figure V.5.**

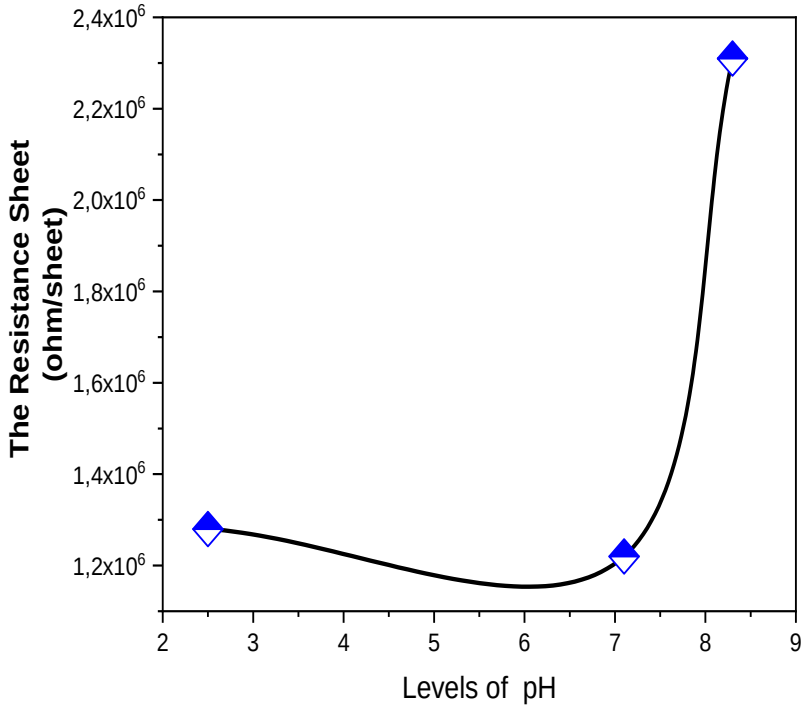

Figure V.8. The resistance Sheet of of Zn $_{0.5}$Mg $_{0.5}$O thin films at different pH solutions.

V. 3.Conclusion

$Mg_{0.5}Zn_{0.5}O$ thin films have been grown on glass substrates by spray pyrolysis technique at different pH solution values (2.5; 7.10 and 8.30 of pH) was successfully investigated. The Zn $_{0.5}$Mg $_{0.5}$O thin films were observed in high crystallinity with a cubic structure with a strong preferential, the maximum value of crystallite size 72.28 nm is attained of deposit $Mg_{0.5}Zn_{0.5}O$ thin film at 450 °C with 8.30 of pH. The optical transmission spectra

showed all the sprayed $Mg_{0.5}Zn_{0.5}O$ thin films are transparent within the visible wavelength region. The band gap of $Mg_{0.5}Zn_{0.5}O$ thin films increases from 3.77 to 4.09 eV as the pH increases, The Urbach energy values decreased as the pH increased from 397 to 321 meV. The FTIR absorbance spectra measurements confirmed the presence of functional groups and chemical bonding in these films. With increasing pH of the solution. From the SEM images, it has been perceived that the grain sizes and shapes change to some extent by changing the levels of pH the resistance Sheet value increases of the films exhibit a high of 2,31E+06 ohm/sheet.

References

[1] K. Y. Æ. S. O. Æ. M. Yoneta, "Structural , optical and electrical characterization of undoped ZnMgO film grown by spray pyrolysis method," pp. 203–209, 2008.

[2] V. Revathi and K. Karthik, "Microwave assisted CdO–ZnO–MgO nanocomposite and its photocatalytic and antibacterial studies," *J. Mater. Sci. Mater. Electron.*, vol. 29, no. 21, pp. 18519–18530, 2018.

[3] H. Wang, Q. Liu, X. Wang, H. Tang, J. Yan, and P. Gao, "Laser sintering method induced c - axis growth of - Mg 0 . 2 Zn 0 . 8 O nano - film for ultraviolet photodetector," *J. Mater. Sci. Mater. Electron.*, no. 0123456789, pp. 1–6, 2019.

[4] R. Schmidt-Grund *et al.*, "Refractive indices and band-gap properties of rocksalt Mg xZn 1-xO (0.68≤x≤1)," *J. Appl. Phys.*, vol. 99, no. 12, pp. 0–7, 2006.

[5] P. Bhattacharya, R. R. Das, R. S. Katiyar, P. Bhattacharya, R. R. Das, and R. S. Katiyar, "Fabrication of stable wide-band-gap ZnO / MgO multilayer thin films Fabrication of stable wide-band-gap ZnO Õ MgO multilayer thin films," vol. 2010, no. 2003, pp. 2009–2012, 2012.

[6] M. Biswas, M. Sharmin, C. Das, J. Poddar, and S. Choudhury, "Structural and Optical Characterization of Magnesium Doped Zinc Oxide Thin Films Deposited by Spray Pyrolysis," vol. 64, no. 1, pp. 1–6, 2016.

[7] K. Huang *et al.*, "Preparation and characterization of Mg-doped ZnO thin films by sol-gel method," *Appl. Surf. Sci.*, vol. 258, no. 8, pp. 3710–3713, 2012.

[8] A. Kaushal and D. Kaur, "Effect of Mg content on structural, electrical and optical properties of Zn1-xMgxO nanocomposite thin films," *Sol. Energy Mater. Sol. Cells*, vol. 93, no. 2, pp. 193–198, 2009.

[9] A. K. Balta, Ö. Ertek, N. Eker, and İ. Okur, "MgO and ZnO Composite Thin Films Using the Spin Coating Method on Microscope Glasses," no. January, pp. 40–47, 2015.

[10] M. Rouchdi, E. Salmani, B. Fares, N. Hassanain, and A. Mzerd, "Synthesis and characteristics of Mg doped ZnO thin films: Experimental and ab-initio study," *Results Phys.*, vol. 7, no. January, pp. 620–627, 2017.

[11] V. G. Krishnan, P. Elango, V. Ganesan, and P. Sathish, "pH deeds on structural, optical, electrical and gas sensing performance of TiO2 nanofilms by automated nebulizer spray pyrolysis technique," *Optik (Stuttg).*, vol. 127, no. 23, pp. 11102–11110, 2016.

[12] M. Rashad, H. O. Tekin, H. M. Zakaly, M. Pyshkina, S. A. M. Issa, and G. Susoy, "Physical and nuclear shielding properties of newly synthesized magnesium oxide and zinc oxide nanoparticles," *Nucl. Eng. Technol.*, vol. 52, no. 9, pp. 2078–2084, 2020.

[13] F. Meydaner. Tezel, O. Özdemir, and I. Afsin Kariper, "THE EFFECTS of pH on STRUCTURAL and OPTICAL CHARACTERIZATION of IRON OXIDE THIN FILMS," *Surf. Rev. Lett.*, vol. 24, no. 4, pp. 1–10, 2017.

[14] A. Kariper, E. Güneri, F. Göde, and C. Gümüş, "Effect of pH on the physical properties of CdS thin films deposited by CBD," *Chalcogenide Lett.*, vol. 9, no. 1, pp. 27–40, 2012.

[15] M. K. Dhahir and H. A. Khyoon, "Study the Effect of PH Variation on the Particle Size of Sio 2 Thin Films," *Iraqi J. Laser, Part A*, vol. 15, pp. 1–8, 2016, [Online]. Available: https://www.iasj.net/iasj?func=fulltext&aId=117415.

[16] N. S. Tezel, F. M. Tezel, and I. A. Kariper, "The impact of pH on the structural, surface, electrical and optical properties of nanostructured PbSe thin films," *Mater.*

Res. Express, vol. 6, no. 7, 2019.
[17] V. S. Raut, "Studies on effect of pH on structural , optical and morphological properties of chemisynthesizedCdSe grains," vol. 10, no. 1, pp. 568–572, 2017.
[18] I. Journal and O. F. Engineering, "INTERNATIONAL JOURNAL OF ENGINEERING SCIENCES & RESEARCH TECHNOLOGY STRUCTURAL AND OPTICAL PROPERTIES OF (ZnO/MgO) NANOCOMPOSITES," vol. 7, no. 8, pp. 493–499, 2018.
[19] M. W. Lekota, K. M. Dimpe, and P. N. Nomngongo, "MgO-ZnO/carbon nanofiber nanocomposite as an adsorbent for ultrasound-assisted dispersive solid-phase microextraction of carbamazepine from wastewater prior to high-performance liquid chromatographic detection," *J. Anal. Sci. Technol.*, vol. 10, no. 1, pp. 1–12, 2019.
[20] L. Z. Peia, L. Z. Yinb, J. F. Wanga, J. Chena, C. G. Fana, and Q. F. Zhanga, "Low temperature synthesis of magnesium oxide and spinel powders by a sol-gel process," *Mater. Res.*, vol. 13, no. 3, pp. 339–343, 2010.
[21] A. Nada, "Synthesis and Photocatalytic Activity of Single Crystal Titanate :," vol. 6, no. 10, pp. 40–50, 2014.
[22] S. Nisatharaju, R. Ayyappa, D. Balamurugan. Structural, Morphological and Optical Characterization of Spray Deposited MgO Thin Film. August 2014 Asian Journal of Applied Sciences 7(8):780-785.

General conclusion and perspectives

General conclusion

The interest in magnesium oxide thin films is fast growing due to their importance in many applications in science and technology. Besides acting as an EC material, it can also be used as a functional layer material for photovoltaic applications. MgO is an insulator with a resistivity of the order of 1010 Ω.cm at room temperature.

In conclusion, highly transparent conductive MgO-ZnO thin films have been deposited on glass substrate by spray pneumatic method.The aim of this work is to prepare thin films of MgO-ZnO by the spray pyrolysis technique and to study the effect of different experimental parameters on the fundamental properties of MgO-ZnO films. The parameters investigated are (substrate temperature, molarity and PH). The understand the effects of these parameters on the properties of this material in order to optimize their performance for use in optoelectronic applications. The layers developed have undergone morphological, structural, optical and electrical characterizations.

Firstly, we have prepared the MgO thin films on a glass substrate at 450°C at different MgO concentrations (0.05, 0.10, 0.15 and 0.2 mol.l-1). Polycrystalline MgO films with a cubic structure with a strong (002) preferred orientation were observed at all sprayed films with maximum crystallite size of 21.4 nm was attained of sprayed film at 0.2 mol.l-1. The good transmission was found in the deposited MgO thin film with the lowest molarity. The transmission of MgO thin films decreases rapidly as the wavelength increases in the range of (300-400) nm, and then increases slowly at higher wavelengths. The band gap of MgO thin films decreases as the molarity increases and the band gap values range between 4.8-4.3 eV. The Urbach energy values range between 375-519 meV. The electrical resistance of our films in the order 2*107Ω.

Secondly, the MgO Thin Films have been grown on glass substrates at 450°C by various pH solution values (2.5; 5; 8.3 and 10 of pH). The MgO thin films have a strong preferential crystallinity with a cubic structure with high (200) phase, the minimum value of crystallite size 9.9 nm is attained of deposit MgO thin film at 450 °C with 10 of PH. The optical transmission spectra showed all the sprayed MgO thin films are transparency within the visible wavelength region. The band gap of MgO thin films decreases from 3.91 to 3.7 eV as the PH increases from 2.5 to 6.8, and the

urbach energy was increased. The surface morphology by SEM was indicated that the MgO prepared with PH= 5 and 6.80 the grains become nearly spherical and bigger, and for the pH increased to pH =10, showing spherical particles and smaller, this may be when coalescence occurs. The thin film obtained with 2.5 of pH has a lower electrical resistance.

Thirdly, Mg0.5Zn0.5O thin films have been grown on glass substrates at 450°C by various pH solution values (2.5; 7.10 and 8.30 of pH). The Zn 0.5Mg 0.5O thin films were observed in high crystallinity with a cubic structure with a strong preferential, the maximum value of crystallite size 20.63 nm is attained of deposit Mg0.5Zn0.5O thin film at 450 °C with 8.30 of PH. The optical transmission spectra showed all the sprayed Mg0.5Zn0.5O thin films are transparency within the visible wavelength region. The band gap of Mg0.5Zn0.5O thin films increases from 3.77 to 4.09 eV as the PH increases, The Urbach energy values decreased as the PH increased from 397 to 321 meV. FTIR absorbance spectra revealed the presence of the stretching vibration mode of Mg–O. peaks stretching vibration bond in MgO thin film network.

perspectives

- Elaboration of ZrO_2 , MgS thin films by varying other parameters like precursor, the substrates and solvent….etc.
- Investigating the use of deposited films in PN junctions, photocatalysts, and antibacterial applications, among others.

Abstract

The aim of this work is to prepare thin films of MgO and alloys MgO-ZnO by the spray pyrolysis technique. and to study the effect of different experimental parameters on the fundamental properties of thin films, The parameters investigated are (substrate temperature, molarity, and pH). Firstly, we prepared the MgO thin films on a glass substrate at 450°C at different MgO concentrations (0.05, 0.10, 0.15, and 0.2 mol.l-1). the MgO thin films show a cubic structure with a strong (002) preferred orientation and a maximum crystallite size of 21.4 nm attained of sprayed film at 0.2 mol.l-1.Good transmission was found in MgO thin film with the lowest molarity. The transmission of MgO thin films decreases rapidly as the wavelength increases in the range of (300-400) nm and then increases slowly at higher wavelengths. The band gap of MgO thin films decreases as the molarity increases and the band gap values range between 4.8-4.3 eV. The electrical resistance of our films is in the order of $2.10^7\Omega$. Secondly, the MgO Thin Films have been grown on glass substrates at 450°C by various pH solution values (2.5; 5;6.8; 8.3, and 10 pH). The MgO thin films have a strong preferential crystallinity with a cubic structure with a high (200) phase, the minimum value of crystallite size 9.9 nm is attained of deposit MgO thin film at 450 °C with 10 of pH. The optical transmission spectra showed all the sprayed MgO thin films are transparent within the visible wavelength region. The band gap of MgO thin films decreases from 3.91 to 3.7 eV as the pH increases from 2.5 to 6.8, and the Urbach energy was increased. The surface morphology by SEM indicated that in the MgO prepared with pH = 5 and 6.80 the grains become nearly spherical and bigger, and for the pH increased to pH =10, showing spherical particles and smaller, this may be when coalescence occurs. The thin film obtained with 2.5 pH has a lower electrical resistance. Thirdly, Zn 0.5Mg 0.5O thin films have been grown on glass substrates at 450°C by various pH solution values (2.5; 7.10, and 8.30 pH). The Zn 0.5Mg 0.5O thin films were observed in high crystallinity with a cubic structure with a strong orientation preferential at (200) , corresponding to the maximum value of crystallite size 72.28 nm attained of deposit Zn0.5Mg0.5O thin film at 450 °C with 8.30 of pH. The optical transmission spectra showed all the sprayed $Zn_{0.5}Mg_{0.5}O$ thin films are transparent within the visible wavelength region. The band gap of Zn 0.5Mg 0.5O thin films increases from 3.77 to 4.09 eV as the pH increases, The surface morphology of the $Zn_{0.5}Mg_{0.5}O$ appears at pH=2.5 big grains sphere and rod-like, whereas at pH=7.10 and 8.30 the grains become nearly spherical. The thin film obtained with 2.5 and 7.10 pH has a lower electrical resistance.

Key words: MgO; MgO-ZnO; Thin films; pH solution; Spray technique

ملخص

الهدف من هذا العمل هو تحضير أغشية رقيقة من MgO وسبائك MgO-ZnO بتقنية الانحلال الحراري بالرش. ودراسة تأثير العوامل التجريبية المختلفة على الخواص الأساسية للأغشية الرقيقة ، المتغيرات التي تم دراستها هي (درجة حرارة الركيزة ، المولارية ، ودرجة الحموضة). أولاً ، قمنا بإعداد الأغشية الرقيقة MgO على ركيزة زجاجية عند 450 درجة مئوية بتركيزات مختلفة من (0.05 MgO، 0.10، 0.15 ، و 0.2 مول / لتر). تُظهر الأغشية الرقيقة MgO بنية مكعبة ذات اتجاه مفضل قوي (002) وحجم بلوري أقصى يبلغ 21.4 نانومتر تم الحصول عليه من الغشاء المرشو عند 0.2 مول لتر -1 تم العثور على انتقال جيد في غشاء رقيق MgO مع أقل مولارية. يتناقص انتقال الأغشية الرقيقة MgO بسرعة حيث يزداد الطول الموجي في نطاق (300-400) نانومتر ثم يزداد ببطء عند الأطوال الموجية الأعلى. تقل فجوة النطاق للأغشية الرقيقة MgO مع زيادة المولارية وتتراوح قيم فجوة النطاق بين 4.8-4.3 فولت. المقاومة الكهربائية لأفلامنا في حدود Ω2.107. ثانيًا ، تمت زراعة الأغشية الرقيقة MgO على ركائز زجاجية عند 450 درجة مئوية بواسطة قيم مختلفة لمحلول الأس الهيدروجيني (2.5 ، 5 ، 6.8 ، 8.3 ، و 10 درجة حموضة). تحتوي الأغشية الرقيقة MgO على تبلور تفضيلي قوي مع هيكل مكعب ذو طور مرتفع (200) ، ويتم الوصول إلى الحد الأدنى لقيمة حجم البلورة 9.9 نانومتر من غشاء رقيق MgO عند 450 درجة مئوية مع 10 درجة حموضة. أظهر أطياف الإرسال البصري أن جميع الأغشية الرقيقة MgO التي تم رشها شفافة داخل منطقة الطول الموجي المرئي. تقل فجوة النطاق للأغشية الرقيقة MgO من 3.91 إلى 3.7 فولت مع زيادة الأس الهيدروجيني من 2.5 إلى 6.8. أشار شكل السطح بواسطة SEM إلى أنه في MgO المحضر مع الأس الهيدروجيني = 5 و 6.80 تصبح الحبوب كروية تقريبًا وأكبر ، ولزيادة الرقم الهيدروجيني إلى الرقم الهيدروجيني = 10 ، مما يُظهر جزيئات كروية وأصغر ، قد يحدث هذا عند حدوث الاندماج. تتميز الطبقة الرقيقة التي تم الحصول عليها بـ 2.5 درجة حموضة بمقاومة كهربائية أقل. ثالثًا ، تمت زراعة أغشية رقيقة Zn 0.5Mg 0.5O على ركائز زجاجية عند 450 درجة مئوية بقيم مختلفة لمحلول الأس الهيدروجيني (2.5 ، 7.10 ، 8.30 درجة حموضة). لوحظت الأغشية الرقيقة Zn 0.5Mg 0.5O في درجة تبلور عالية مع هيكل مكعب ذو اتجاه تفضيلي قوي عند (200) ، وهو ما يقابل القيمة القصوى لحجم البلورات 72.28 نانومتر التي تم الحصول عليها من رواسب Zn0.5Mg0.5O غشاء رقيق عند 450 درجة C مع 8.30 من الرقم الهيدروجيني. أظهر أطياف النقل البصري أن جميع الأفلام الرقيقة التي تم رشها من Zn 0.5Mg 0.5O شفافة داخل منطقة الطول الموجي المرئية. تزداد فجوة النطاق للأغشية الرقيقة Zn 0.5Mg 0.5O من 3.77 إلى 4.09 eV مع زيادة الرقم الهيدروجيني ، يظهر الشكل السطحي لـ Zn 0.5Mg 0.5O عند درجة الحموضة = 2.5 كرة حبيبات كبيرة وشبيهة بالقضيب ، بينما عند درجة الحموضة = 7.10 و 8.30 تصبح الحبيبات شبه كروية. تتميز الطبقة الرقيقة التي تم الحصول عليها برقم 2.5 و 7.10 pH بمقاومة كهربائية أقل.

الكلمات الأساسية: MgO ؛ MgO-ZnO ؛ الأغشية الرقيقة؛ محلول الأس الهيدروجيني تقنية الرش

RÉSUME

L'objectif de ce travail est de préparer des couches minces de MgO et d'alliages MgO-ZnO par la technique de pyrolyse par pulvérisation. et d'étudier l'effet de différents paramètres expérimentaux sur les propriétés fondamentales des films minces, Les paramètres étudiés sont (température du substrat, molarité et pH). Dans un premier temps, nous avons préparé les couches minces de MgO sur un substrat de verre à 450°C à différentes concentrations de MgO (0,05, 0,10, 0,15 et 0,2 mol.l-1). les films minces de MgO présentent une structure cubique avec une orientation préférée forte (002) et une taille de cristallite maximale de 21,4 nm atteinte du film pulvérisé à 0,2 mol.l-1. Une bonne transmission a été trouvée dans le film mince de MgO avec la molarité la plus faible. La transmission des films minces de MgO diminue rapidement à mesure que la longueur d'onde augmente dans la plage de (300-400) nm, puis augmente lentement à des longueurs d'onde plus élevées. La bande interdite des couches minces de MgO diminue à mesure que la molarité augmente et les valeurs de la bande interdite se situent entre 4,8 et 4,3 eV. La résistance électrique de nos films est de l'ordre de 2.107Ω. Deuxièmement, les couches minces de MgO ont été développées sur des substrats de verre à 450 ° C par différentes valeurs de pH de la solution (2,5 ; 5 ; 6,8 ; 8,3 et 10 pH). Les films minces de MgO ont une forte cristallinité préférentielle avec une structure cubique à phase élevée (200), la valeur minimale de taille de cristallite 9,9 nm est atteinte de dépôt de film mince de MgO à 450 °C avec 10 de pH. Les spectres de transmission optique ont montré que tous les films minces de MgO pulvérisés sont transparents dans la région des longueurs d'onde visibles. La bande interdite des couches minces de MgO diminue de 3,91 à 3,7 eV lorsque le pH augmente de 2,5 à 6,8. La morphologie de surface par SEM a indiqué que dans le MgO préparé avec pH = 5 et 6,80, les grains deviennent presque sphériques et plus gros, et pour le pH augmenté à pH = 10, montrant des particules sphériques et plus petites, cela peut être le cas lorsque la coalescence se produit. Le film mince obtenu avec un pH de 2,5 a une résistance électrique plus faible. Troisièmement, des couches minces de Zn 0,5 Mg 0,5 O ont été développées sur des substrats de verre à 450°C avec différentes valeurs de pH de solution (2,5 ; 7,10 et 8,30 pH). Les films minces de Zn 0,5Mg 0,5O ont été observés en haute cristallinité avec une structure cubique avec une forte orientation préférentielle à (200) , correspondant à la valeur maximale de taille de cristallite 72,28 nm atteinte du dépôt de film mince de Zn0,5Mg0,5O à 450° C à 8.30 de pH. Les spectres de transmission optique ont montré que tous les films minces de Zn 0,5 Mg 0,5 O pulvérisés sont transparents dans la région des longueurs d'onde visibles. La bande interdite des couches minces de Zn 0,5 Mg 0,5 O augmente de 3,77 à 4,09 eV lorsque le pH augmente. La morphologie de surface du Zn 0,5 Mg 0,5 O apparaît à pH = 2,5 gros grains sphériques et en forme de bâtonnet, alors qu'à pH = 7,10 et 8.30 les grains deviennent presque sphériques. Le film mince obtenu avec 2,5 et 7,10 pH a une résistance électrique plus faible.

Mots clés : MgO ; MgO-ZnO; Films minces; solution pH ; Technique de pulvérisation.

Abstract

The aim of this work is to prepare thin films of MgO and alloys MgO-ZnO by the spray pyrolysis technique. and to study the effect of different experimental parameters on the fundamental properties of thin films, The parameters investigated are (substrate temperature, molarity, and pH). Firstly, we prepared the MgO thin films on a glass substrate at 450°C at different MgO concentrations (0.05, 0.10, 0.15, and 0.2 mol.l-1). the MgO thin films show a cubic structure with a strong (002) preferred orientation and a maximum crystallite size of 21.4 nm attained of sprayed film at 0.2 mol.l-1.Good transmission was found in MgO thin film with the lowest molarity. The transmission of MgO thin films decreases rapidly as the wavelength increases in the range of (300-400) nm and then increases slowly at higher wavelengths. The band gap of MgO thin films decreases as the molarity increases and the band gap values range between 4.8-4.3 eV. The electrical resistance of our films is in the order of $2.10^7\Omega$. Secondly, the MgO Thin Films have been grown on glass substrates at 450°C by various pH solution values (2.5; 5;6.8; 8.3, and 10 pH). The MgO thin films have a strong preferential crystallinity with a cubic structure with a high (200) phase, the minimum value of crystallite size 9.9 nm is attained of deposit MgO thin film at 450 °C with 10 of pH. The optical transmission spectra showed all the sprayed MgO thin films are transparent within the visible wavelength region. The band gap of MgO thin films decreases from 3.91 to 3.7 eV as the pH increases from 2.5 to 6.8, and the Urbach energy was increased. The surface morphology by SEM indicated that in the MgO prepared with pH = 5 and 6.80 the grains become nearly spherical and bigger, and for the pH increased to pH =10, showing spherical particles and smaller, this may be when coalescence occurs. The thin film obtained with 2.5 pH has a lower electrical resistance. Thirdly, Zn 0.5Mg 0.5O thin films have been grown on glass substrates at 450°C by various pH solution values (2.5; 7.10, and 8.30 pH). The Zn 0.5Mg 0.5O thin films were observed in high crystallinity with a cubic structure with a strong orientation preferential at (200) , corresponding to the maximum value of crystallite size 72.28 nm attained of deposit Zn0.5Mg0.5O thin film at 450 °C with 8.30 of pH. The optical transmission spectra showed all the sprayed $Zn_{0.5}Mg_{0.5}O$ thin films are transparent within the visible wavelength region. The band gap of Zn 0.5Mg 0.5O thin films increases from 3.77 to 4.09 eV as the pH increases, The surface morphology of the $Zn_{0.5}Mg_{0.5}O$ appears at pH=2.5 big grains sphere and rod-like, whereas at pH=7.10 and 8.30 the grains become nearly spherical. The thin film obtained with 2.5 and 7.10 pH has a lower electrical resistance.

Key words: MgO; MgO-ZnO; Thin films; pH solution; Spray technique

ملخص

الهدف من هذا العمل هو تحضير أغشية رقيقة من MgO وسبائك MgO-ZnO بتقنية الانحلال الحراري بالرش. ودراسة تأثير العوامل التجريبية المختلفة على الخواص الأساسية للأغشية الرقيقة ، المتغيرات التي تم دراستها هي (درجة حرارة الركيزة ، المولارية ، ودرجة الحموضة). أولاً ، قمنا بإعداد الأغشية الرقيقة MgO على ركيزة زجاجية عند 450 درجة مئوية بتركيزات مختلفة من (0.05 MgO، 0.10، 0.15 ، و 0.2 مول / لتر). تُظهر الأغشية الرقيقة MgO بنية مكعبة ذات اتجاه مفضل قوي (002) وحجم بلوري أقصى يبلغ 21.4 نانومتر تم الحصول عليه من الغشاء المرشو عند 0.2 مول لتر -1 تم العثور على انتقال جيد في غشاء رقيق MgO مع أقل مولارية. يتناقص انتقال الأغشية الرقيقة MgO بسرعة حيث يزداد الطول الموجي في نطاق (300-400) نانومتر ثم يزداد ببطء عند الأطوال الموجية الأعلى. تقل فجوة النطاق للأغشية الرقيقة MgO مع زيادة المولارية وتتراوح قيم فجوة النطاق بين 4.8-4.3 فولت. المقاومة الكهربائية لأفلامنا في حدود Ω2.107. ثانيًا ، تمت زراعة الأغشية الرقيقة MgO على ركائز زجاجية عند 450 درجة مئوية بواسطة قيم مختلفة لمحلول الأس الهيدروجيني (2.5 ، 5 ، 6.8 ، 8.3 ، و 10 درجة حموضة). تحتوي الأغشية الرقيقة MgO على تبلور تفضيلي قوي مع هيكل مكعب ذو طور مرتفع (200) ، ويتم الوصول إلى الحد الأدنى لقيمة حجم البلورة 9.9 نانومتر من غشاء رقيق MgO عند 450 درجة مئوية مع 10 درجة حموضة. أظهر أطياف الإرسال البصري أن جميع الأغشية الرقيقة MgO التي تم رشها شفافة داخل منطقة الطول الموجي المرئي. تقل فجوة النطاق للأغشية الرقيقة MgO من 3.91 إلى 3.7 فولت مع زيادة الأس الهيدروجيني من 2.5 إلى 6.8. أشار شكل السطح بواسطة SEM إلى أنه في MgO المحضر مع الأس الهيدروجيني = 5 و 6.80 تصبح الحبوب كروية تقريبًا وأكبر ، ولزيادة الرقم الهيدروجيني إلى الرقم الهيدروجيني = 10 ، مما يُظهر جزيئات كروية وأصغر ، قد يحدث هذا عند حدوث الاندماج. تتميز الطبقة الرقيقة التي تم الحصول عليها بـ 2.5 درجة حموضة بمقاومة كهربائية أقل. ثالثًا ، تمت زراعة أغشية رقيقة Zn 0.5Mg 0.5O على ركائز زجاجية عند 450 درجة مئوية بقيم مختلفة لمحلول الأس الهيدروجيني (2.5 ، 7.10 ، 8.30 درجة حموضة). لوحظت الأغشية الرقيقة Zn 0.5Mg 0.5O في درجة تبلور عالية مع هيكل مكعب ذو اتجاه تفضيلي قوي عند (200) ، وهو ما يقابل القيمة القصوى لحجم البلورات 72.28 نانومتر التي تم الحصول عليها من رواسب Zn0.5Mg0.5O غشاء رقيق عند 450 درجة C مع 8.30 من الرقم الهيدروجيني. أظهر أطياف النقل البصري أن جميع الأفلام الرقيقة التي تم رشها من Zn 0.5Mg 0.5O شفافة داخل منطقة الطول الموجي المرئية. تزداد فجوة النطاق للأغشية الرقيقة Zn 0.5Mg 0.5O من 3.77 إلى 4.09 eV مع زيادة الرقم الهيدروجيني ، يظهر الشكل السطحي لـ Zn 0.5Mg 0.5O عند درجة الحموضة = 2.5 كرة حبيبات كبيرة وشبيهة بالقضيب ، بينما عند درجة الحموضة = 7.10 و 8.30 تصبح الحبيبات شبه كروية. تتميز الطبقة الرقيقة التي تم الحصول عليها برقم 2.5 و 7.10 pH بمقاومة كهربائية أقل.

الكلمات الأساسية: MgO ؛ MgO-ZnO ؛ الأغشية الرقيقة؛ محلول الأس الهيدروجيني تقنية الرش

RÉSUME

L'objectif de ce travail est de préparer des couches minces de MgO et d'alliages MgO-ZnO par la technique de pyrolyse par pulvérisation. et d'étudier l'effet de différents paramètres expérimentaux sur les propriétés fondamentales des films minces, Les paramètres étudiés sont (température du substrat, molarité et pH). Dans un premier temps, nous avons préparé les couches minces de MgO sur un substrat de verre à 450°C à différentes concentrations de MgO (0,05, 0,10, 0,15 et 0,2 mol.l-1). les films minces de MgO présentent une structure cubique avec une orientation préférée forte (002) et une taille de cristallite maximale de 21,4 nm atteinte du film pulvérisé à 0,2 mol.l-1. Une bonne transmission a été trouvée dans le film mince de MgO avec la molarité la plus faible. La transmission des films minces de MgO diminue rapidement à mesure que la longueur d'onde augmente dans la plage de (300-400) nm, puis augmente lentement à des longueurs d'onde plus élevées. La bande interdite des couches minces de MgO diminue à mesure que la molarité augmente et les valeurs de la bande interdite se situent entre 4,8 et 4,3 eV. La résistance électrique de nos films est de l'ordre de 2.107Ω. Deuxièmement, les couches minces de MgO ont été développées sur des substrats de verre à 450 ° C par différentes valeurs de pH de la solution (2,5 ; 5 ; 6,8 ; 8,3 et 10 pH). Les films minces de MgO ont une forte cristallinité préférentielle avec une structure cubique à phase élevée (200), la valeur minimale de taille de cristallite 9,9 nm est atteinte de dépôt de film mince de MgO à 450 °C avec 10 de pH. Les spectres de transmission optique ont montré que tous les films minces de MgO pulvérisés sont transparents dans la région des longueurs d'onde visibles. La bande interdite des couches minces de MgO diminue de 3,91 à 3,7 eV lorsque le pH augmente de 2,5 à 6,8. La morphologie de surface par SEM a indiqué que dans le MgO préparé avec pH = 5 et 6,80, les grains deviennent presque sphériques et plus gros, et pour le pH augmenté à pH = 10, montrant des particules sphériques et plus petites, cela peut être le cas lorsque la coalescence se produit. Le film mince obtenu avec un pH de 2,5 a une résistance électrique plus faible. Troisièmement, des couches minces de Zn 0,5 Mg 0,5 O ont été développées sur des substrats de verre à 450°C avec différentes valeurs de pH de solution (2,5 ; 7,10 et 8,30 pH). Les films minces de Zn 0,5Mg 0,5O ont été observés en haute cristallinité avec une structure cubique avec une forte orientation préférentielle à (200) , correspondant à la valeur maximale de taille de cristallite 72,28 nm atteinte du dépôt de film mince de Zn0,5Mg0,5O à 450° C à 8.30 de pH. Les spectres de transmission optique ont montré que tous les films minces de Zn 0,5 Mg 0,5 O pulvérisés sont transparents dans la région des longueurs d'onde visibles. La bande interdite des couches minces de Zn 0,5 Mg 0,5 O augmente de 3,77 à 4,09 eV lorsque le pH augmente. La morphologie de surface du Zn 0,5 Mg 0,5 O apparaît à pH = 2,5 gros grains sphériques et en forme de bâtonnet, alors qu'à pH = 7,10 et 8.30 les grains deviennent presque sphériques. Le film mince obtenu avec 2,5 et 7,10 pH a une résistance électrique plus faible.

Mots clés : MgO ; MgO-ZnO; Films minces; solution pH ; Technique de pulvérisation.